MINISTRY OF NATIONAL EDUCATION
AND SCIENTIFIC RESEARCH

THE ANNALS OF "DUNAREA DE JOS" UNIVERSITY OF GALATI

Fascicle IX
METALLURGY AND MATERIALS SCIENCE

YEAR XXXIV (XXXIX)
June 2016, no. 2

ISSN 1453-083X

2016
GALATI UNIVERSITY PRESS

EDITORIAL BOARD

Table of Contents

THE ANNALS OF "DUNAREA DE JOS" UNIVERSITY OF GALATI
FASCICLE IX. METALLURGY AND MATERIALS SCIENCE
Nº. 2 - 2016, ISSN 1453 – 083X

TREATMENT OF WASTEWATER RESULTING FROM THE METALLIC COATINGS PROCESS

Tamara RADU
„Dunarea de Jos" University of Galati, Romania
e-mail: tradu@ugal.ro

ABSTRACT

The technological cleaning processes of steel strip surfaces used in metal coatings require organic or inorganic chemicals with a high risk of toxicity. To avoid pollution, the water resulting from these processes must be neutralized.

During the degreasing process, alkaline solutions containing caustic soda (NaOH), tri-sodium phosphate (Na_3PO_4) and detergents are used and the pickling process is made in 15-20% HCl solution. Rinse waters resulting from these operations will have an alkaline pH respectively acid pH, with values depending on the duration of use or refresh solution.

Neutralization was done with sulfuric acid solutions for alkaline water and sodium hydroxide solutions for acid water. The research aimed to establish the optimal conditions for neutralization and the optimal reagent consumptions.

KEYWORDS: cleaning surfaces, rinse waters, alkaline water, acid water, neutralization

1. Introduction

Treatment of wastewater generated by metallic coatings processes is essential prior to discharge of these wastewaters to wastewater collection systems or to the environment. Adequate treatment or pretreatment before discharge in wastewater collection systems is important to prevent toxic, corrosive, flammable or explosive wastes [1].

The wastewaters come from several different sources such as cleaning surfaces, preparation, production and rinsing processes, as well as the washing of equipment and production facilities [2, 3]. These processes produce various types of industrial wastes such as toxic organic solvents used as degreasing and cleansing agents, highly acidic or basic solutions used for the surfaces cleaning [4, 5].

Most of the hazardous wastewater comes from the rinsing operations applied after surfaces cleaning of the steel support. These waters may be highly acidic (low pH) or highly basic (high pH).

Different technologies exist for treatment of wastewater and effluents generated by the metal surface treatment industry. Treatment choice will depend on the composition of the effluents as well as the objectives and environmental needs of the company: zero liquid discharge, water reuse, adjustment of discharge limits, obtaining by-products, etc. [6].

Wastewaters with high pH levels are neutralized by the addition of acids such as sulfuric acid (H_2SO_4) and hydrochloric acid (HCl). Also, carbon dioxide (CO_2) and sulfur dioxide (SO_2) can be applied in the gaseous form to decrease the pH of liquids [1].

Wastewaters with low pH levels are neutralized by oxides (CaO; MgO), hydroxides ($Ca(OH)_2$; $Mg(OH)_2$; NaOH) or soda ash (Na_2CO_3). Neutralization may be accomplished by either batch or continuous processes, depending on the amount of wastewater that will be treated [1].

The main methods of neutralizing these waters can be classified in three categories [7]:

- neutralization without water recirculation (open circuit) - applied before these waters are discharged to the sewer or in environment;

- with partial recirculation (semi-open circuit) - water treatment is done on the technological flow and recycled water is partially neutralized in the washing tanks. This method does not allow total reuse of the neutralized water because soluble ions (Na^+, Cl^-) remain in solution and, upon each reuse, their concentration increases;

- with total recirculation (closed circuit) - the neutralized water is completely recycled in the technological flow. The neutralization in closed

circuit is becoming more popular because it ensures a significant reduction in water consumption.

The research presented in this paper was aimed at neutralization of waters resulted from cleaning the steel strip surfaces in hot dip galvanizing processes. Were targeted the rinsing waters resulted after the degreasing and pickling processes.

In the process of alkaline degreasing of the steel strips surfaces for galvanizing, solutions which contain caustic soda (NaOH), trisodium phosphate (Na_3PO_4), detergents and other are usually used.

Pickling is made in acid solutions and the hydrochloric acid, 15-20% HCl solution is commonly used. In the technological flow, degreasing operations and pickling are followed by washing processes.

The wastewaters results will have an alkaline pH, respectively acid pH, with pH values depending on duration of use or refresh. These waters are treated for neutralizations up to a pH reaching 6.5-8.5 values, as required by normative (NTPA 002/2002).

2. Experimental researches

For the purpose of this research were intentionally prepared solutions with different pH values, respectively: acid solutions (with HCl): pH 2.64, 3.57, 4.30 and alkaline solutions (with NaOH) pH: 11.14; 12.27; 13.44.

2.1. Treating acidic waters

To treat acidic waters resulting from the washing process after pickling, the literature [8-10] indicates the use of a NaOH solution because it ensures simultaneous precipitation of metal ions through the following reaction:

$$Me^{2+} + 2NaOH \rightarrow Me(OH)_2 + 2Na^+$$

Work safety limits the concentration of caustic soda solution because it is a highly toxic and corrosive. Concentrated solutions can also affect the working installations.

For the treatment of acidic waters in the laboratory, there were introduced, while stirring and at room temperature, 5 mL 10% NaOH solution in 200 mL solution having an acid pH. After introducing the NaOH solution, we waited for 5 minutes for producing reactions and stabilizing pH.

It was recorded the resulting pH and the operation was repeated until the pH was neutral. Figure 1 presents the experimental results of the neutralization of the water with a pH of 2.64. It is observed that, for bringing the pH at value 6.83-7.50, which fits the normative, 25-30 mL NaOH solution was needed.

Figure 2 presents the experimental results of the water neutralization process with an initial pH of 3.57. It can be observed, similarly to the solution with pH 2.64, a rapid increase of the pH at introducing the first 5 mL NaOH solution and subsequently slower increase of pH values.

This evolution is explained by salt formation that has a buffering effect for the solutions that will be treated further.

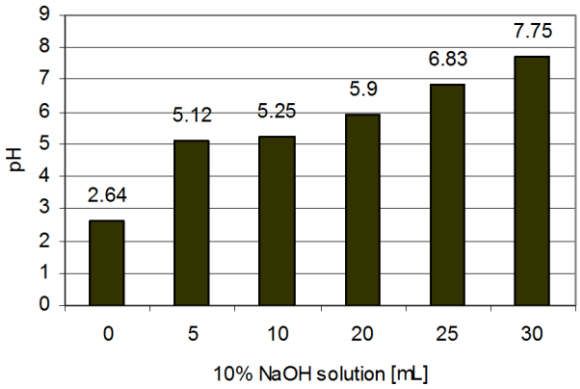

Fig. 1. *The variation of the pH for the solution with initial pH 2.64 depending on the amount of alkaline solution added*

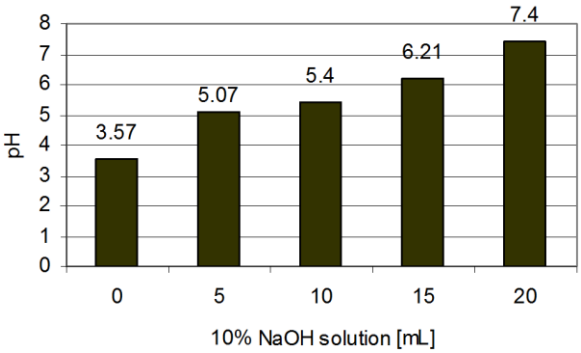

Fig. 2. *The variation of the pH for the solution with initial pH 3.57 depending on the amount of alkaline solution added*

As shown in Figure 3 if the initial pH is 4.30, neutralization occurs at the addition of 15 mL of NaOH solution.

The consumption of 10% NaOH solution to neutralize 100 L rinse water, with the different low values of pH is shown in Table 1.

Ii is observed that, to neutralize rinse water, with initial 2.5-3 pH, it is required a higher reagent consumption by 60% compared to the waters with pH value of 4-4.5. It is therefore indicated that the neutralization of the rinse water after pickling to be performed when they have a minimum pH value of 4.5. This reduces water consumption duration of the

neutralization process, the amount of reagents and financial costs.

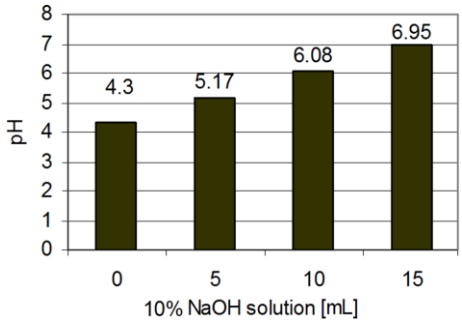

Fig. 3. *The variation of the pH for the solution with initial pH 4.30 depending on the amount of alkaline solution added*

Table 1. *Consumption of reagents required to neutralize the 100 L rinse water after pickling*

pH	2.5-3	3-3.5	4-4.5
10% NaOH solution [L]	12.5	10	7.5

2.2. Treating alkaline waters

To treat alkaline waters resulting from the washing process after degreasing, the literature indicates the use of an acid solution [10, 11]. For the treatment of alkaline waters in the laboratory we introduced, through stirring at ambient temperature, 2 mL of 25% H_2SO_4 solution in 200 mL solution having a basic pH determined. The results of the neutralization process are shown in Figures 4-6. In Figure 4 it is shown the neutralization results of the alkaline water with initial pH of 13.44. It is observed that, for bringing the pH at a value of 7.21, 10 mL of H_2SO_4 solution was needed.

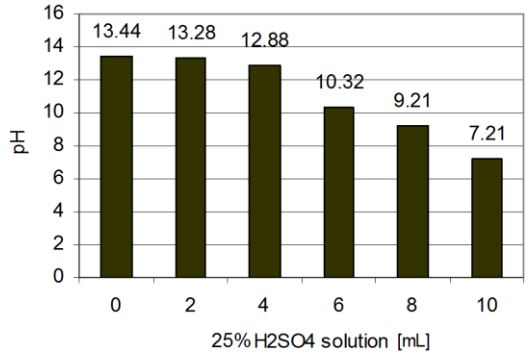

Fig. 4. *The variation of the pH for the solution with initial pH 13.44 depending on the amount of acid solution added*

Initial additions of the H_2SO_4 have a minor effect upon pH because the result product, Na_2SO_4 has little buffer capacity [6].

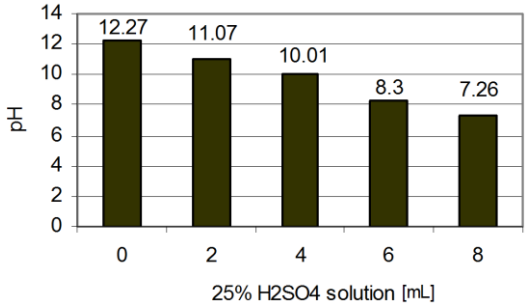

Fig. 5. *The variation of the pH for the solution with initial pH 12.27depending on the amount of acid solution added*

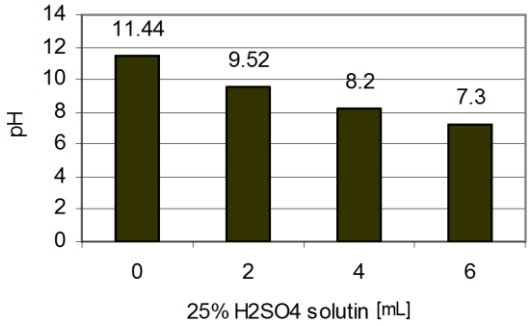

Fig. 6. *The variation of the pH for the solution with initial pH 11.44 depending on the amount of acid solution added*

The consumption of 25% H_2SO_4 solution to neutralize 100 L rinse water, with the different alkaline pH values, is shown in Table 2. The alkaline waters resulted after the rinse applied after degreasing are more easily neutralized for a pH minim 11 value.

Table 2. *Consumption of reagents required to neutralize the 100 L rinse water after degreasing*

pH	10-11.5	12-12.5	13-13.5
25% H_2SO_4 solution [L]	2	3	5

3. Conclusions

Neutralizing waters with acid pH, resulting following pickling process, should be made with less concentrated solution of caustic soda, because it favors the simultaneous precipitation of present metal ions. During neutralization with sodium hydroxide solutions, salts with buffering effect form quickly, stabilizing the pH.

Neutralizing alkaline waters, formed when rinsing following pickling process was performed with sulfuric acid solution of 25%. Following the process sodium sulfate will result, with reduced buffering effect.

Neutralization used for technological purpose or to avoid environmental pollution is performed up to a pH value of 6.5-8.5. Achieving these values through neutralization is done with lower reagents consumption and reduced process duration for acid waters with a maxim pH of 4.5, and for alkaline waters with a maxim pH of 11.

References

[1]. ***, *Treatment of wastewater from electroplating, metal finishing and printed circuit board manufacturing*, California State University, Sacramento Department of Civil Engineering Office of Water Programs.

[2]. Maria Vlad, Tamara Radu, Olga Mitoseru, Florentina Potecasu, *Environment Quality Improvement at Hot-dip Galvanisation and the Recycling of Zinc By-products*, Journal of Environmental Protection and Ecology, 12, No 3A, p. 1415-1423 2011.

[3]. Maria Vlad, Gelu Movileanu, Tamara Radu, Lucica Balint, *Recycling of zinc by products*, 11th International Multidisciplinary Scientific GeoConference, SGEM 2011, Proceedings, vol. 3, p. 875-882, 2011.

[4]. Tamara Radu, Anisoara Ciocan, Maria Vlad, Simion Ioan Balint, Viorel Dragan, *Environmental risk assessment in the galvanizing of steel sheets*, 12th International Multidisciplinary Scientific GeoConference, SGEM 2012, Proceedings, vol. 5, p. 391-397, 2012.

[5]. ***, www.ebrd.com.

[6]. ***, www.blog-en.condorchem.com.

[7]. Marcos von Sperling, *Biological Wastewater Treatment Series*, vol. 2, IWA Publishing, London, 2007.

[8]. Metcalf and Eddy, *Wastewater engineering: treatment and reuse*, McGraw Hill, 4th ed., p. 1819, 2003.

[9]. Metcalf and Eddy, *Wastewater engineering: treatment, disposal and reuse*, Metcalf & Eddy Inc., 3th ed., p. 1334, 1991.

[10]. Elson R., Shaw R. J., *Wastewater treatment options*, *in Running Water*, p. 41, IT Publications, London, 1999.

[11]. ***, www.lboro.ac.uk.

THE ANNALS OF "DUNAREA DE JOS" UNIVERSITY OF GALATI
FASCICLE IX. METALLURGY AND MATERIALS SCIENCE
Nº. 2 - 2016, ISSN 1453 – 083X

RESEARCH ON OBTAINING AND CHARACTERIZATION OF POLYMERIC MEMBRANES FOR WASTEWATER TREATMENT

Laurenția Geanina TIRON*, Maria VLAD, Ștefan Cătălin PINTILIE, Ștefan BALTĂ
"Dunarea de Jos" University of Galati, Romania
*e-mail: geanina.tiron@ugal.ro

ABSTRACT

Some of the most common polymeric membranes are used in wastewater treatment. Over the years, these membranes have been studied from different points of view: their aim to improve the retention of impurities, membrane affinity to water and degree of fouling of polymeric membranes. By analysing the surface of the membrane material by chemical characteristics information can be offered regarding the polymer's hydrophilicity or hydrophobicity. Improving membrane properties can be achieved during the stage of obtaining the polymer solution and during the thin film deposition step. To obtain polymeric membranes, the phase inversion method was used, following the influencing factors on membrane properties during the manufacturing process. The performance of membranes was studied using various parameters which lead to different results in terms of flux, permeability and hydrophilicity. This paper presents the influence of different polymer concentration, the influence of relative air humidity and the membrane thickness gradient on membrane flux and permeability.

KEYWORDS: polymeric membranes, pure water flux, relative air humidity, thickness gradient

1. Introduction

Membrane filtration is an important alternative for wastewater treatment and was developped after the XVIIIth century when Abb'e Nolet discovered water permeation through a diaphragm, a phenomenon called osmosis [1]. Widely recognized as the technology used for superior wastewater treatment, membranes provide a physical barrier that effectively removes solids, viruses, bacteria and other unwanted molecules [2].

Membrane water treatment process was applied first in the US and Middle East, but has expanded so much that in the present, to obtain drinking water, there are membranes used all over the world [3]. Membrane technologies are used on a large scale in industries like chemical industry and water treatment [4]. Membrane filtration has become the leading separation technology for water and wastewater treatment in the last 50 years [5].

Water treatment membranes are thin sheets of material (mainly polymers) that are able to separate contaminants based on properties such as size or charge. Water passes through a membrane but not larger particles, microorganisms and other contaminants, depending on their size, are separated and eliminated [6].

Polymeric membranes used in ultrafiltration processes are obtained by applying phase inversion process. The most used polymers are polysulfone (PSF), polyethersulfone (PES) and polyvinylidene fluoride (PVDF). These polymers show a high degree of utilization because it provides high tolerance to pH, chlorine and high temperatures, and are stable from the mechanical point of view [7].

The membrane properties may vary depending on the fabrication steps [8], for example there are many approaches involving either mixing with the hydrophilic components to improve the hydrophilicity of the membrane, or the modification [9] of the surface to improve antifouling [10]. Many factors which can have an influence on the membrane properties were studied by researchers. The most important factors studied are the polymer concentration, relative air humidity and the use of additives in the polymeric casting solution or in the nonsolvent bath (Han and Bhattacharyya, 1994;

Swinyard and Barnie, 1988) [11, 12], the temperature of the nonsolvent bath [13, 14] etc.

A major problem for membranes is fouling. Membrane fouling can be defined as a pollutant deposition to the membrane surface or the absorption of pollutants in the membrane pores [15]. Generally, fouling occurs either on the surface of a membrane or within its pores, and it causes a decrease in flux. There are four major types of fouling: biofouling, scaling, organic, and colloidal [16]. Biofouling results from microbial contamination of feed water and produces a biofilm on the surface of the membrane, which increases the resistance to water permeation. Scaling arises from the precipitation and deposition of salts on the membrane surface. Organic fouling comes from substances such as hydrocarbons which coat the surface and/or plug pores in the porous support layer. Colloidal fouling mainly stems from particles, such as clay or silica, accumulating on the surface of the membrane. Fouling can be controlled to some extent by adding disinfectants, anti-scaling agents, and other pre-treatment steps. However, these are not remedies to the problem, and fouling remains a key area in definite need of improvement for reverse osmosis (RO) membranes [17].

2. Equipment and process

The separation of impurities from the fluid using water flow filtration is achieved by the filters or filter media (permeable porous media) as illustrated in Figure 1 [16].

Using the pressure difference (Δp), the suspension (fluid subjected to filtration) has a flow rate Q that passes through the filter medium. The difference between the pressure of the fluid subjected to the filtration (p_1) and the permeate pressure (p_2) called the pressure drop may be provided by gravity, fluid pressure, filter vacuum downstream.

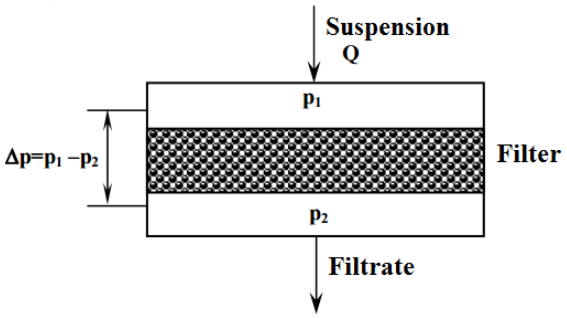

Fig. 1. *The scheme of the filtration principle* [16]

In the dead-end filtration, the influent flow is perpendicular to the membrane (Figure 2). Any solid particles in the influent which is greater than the pore size of the membrane is deposited on the surface, forming a "cake" layer of the solid particles. The fluid passing through the membrane is called filtered [17].

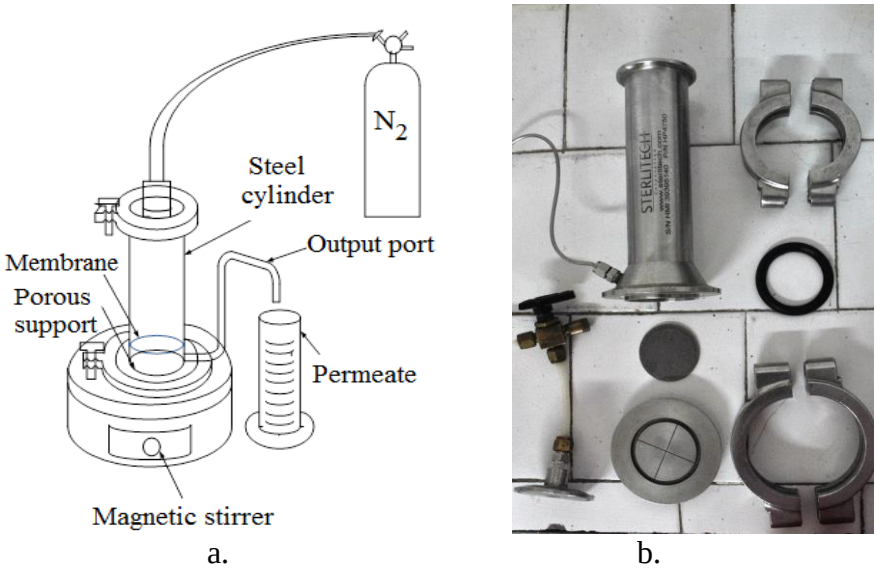

Fig. 2. *Dead-End Filtration System: a. filtration plant; b. filtration cell*

The laboratory filtration dead-end system is often conducted in a stirred-cell which is merely a cylindrical vessel, usually made of stainless steel, fitted with a porous support on top of which is placed the membrane [18]. An output port is designed for the filtrate to be collected and weighed on a digital balance. For accurate measurements and efficient data collection, this measurement system can be connected to a personal computer. The flow is calculated by measuring the mass (or the volume if the density is

known) of filtrate collected in a known time. The pressure inside the vessel was kept constant by connecting it to a cell with a compressed inert gas (e.g.: nitrogen) [17].

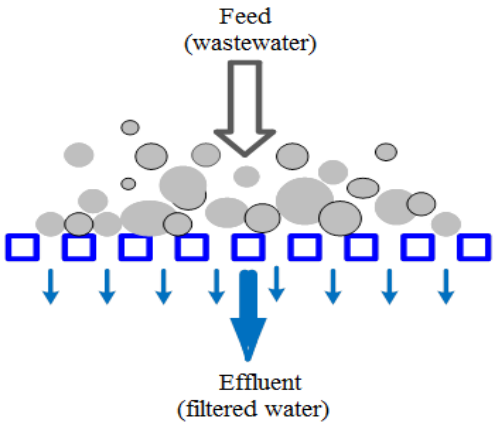

Fig. 3. *Filtration process in a dead-end stirred-cell* [19]

Pure water permeability is based on the Darcy's Law, which explains that the flow rate of water through a porous medium under the action of a driving pressure ΔP is expressed by the equation [20]

$$dV / (A \times dt) = J = \Delta P / (\eta \times Rm) \qquad (1)$$

where:

- J is the linear flux of the fluid (the water volume „V" that passes in the known time „t" through a known area „A") [L / m² · h];
- ΔP is the pressure gradient [N / m²] or [bar];
- η is the fluid viscosity [Ns / m²];
- Rm refers to the permeability of the filter media.

3. Materials used for membrane fabrication

3.1. Types of polymers used to obtain the polymeric membrane

The hydrophilicity of the membrane's surface can be studied using a contact angle analyzer with the sessile drop method by measuring the dynamic contact angle [21].

In the category of hydrophobic materials there are polysulfone (PSF) and polyethersulfone (PES) that are used for ultrafiltration (UF) membranes or for support for the reverse osmosis (RO) membranes. In the category of hydrophilic membranes there are polymers such as polyethylene (PE), polytetrafluoroethylene (PTFE), isotactic polypropylene (PP) or fluoride (PVDF), which are commonly used to obtain the microfiltration membranes [22, 23].

The membrane permeability can be influenced by the type of polymer. Analyzing the results of S.A. Al Malek *et al.*, in their study on the polyethersulfone membranes (15 wt.%), obtained water permeability of 128.2 L/m²·h·bar, presented in Fig. 1 with PES-1 [24]. The results of the sample PS-1 were obtained by Elizabeth Arkhangelsky *et al.*, using polysulfone with 15 wt.%, resulting pure water permeability of 118.28 L/m²·h·bar [25]. In the sample CA, Toraj Mohammadi *et al.* has used cellulose acetate (CA) with 15 wt.% and a value of pure water permeability of about 58 L/m²·h·bar [26].

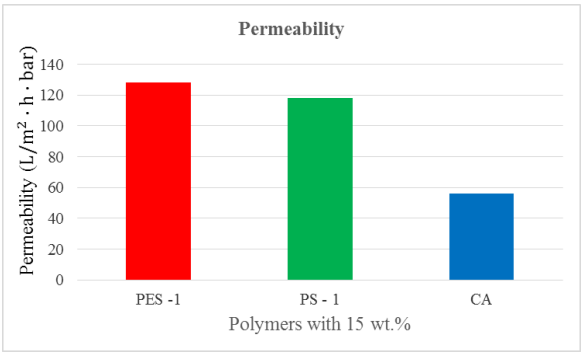

Fig. 4. *Permeability of polymeric membrane*

If we analyse the three types of membranes obtained from different polymers, with the same concentration, it can be seen that the membrane with polyethersulfone has better permeability than the other membranes, but the polyethersulfone and polysulfone have close values of permeability.

3.2. The influence of polymer concentration used in the membranes manufacture

The concentration is the parameter that has the greatest influence on the properties of the polymer membrane [27] and it may affect the performance of membrane structure and thickness [28].

To observe this phenomenon, three different studies were analyzed for polyethersulfone with different concentrations. The results of sample PES-2 were obtained by S. A. Al Malek *et al.*, with the highest value of permeability [24]. The sample PES-3 was obtained by Jiang-Nan Shen *et al.* In this study, polyethersulfone with 18 wt.% was used and obtained a permeability of 124.6 L/m²·h·bar [29]. And Elizabeth Arkhangelsky *et al.* in their study obtained polymeric membranes with 20 wt.% of polyethersulfone and with 50 L/m²·h·bar permeability [25].

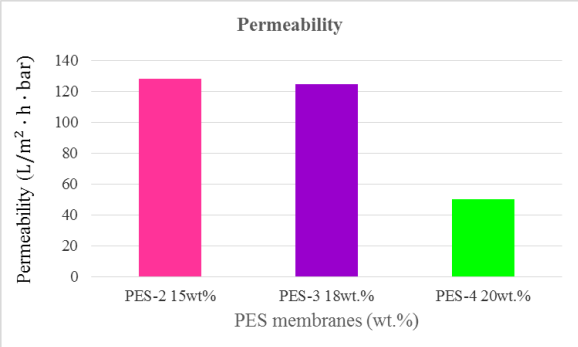

Fig. 5. *The influence of polymer concentration*

3.3. The influence of membrane thickness on the properties of the membrane

A membrane thickness gradient is defined as a flat sheet membrane with a membrane thickness increasing in one direction, which is used to investigate the morphology evolution of the membrane to the membrane thickness.

Experimentally, the gradient of thickness of the membranes is adjusted to the casting with a utility knife, generally being studied the critical structure-transition thickness (Lc) and the thickness of the overall thickness of the structure of a sponge (Lgs). LGS is the thickness of the sponge-like portion below the surface membrane [30].

4. Analysis of the additives used in the preparation of membranes

Polymeric additives (usually a hydrophilic polymer) in a casting solution are also used to increase both porosity and pore size (pore forming agent), and to suppress the formation of macrovoids. However, depending on the polymer used to make the membrane, depending on the solvent and the method of applying the thin film, effects can be observed [31].

Membranes made from hydrophobic materials can be improved by adding copolymer in the membrane matrix solution. The presence of polyethylene glycol (PEG) additive in polymer solution helps form a hydration layer that provides resistance to foulant adsorption [32].

Membranes obtained from polyvinyl chloride (PVC) blended with copolymer (Pluronic F-127) and poly(ethylene oxide) (PEO), used like additive, was studied by Liu *et al.* to increase the antifouling properties [33].

S.A. Al Malek *et al.* studied the pure water flux of membranes obtained from polyethersulfone with 20 wt.% and polyvinylpyrrolidone with 5, 10, 15 and 20 wt.% [24]. Comparing with the membranes with polyethylene glycol having 5, 10, 15 and 20 wt.% in polyethersulfone of 20 wt.% obtained by Ani Idris *et al.* [34], the water flux is higher in the case of polyethylene glycol additive.

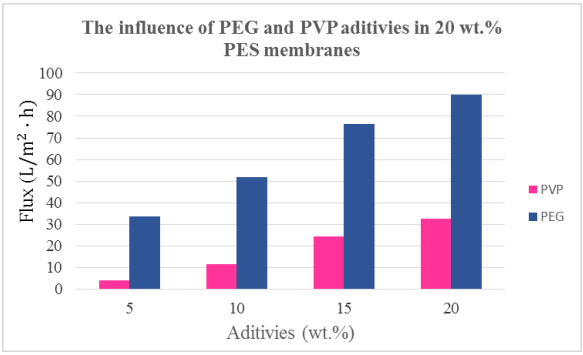

Fig. 6. *The influence of additives on membrane performance*

5. Improving the humidity gradient variation property in the membrane production

Relative air humidity affects membrane performance because during application of polymer solution on a thin film, the cast of this film composition varies by absorbing water vapour. Absorption occurs when the solvent evaporates in the presence of water vapour, dimethylformamide (DMF) and N-Methyl-2-pyrrolidone (NMP) are solvents and absorb a large amount of moisture.

Due to this absorption of water vapour, separation phase occurs in some places of the membrane's surface, preceding the separation phase that occurs when the cast film is placed in a bath of non-solvent with distilled water. Relative air humidity can thus influence the top layer of the surface of the membrane, because the base layer of the membrane is formed only at the time of immersion in the bath of non-solvent.

6. Conclusions

In conclusion, the membranes obtained from polyethersulfone (PES) is one of the most hydrophilic polymer in terms of pure water filtration. Also, the concentration of the polymer has an important influence on the membrane performance. In this situation, the membrane permeability decreases with the increasing polymer concentration. Another important factor influencing the process of obtaining membranes is the addition of additives. The amount of additive and the type of additive in the support layer is an important parameter for membrane permeation.

References

[1]. Richard W. Baker, *Membrane Technology and Applications*, Membrane Technology and Research, Inc., Menlo Park, California, 2004.
[2]. ***, www.kochmembrane.com.
[3]. Johannes Martinus Koen Timmer, *Properties of nanofiltration membranes; model development and industrial application*, Technische Universiteit Eindhoven, Proefschrift, 2001.
[4]. Solanki Sejal J., Rupande N., Desai L. D., *College of Engineering, Ahmedabad, Polymer Membrane Technology*, International Journal of Engineering Science and Innovative Technology, vol. 2, issue 2, 2013.
[5]. ***, www.kochmembrane.com.
[6]. ***, www.koshland-science-museum.org.
[7]. Harmant P., *Contrôle de la structure de dépôts de particules colloidales en filtration frontale et tangentielle*, PhD Thesis, Université Paul Sabatier, Toulouse, 1996.
[8]. Yuzhang Zhu, Dong Wang, Lei Jiang, Jian Jin, *Recent progress in developing advanced membranes for emulsified oil/water separation*, NPG Asia Materials, 2014.
[9]. Hyun J., Jang H., Kim K., Na K., Tak T., *Restriction of biofouling in membrane filtration using a brush-like polymer containing oligoethylene glycol side chains*, J. Membr. Sci. 2006.
[10]. Shi Q., Su Y. L., Zhao W., Li C., Hu Y. H., Jiang Z. Y., Zhu S. P., *Zwitterionic polyethersulfone ultrafiltration membrane with superior antifouling property*, J. Membr. Sci., 2008.
[11]. Han M. J., Bhattacharyya D., *Morphology and transport study of phase inversion polysulfone membranes*, Chemical Engineering Communications, 128, p. 197-209, 1994.
[12]. Swinyard B. T., Barrie J. A., *Phase separation in nonsolvent/ dimethylformamide/polyethersulfone and non-solvent/dimethylformamide/polysulfone systems*, British Polymer Journal, 20, p. 317-321, 1988.
[13]. Chaturvedi B. K., Ghosh A. K., Ramachandhran V., Trivedi M. K., Hanra M. S., Misra B. M., *Preparation, characterization and performance of polyethersulfone ultrafiltration membranes*, Desalination, 133, p. 31-40, 2001.
[14]. Spricigo C. B., Petrus J. C. C., Machado R. A. F., Sarmento L. A. V., Bolzan A., *Preparation and characterization of polyethersulfone membranes for use in supercritical medium*, Journal of Membrane Science, 205, p. 273-278, 2002.
[15]. Norman N. Li, Anthony G. Fane, W. S. Winston Ho, T. Matsuura, *Advance-Membrane-Technology-and-Application*, A John Willey & Sons Inc., Publication, 2008.
[16]. Amjad Z., *Ed. Reverse Osmosis: Membrane Technology*, Water Chemistry and Industrial Applications, Van Nostrand Reinhold: New York, 1993.
[17]. ***, www.texaswater.tamu.edu.
[16]. ***, www.sim.utcluj.ro.
[17]. Jenny Ní Mhurchú, *BE - Dead-End and crossflow microfiltration of yeast and bentonite suspensions: experimental and modelling studies incorporating the use of artificial neural networks*, Journal of Membrane Science, 281, (1-2), p. 325-333, 2006.
[18]. Kaminska G., Bohdziewicz J., Calvo J. I., Prádanos P., Palacio L., Hernández A., *Fabrication and characterization of polyethersulfone nanocomposite membranes for the removal of endocrine disrupting micropollutants from wastewater. Mechanisms and performance*, Journal of Membrane Science, 493, p. 66-79, 2015.
[19]. Mulder M., *Basic Principles of Membrane Technology*, second ed., Kluwer Academic Publishers, Netherlands, 1998.
[20]. Norman N. Li, Anthony G. Fane, Winston Ho W. S., Matsuura T., *Advanced Membrane Technology and Applications*, Published by John Wiley & Sons Inc., Hoboken, New Jersey, 2008.
[21]. Kandlikar S. G., Steinke M. E., *Contact angles of droplets during spread and recoil after impinging on a heated surface*, Mechanical Engineering Department, Rochester Institute of Technology, New York, USA, vol. 79, part A, 2001.
[22]. Heru Susanto, Mathias Ulbricht, *Characteristics, performance and stability of polyethersulfone ultrafiltration membranes prepared by phase separation method using different macromolecular additives*, Journal of Membrane Science, 327, p. 125-135, 2009.
[23]. Jian Zuo, SinaBonyadi, Tai-Shung Chung, *Exploring the potential of commercial polyethylene membranes for desalination by membrane distillation*, Journal of Membrane Science, 497, p. 239-247, 2016.
[24]. Al Malek S. A., Abu Seman M. N., Johnson D., Hilal N., *Formation and characterization of polyethersulfone membranes using different concentrations of polyvinylpyrrolidone*, Desalination, vol. 288, p. 31-39, 2012.
[25]. Elizabeth Arkhangelsky, Denis Kuzmenko, Vitaly Gitis, *Impact of chemical cleaning on properties and functioning of polyethersulfone membranes*, Journal of Membrane Science, vol. 305, p. 176-184, 2007.
[26]. Toraj Mohammadi, Ehsan Saljoughi, *Effect of production conditions on morphology and permeability of asymmetric cellulose acetate membranes*, Desalination, vol. 243, p. 1-7, 2009.
[27]. See Toh Y. H., Limb F. W., Livingston A. G., *Polymeric membranes for nanofiltration in polar aprotic solvents*, Journal of Membrane Science, vol. 301, p. 3-10, 2007.
[28]. Sofiah H., Nora'aini A., Marinah M. A., *The influence of polymer concentration on performance and morphology of asymmetric ultrafiltration membrane for lysozyme separation*, Journal of Applied Sciences, vol. 10, (24), p. 3325-3330, 2010.
[29]. Jiang-Nan Shen, Hui-Min Ruan, Li-Guang Wu, Cong-Jie Gao, *Preparation and characterization of PES–SiO_2 organic–inorganic composite ultrafiltration membrane for raw water pretreatment*, Chemical Engineering Journal, vol. 168, p. 1272-1278, 2011.
[30]. Jingqian Zhou, Jizhong Ren, Li Lin, Maicun Deng, *Morphology evolution of thickness-gradient membranes prepared by wet phase-inversion process*, Separation and Purification Technology, 63, p. 484-486, 2008.
[31]. Heru Susanto, Mathias Ulbricht, *Characteristics, performance and stability of polyethersulfone ultrafiltration membranes prepared by phase separation method using different macromolecular additives*, Journal of Membrane Science, 327, p. 125-135, 2009.
[32]. Zhuang Zhou, Saeid Rajabzadeh, Abdul Rajjak Shaikh, Yuriko Kakihana, Wenzhong Ma, Hideto Matsuyama, *Effect of surface properties on antifouling performance of poly(vinyl chloride-co-poly(ethylene glycol)methyl ether methacrylate)/PVC blend membrane*, Journal of Membrane Science, vol. 514, p. 537-546, 2016.
[33]. Liu B., Chen C., Zhang W., Crittenden J., Chen Y., *Low-cost antifouling PVC ultrafiltration membrane fabrication with Pluronic F127: Effect of additives on properties and performance*, Desalination, 307, p. 26-33, 2012.
[34]. Ani Idris, Norashikin Mat Zain, Noordin M. Y., *Synthesis, characterization and performance of asymmetric polyethersulfone (PES) ultrafiltration membranes with polyethylene glycol of different molecular weights as additives*, Desalination, vol. 207, p. 324-339, 2007.

THE ANNALS OF "DUNAREA DE JOS" UNIVERSITY OF GALATI
FASCICLE IX. METALLURGY AND MATERIALS SCIENCE
Nº. 2 - 2016, ISSN 1453 – 083X

CORROSION BEHAVIOR OF 1050 AND 3003 ALUMINUM ALLOYS USED IN NAVAL INDUSTRY

Valentin Marian DUMITRAȘCU, Camelia STAICU, Lidia BENEA*
Research (Competences) Centre: Interfaces-Tribocorrosion and Electrochemical Systems (CC-ITES), Faculty of Engineering, "Dunarea de Jos" University of Galati, 47 Domneasca Street, RO-800008, Galati, Romania
e-mail: lidia.benea@ugal.ro

ABSTRACT

The most important requests for new materials used in marine aggressive corrosion environment are the corrosion resistance and the susceptibility to localized and pitting corrosion. The corrosion behavior of 1050 and 3003 aluminum alloys in natural seawater were characterized by electrochemical measurements, including open circuit potential, linear polarization, polarization resistance and cyclic voltammetry. Stability, polarization resistance, corrosion rate and pitting susceptibility were determined. 1050 aluminum alloy shows an increase of polarization resistance and improved corrosion resistance in natural seawater compared to 3003 aluminum alloy. The optical micrographs taken after corrosion assays are in good agreement with the recorded electrochemical measurements.

KEYWORDS: aluminum alloys, corrosion behavior, marine environment, electrochemical measurements

1. Introduction

Material competition in the marine industry has been traditionally intensive. Even if steel is the most common material used for ship and off-shore constructions, new materials are developed in order to decrease the weight, to increase the life time and also to decrease the maintenance costs and exhaust emissions. The increase of corrosion resistance and enhance the environmental protection are the most important requests for new materials used in marine aggressive corrosion environment. Weight reduction associated with increasing corrosion resistance have led to the development of lightweight materials such as aluminum alloys or polymeric materials.

Due to their workability and low density, aluminum and its alloys have been the first-choice material for different industries [1, 2]. Different aluminum alloys are used in marine industry, due to their mechanical properties such as: hardness, elongation, tensile strength or thermal conductivity. Generally, these properties are offered by the alloying elements or impurities entrapped into aluminum matrix.

Usually aluminum alloys of 1xxx and 3xxx series have been widely used for cooling exchange or heat exchange systems due to their high thermal conductivity and corrosion resistance in comparison with traditional material used such as stainless steel or copper alloys [3, 4].

After exposure to an oxygen-containing environment, aluminum and its alloys are immediately covered by a dense thin aluminum oxide film. Unfortunately, the native aluminum oxide film has thickness of a few nanometers and present vacancies, faults and voids [5, 6] or inclusions, second phase particles [7], that cause the susceptibility to corrosion in the presence of chloride ions and therefore restricting their applications [8]. Different forms of corrosion such as localized corrosion (pitting corrosion, intergranular corrosion) or generalized corrosion, exfoliation corrosion even stress corrosion may occur after exposure of aluminum and its alloys in corrosive environments [1].

The mechanism of the corrosion process is not established considering the specific role of alloying elements. The increased number of alloying elements in the materials led to a very complex corrosion behavior [9].

The corrosion initiation is generally believed to begin by the rupture or breakdown of the passive film upon the metallic surface, usually into defects zone or around intermetallic particles which exhibits different surface film characteristics to the aluminum matrix [10, 11].

This study intends to investigate by electrochemical methods and optical microscopy the corrosion resistance of two different aluminum alloys: 1050 aluminum alloys (Al1050) and 3003 aluminum alloy (Al3003) after immersion in natural seawater sampled from Black Sea, Navodari port.

2. Materials and methods

The samples with dimensions of 40 mm x 20 mm x 2 mm were cut from Al1050 and Al3003 sheets. The chemical compositions are presented in Table 1. The samples were mechanically wet-polished with SiC grinding paper (between #1500 and #2000), cleaned with alcohol, etched with NaOH 5M for 30 seconds, rinsed with deionized water, cleaned with alcohol into ultrasonic bath for 5 minutes, rinsed again with deionized water and finally dried with hot air at 60 ºC for 60 minutes. As prepared Al1050 and Al3003 samples were isolated with epoxy resin in order to obtain 1 cm^2 active surface area.

Table 1. *Chemical composition of Al1050 and Al3003*

	Si [%]	Fe [%]	Cu [%]	Mn [%]	Ti [%]	Cr [%]	Zn [%]	Others [%]	Al [%]
Al1050	0.5	0.5	0.05	0.1	0.05	0.01	0.1	0.01	Balance
Al3003	0.6	0.7	0.2	1	-	-	0.1	0.015	Balance

The electrochemical corrosion assays were performed in aerated natural seawater with chemical parameters presented in Table 2, using a Potentiostat/Galvanostat VoltaLab – PGZ301 controlled with VoltaMaster 4 software. For corrosion experiments it was used a standard electrochemical cell with Pt-Rh grid as counter electrode, Saturated Calomel Electrode–SCE (saturated KCl solution, E= +241 mV vs. Normal Hydrogen Electrode-NHE) as reference electrode and the prepared samples (Al1050 and Al3003) as working electrode.

Table 2. *Chemical parameters of natural seawater harvested from Black Sea*

	pH	**Conductivity [mS]**	**Salinity [‰]**
Natural Seawater	7.98	22	13.1

The open circuit potential (OCP) was measured for 60 minute after 90 minutes of immersion into electrolyte. The evolution of polarization resistance and corrosion rate were investigated using linear polarization method around free potential value with a very small overvoltage of ± 40 mV in order to keep the steady state of analyzed surface [12].

The cyclic voltammetry was initiated from negative direction (-1.5 V vs. SCE) to positive direction (+0.5 V vs. SCE) with the sweep rate of 5 mV/s. The scan direction was reversed after the anodic current reached +0.5 mV vs. SCE.

In order to see the influence of chloride ions on surface morphology of the studied samples, optical images were taken before and after corrosion assays using the optical microscope OPTIKA XDS3 MET connected to a computer and controlled with Vision Pro Plus 5.0 software.

3. Results and discussions

3.1. Open circuit potential

The open circuit potential represents the potential difference between the working electrode with respect to the saturated calomel electrode (SCE) and was continuously monitored during 60 min after 90 minutes immersion of aluminum samples into the electrolyte (aerated natural seawater at room temperature).

The variation of OCP for the analyzed samples are illustrated in Fig. 1. For both diagrams, it can be seen that the aluminum alloys try to reach a steady state value of potential, with some fluctuations due to the fact that chloride ions destroy the passive aluminum oxide film and prevents the equilibrium of metallic aluminum alloy – electrolyte interface.

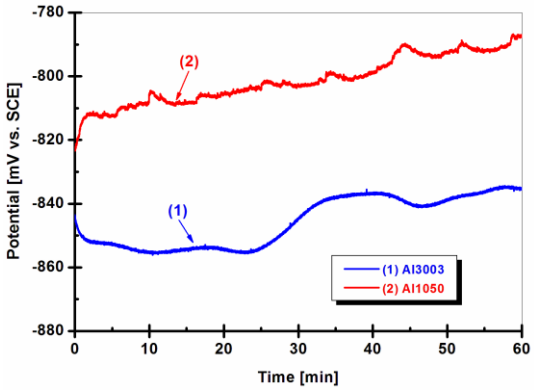

Fig. 1. *Variation of the open circuit potential after 90 minutes immersion into natural seawater: (1) Al3003 and (2) Al1050*

From the diagrams presented in Fig. 1. it can be observed that the potential values of Al1050 changed continuously into anodic direction from -825 mV vs. SCE to -790 mV vs. SCE. That shift can be attributed to the formation of a compact adherent aluminum oxide layer on the Al1050 surface. S. Lameche-Djeghaba and his co-workers [13] observed this behavior for pure aluminum immersed in 3% NaCl electrolyte.

For Al3003, the potential values shift slowly to the cathodic direction from -845 mV vs. SCE to -855 mV vs. SCE, but after 25 minutes of monitoring, the potential values are shifted to the anodic direction, around -835 mV vs. SCE. This behavior can be related with the preferential dissolution of copper presented into Al3003 composition.

3.2. Evolution of polarization resistance (R_p) during immersion time

The linear polarization method was used to determine the polarization resistance of analyzed samples around the free potential with a very small overvoltage of ± 40 mV. In Fig. 2. are illustrated the diagrams for both aluminum alloys recorded after 3 hours of immersion.

The corrosion reactions for simple corrosion systems are strictly controlled by the charge transfer resistance and the corrosion current density (i_{corr}) is related to polarization resistance by the Stern Geary [14] equation (1)

$$i_{corr} = \frac{B}{R_p} \quad (1)$$

where B is a specific constant of material-environment given by equation (2):

$$B = \frac{b_a |b_c|}{2.303(b_a + b_c)} \quad (2)$$

where b_a and b_c are the Tafel slopes for anodic and respectively cathodic reaction.

It can be observed from Fig. 2. that the Al3003 have the lowest value of polarization resistance, which fluctuate around 37 kohm.cm^2, but with an upward trend. For Al1050, the value of polarization resistance fluctuates around 43 kohm.cm^2 with the same upward trend caused by the growth of oxide layer. The increasing of aluminum oxide layer thickness lead to the increasing of polarization resistance and lowering of corrosion current density.

The evolution of corrosion rate in time, corresponding to the polarization resistance from Fig. 2. is calculated as thickness loss and it is illustrated in Fig. 3.

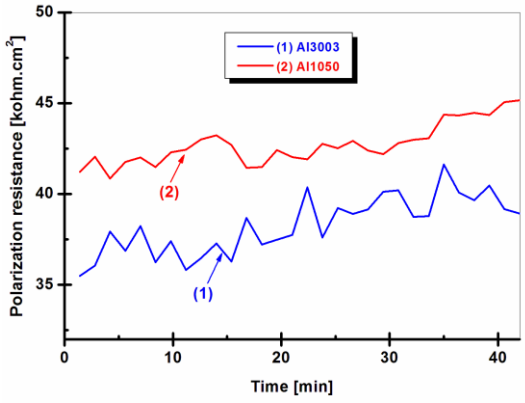

Fig. 2. *The evolution of polarization resistance of (1) Al3003 and (2) Al1050 during immersion in natural seawater*

The increased polarization resistance of Al1050 compared to the polarization resistance of Al3003 means the lowering of the corrosion current density and therefore the decreasing of corrosion rate (the loss of thickness).

These results suggest that the increased purity of Al1050 in comparison with Al3003 lead to an increased polarization resistance due to the increased homogeneity of aluminum oxide layer formed on their surface resulting an improved corrosion resistance.

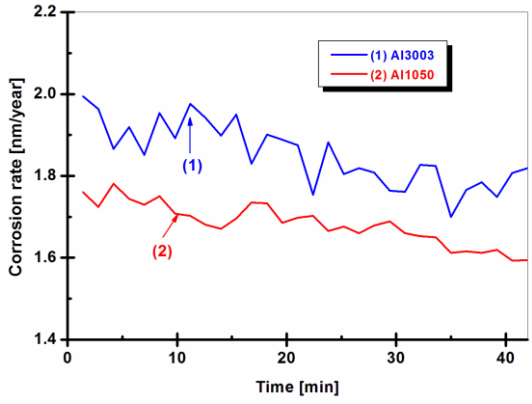

Fig. 3. *The evolution of corrosion current density (corrosion rate) of (1) Al3003 and (2) Al1050 during immersion in natural seawater*

3.3. Cyclic voltammetry

The cyclic voltammetry was initiated from negative direction (-1.5 V vs. SCE) to positive direction (+0.5 V vs. SCE) with the sweep rate of 5 mV/s. The scan direction was reversed after the

anodic current reached + 0.5 mV vs. SCE to form a complete cycle and the recorded diagrams for both aluminum alloys are presented in Fig. 4.

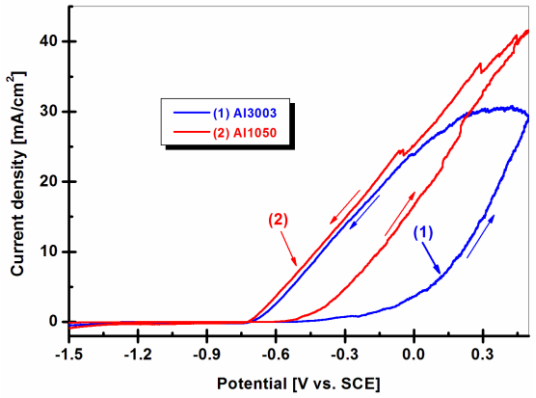

Fig. 4. *The cyclic voltammograms of (1) Al3003 and (2) Al1050 performed at 5mV/sec sweep rate during immersion in natural seawater*

Highlighting the localized corrosion susceptibility in the presence of chloride ions from natural seawater for both aluminum alloys can be seen very well due to the specific hysteresis formed in the anodic transpasivation part of the diagrams. For both materials, in the transpassive region the current density rises up until the potential is reversed and this indicates the breakdown of the passive aluminum oxide layer and a delay in the repassivation of an existing pit when the potential is scanned towards negative direction [15].

Analyzing the area of the hysteresis loop it could be observed that a larger area is present on Al3003 surface, which makes it more difficult to repasivate the pit [15, 16].

Analyzing the voltammograms presented in Fig. 4. it can be seen that the Al3003 presents a larger area of hysteresis loop in comparison with Al1050, confirming the previous behaviors in measuring the polarization resistance or corrosion current density.

3.4. Optical microscopy

The optical micrograph of analyzed Al1050 and Al3003 were taken before and after the corrosion assays. From Fig. 5 (a and b) it can be observed different aspects of aluminum alloy surfaces after the pretreatment process. Al1050 shows a uniform polished surface while Al3003 presents some inclusion or impurities, as it can be observed in Fig. 5 (a) and (b).

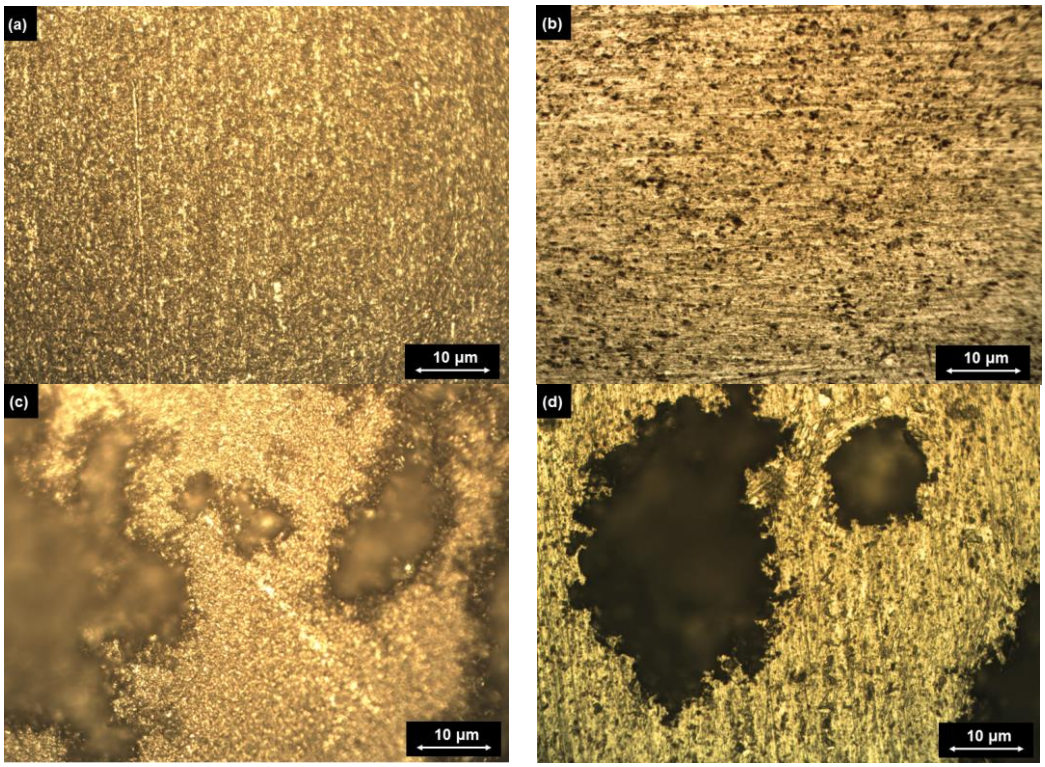

Fig. 5*. Optical micrographs of Al1050 and Al3003: (a) Al1050 polished before corrosion tests; (b) Al3003 polished before corrosion tests; (c) Al1050 after corrosion tests; (d) Al3003 after corrosion tests*

Conclusions

The aim of this paper was to study the corrosion behavior of Al1050 and Al3003 immersed in natural seawater. From the presented results, the following conclusions can be drawn:

- due to the decreased number of alloying elements, the open circuit potential value of Al1050 is nobler in comparison with the open circuit potential value of Al3003 which means a homogenous native aluminum oxide film for Al1050 and a low interaction with the electrolyte;
- equally, the homogeneity of aluminum oxide offers an increased polarization resistance for Al1050 in comparison with Al3003;
- the increased polarization resistance led to a decreased corrosion current density and thus to a lower corrosion rate for Al1050 in comparison with Al3003;
- the cyclic voltammograms reveal the susceptibility to pitting corrosion for both analyzed aluminum alloys, with a higher hysteresis area for Al3003;
- the electrochemical results illustrate the susceptibility of aluminum alloys to localized and pitting corrosion in presence of chloride ions, confirmed by optical micrographs performed after corrosion.

Acknowledgements

UEFISCDI – Ministry of Education and research is acknowledged for the financial support to Competences Centre Interfaces-Tribocorrosion and Electrochemical Systems (CC-ITES) – Dunarea de Jos University of Galati – Research project: HyBioElect, contract 10/30-08-2013 (2013 – 2016) in the frame of National Research Programme Romania – PN II PCE.

References

[1]. Cui Z., Li X., Zhang H., Xiao K., Dong C., Liu Z., Wang L., *Atmospheric corrosion behavior of 2A12 aluminum alloy in a tropical marine environment*, Advances in Materials Science and Engineering, vol. 2015, Article ID 163205, 2015.

[2]. Johansen H. D., Brett C. M. A., Motheo A. J., *Corrosion protection of aluminium alloy by cerium conversion and conducting polymer duplex coatings*, Corrosion Science, 63, p. 342-350, 2012.

[3]. Liu Y., Meng G. Z., Cheng Y. F., *Electronic structure and pitting behavior of 3003 aluminum alloy passivated under various conditions*, Electrochmica Acta, 54, p. 4155-4163, 2009.

[4]. Yazdzad A. R., Shahrabi T., Hosseini M. G., *Inhibition of 3003 aluminum alloy corrosion by propargyl alcohol and tartrate ion and their synergistic effects in 0.5% NaCl solution*, Materials Chemistry and Physics, 109, p. 199-205, 2008.

[5]. Allachi H., Chaouket F., Draoui K., *Protection against corrosion in marine environments of AA6060 aluminium alloy by cerium chlorides*, Journal of Alloys and Compounds, 491, p. 223-229, 2010.

[6]. Rosliza R., Senin H. B., Wan Nik W. B., *Electrochemical properties and corrosion inhibition of AA6061 in tropical seawater*, Colloids and Surfaces A: Physicochemical and Engineering Aspects, 312, p. 185-189, 2008.

[7]. Andreatta F., Terryn H., de Wit J. H. W., *Corrosion behavior of different tempers of AA7075 aluminium alloy*, Electrochimica Acta, 49, p. 2851-2862, 2004.

[8]. Xiangfeng M., Guoying W., Hongliang G., Yundan Y., Ying C., Dettinger H., *Anodization for 2024 Al alloy from sulfuri-citric acid and anticorrosion performance of anodization films*, International Journal of Electrochemical Science, 8, p. 10660-10671, 2013.

[9]. Zahs A., Spiegel M., Grabke H. J., *Influence of alloying elements on the chloride-induced high temperature corrosion of Fe-Cr alloys in oxidizing atmospheres*, Materials and Corrosion, 50, p. 561-578, 1999.

[10]. Birbilis N., Buchheit R. G., *Electrochemical characteristics of intermetallic phases in aluminum alloys*, Journal of the Electrochemical Society, 152, (4), p. B140-B151, 2005.

[11]. Na K.-H., Pyun S.-I., *Comparison of susceptibility to pitting corrosion of AA2024-T4, AA7075-T651 and AA7475-T671 aluminium alloys in neutral chloride solutions using electrochemical noise analysis*, Corrosion Science, 50, p. 248-258, 2008.

[12]. Mardare L., Benea L., Dănăilă E., Dumitrașcu V., *Polymeric coatings used against marine corrosion of naval steel EN32*, Key Engineering Materials, 699, p. 71-79, 2016.

[13]. Lameche-Djeghaba S., Benchettare A., Kellou F., Ji V., *Electrochemical behavior of pure aluminium and Al-5%Zn alloy in 3% NaCl solution*, Arabian Journal for Science and Engineering, 39, p. 113-122, 2014.

[14]. Geary S. M. L., *Electrochemical polarization. I. A theoretical analysis of the shape of polarization curves*, Journal of Electrochemical Society, 104, (1), p. 56-63, 1957.

[15]. Amin M. A., *Pitting of Al and Al-Si alloys in KSCN solutions and effect of light*, Arabian Journal of Chemistry, 6, p. 87-92, 2013.

[16]. Szklarska-Smialowska Z., *Pitting Corrosion of Metals*, NACE, Houston, TX, 1986.

THE ANNALS OF "DUNAREA DE JOS" UNIVERSITY OF GALATI
FASCICLE IX. METALLURGY AND MATERIALS SCIENCE
Nº. 2 - 2016, ISSN 1453 – 083X

COMPARATIVE CORROSION BEHAVIOR OF PURE COPPER AND BRASS IN 3.5% NaCl SOLUTION

Lidia BENEA, Eliza DĂNĂILĂ
Competences Center: Interfaces-Tribocorrosion-Electrochemical Systems (CC-ITES), Faculty of Engineering, Dunarea de Jos University of Galati, 47 Domneasca Street, RO-800008 Galati, Romania
e-mail: lidia.benea@ugal.ro

ABSTRACT

Copper and brass are used in many economic sectors as electrical, construction, transport and others. From common household electrical wiring to boat propellers and from photovoltaic cells to saxophones, copper and its alloys are employed in a variety of end-uses. Copper tubing is now the standard material for potable water and heating systems in most developed countries. This is in part due to its bacteriostatic properties, or in other words due to the ability of copper to inhibit the growth of bacterial and viral organisms in water. Therefore, the corrosion resistance of copper and brass are important in defining the field of use as construction parts. This paper aims at investigating the comparative corrosion behavior of pure copper and brass in 3.5 % NaCl solution. The corrosion behavior of both type samples in 3.5% NaCl solution was investigated by the use of electrochemical methods as open circuit potential and linear polarization resistance measurements. The results show an improved corrosion resistance of pure copper sample in 3.5 wt. % NaCl solution as compared with brass sample.

KEYWORDS: copper, corrosion rate, cyclic voltametry

1. Introduction

Corrosion process is certainly one of the most common causes of failure of engineered components and structures. The corrosion phenomenon leads to deterioration of the material (usually a metal) and its properties, being caused by the reaction of the metal with the environment. The corrosion behavior of the material depends on the environment to which it is subjected, and the corrosive action of an environment depends on the material exposed to that environment [1]. Therefore, it is very important to know the corrosion resistance of a material before being designed for a specific application.

Copper tubes are used for plumbing, heating, air-conditioning and refrigeration systems which can be found in the residential, industrial or commercial installations. For several decades, copper has been used as a plumbing material for potable water distribution systems [2]. Also, copper alloys like brass are widely used in domestic water-distribution systems in valves, heat exchangers, pumps, heating components, plumbing fittings and plumbing fixtures [3]. Localized or pitting corrosion is recognized as one of the major problems, with copper tubing or brass failure in tap water being a major and ongoing problem in many countries [2].

The aim of the present work is to systematically study the comparative corrosion behavior on pure copper and brass. Different electrochemical techniques were explored and complemented by surface optical microscopy.

2. Materials and methods

An VoltaLab PGZ 100 potentiostat / galvanostat controlled by VoltaMaster software was used for electrochemical measurements. A conventional three-electrode setup was used for electrochemical studies, in which a Pt-Rh grid served as the auxiliary electrode and an Ag/AgCl with KCl saturated solution (E = 200 mV vs. standard hydrogen electrode – SHE) as the reference electrode. The copper electrode and brass respectively served as the working electrode. The chemical composition of tested samples was 99.97 % for pure copper and the following Cu-57.8%, Zn-39.02%, Pb-2.99%, Fe-0.19% for brass. Prior to the corrosion tests, the surfaces of the samples exposed to the solution were mechanically polished to a mirror finish by using SiC

grinding paper (320-2000 µm), degreased with acetone and dried with hot air. The exposure surface area of the working electrode was 6.25 cm^2. As the corrosive electrolyte was selected 3.5 % NaCl aqueous solution and electrochemical measurements were conducted at room temperature. The pH of this solution was 6.43. The volume for each experiment was 135 mL of 3.5 % NaCl aqueous solution.

3. Results and discussion

3.1. Open Circuit Potential (OCP)

The open circuit potential measurements give the information about thermodynamic stability of the sample surface to electrochemical oxidation in a particular corrosive environment [4]. This potential may vary with time due to change in the oxidation tendency of the surface (oxidation, formation of the passive layer or immunity) [4-5]. Figure 1 shows the variation of the open-circuit potential (E_{OC}) with time, for copper and brass electrodes immersed in 3.5 % NaCl aqueous solution, over a period of 60 minutes. The E_{OC} of the pure Cu electrode stabilizes at a more positive value as compared with that of brass electrode reaching a mean value of -189 mV versus Ag/AgCl. On the other hand, the E_{corr} of the brass electrode reached a more negative steady state value, revealing an average value of -205 mV versus Ag/AgCl.

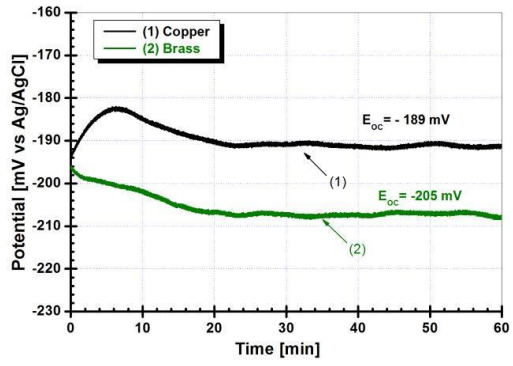

Fig. 1. *Open circuit potential (E_{OC}) for: (1) pure copper and (2) brass electrodes over a period of 60 minutes, immersed in 3.5 % NaCl aqueous solution*

The both type of studied samples reach the steady states after approximatively 22 minutes from immersion and did not exhibit potential drops associated with surface activation during 60 minutes exposure in the 3.5 % NaCl solution. This kind of behavior strongly suggests that the native oxide films from the both studied surfaces are thermodynamically resistant to chemical dissolution in 3.5 % NaCl solution.

Since the difference between the steady states revealed by both electrodes (pure copper and brass) is not so big, of only 16 mV, it could be assumed that the processes which occur, on the brass surface are mainly governed by copper. Similar observations have been made earlier for Cu–16%Zn–6.5%Al alloy as compared with pure copper and pure zinc immersed in borate buffer solution [6]. In other words, it can be said that Zn element has a little influence in defining the potential of the brass/solution interface.

3.2. Linear polarization resistance (LPR)

Linear polarization resistance (LPR) is a rapid response testing technique commonly used in material corrosion studies which allow the calculation of the corrosion rate. For this method, the tested material was polarized with a small overvoltage in the range of ±40 mV, relative to its Open Circuit Potential (OCP) and the resulting ("linear") current response was measured. The measured resistance is inversely related to the corrosion rate. The linear polarization resistance measurements were carried out at a scan rate of 5 mV/sec.

The polarization resistance values of the both tested surfaces studied in 3.5 % NaCl solution are shown in Fig. 2.

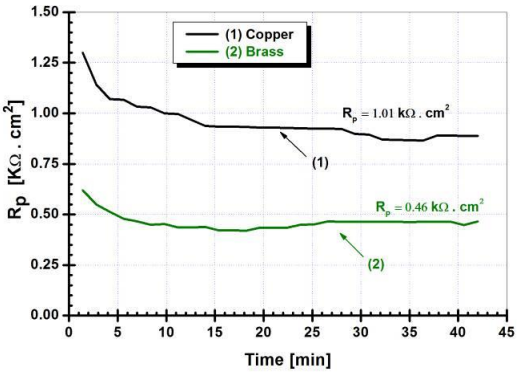

Fig. 2. *The evolution of R_p values during immersion time of: (1) pure copper and (2) brass electrodes*

From Fig. 2 it can be seen that the lowest polarization resistance (R_p) value is attained by the brass electrode being equal to 0.46 kohm cm^2, while the pure copper electrode reveals a mean value of polarization resistance equal to 1 kohm cm^2. An increased value of polarization resistance for pure copper electrode means lower corrosion current density and therefore a lower corrosion rate, as

compared with brass electrode as it can be seen in Fig. 3.

Corrosion rate can be defined as the amount of corrosion loss per year in thickness. From Fig. 3 it can be seen that the lowest corrosion rate value is attained by the pure copper electrode being equal to 0.082 mm/year, while the brass electrode reveals a mean value of corrosion rate equal to 0.164 mm/year. According with the data presented in Fig. 3 it can be clearly seen that the corrosion rate of brass shows a double value as compared with pure cooper electrode. The higher corrosion rate corresponding to brass as compared with copper can be attributed to the presence of zinc as an alloying element, which leads to the incorporation of ZnO (as the main oxidation product on Zn metal) in the passive layer. Similar results were reported earlier by Kosec *et al.* [7] who studied the electrochemical behaviors of copper, Cu-10Zn and Cu-40Zn alloys and zinc in inhibited and uninhibited 0.5 M NaCl solution and by Valcarce and collaborators [8] who investigated the susceptibility to pitting corrosion of copper and 70/30 brass in artificial tap water with or without Pseudomonas fluorescens.

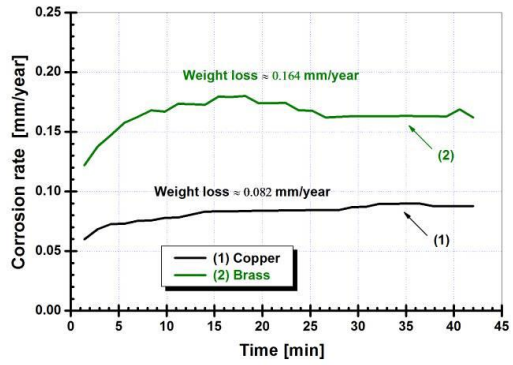

Fig. 3. *Variation of corrosion rate vs. exposure time for: (1) pure copper and (2) brass electrodes*

Corrosion resistance is certainly an important consideration in constructive parts as automotive screw machine components. Despite exposure to corrosive conditions, the constructive parts must continue to function, threads and fittings must continue to fit properly, and an image of quality should be maintained. Affected by corrosion, many constructive parts can conduct to system failure.

3.3. Cyclic voltammetry diagrams (CV)

The cyclic voltammetry was initiated from negative direction (-1.0 V vs. Ag/AgCl) to positive direction (+0.3 V vs. Ag/AgCl) with the sweep rate of 5 mV/s. The scan direction was reversed after the anodic current reached + 0.3 mV vs. Ag/AgCl to form a complete cycle and the recorded diagrams for both copper and brass are presented in Fig. 4.

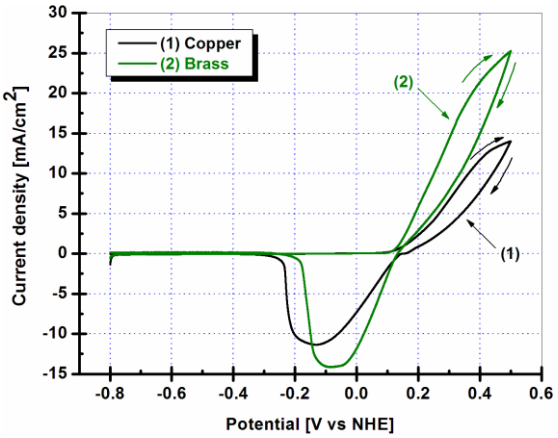

Fig. 4. *Cyclic voltammograms of (1) copper and (2) brass performed at 5mV/sec sweep rate during immersion in 3.5 % NaCl aqueous solution expressed versus Normal Hydrogen Electrode (NHE)*

As it is shown in Fig. 4 the shape of both voltammograms are similar, but the anodic current for brass is higher as compared with anodic current for copper.

The reversed diagrams from positive to negative potentials is drawn under the direct diagram from negative to positive direction for copper as well for brass confirming the repassivation of both surfaces. The reactions taking place at specific potentials for copper and copper corrosion compounds (products) are presented in Fig. 5.

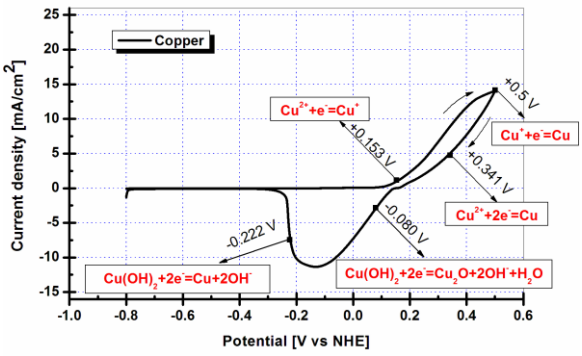

Fig. 5. *Specific corrosion reactions of copper on cyclic voltammograms of copper at different potentials expressed versus Normal Hydrogen Electrode (NHE)*

The shape of cyclic voltammograms for brass is similar with those of copper explained by the fact that the corrosion process of brass is dominated by copper corrosion reactions.

For zinc corrosion in brass on cyclic voltammograms we did not identify the specific reactions of zinc in the measured potentials range, confirming that the entire corrosion process of brass in sodium chloride solution is dominated by copper reactions.

3.4. Optical Microscopy

The optical micrographs of copper and brass surfaces performed before and after the corrosion tests are shown in Figures 6 and 7.

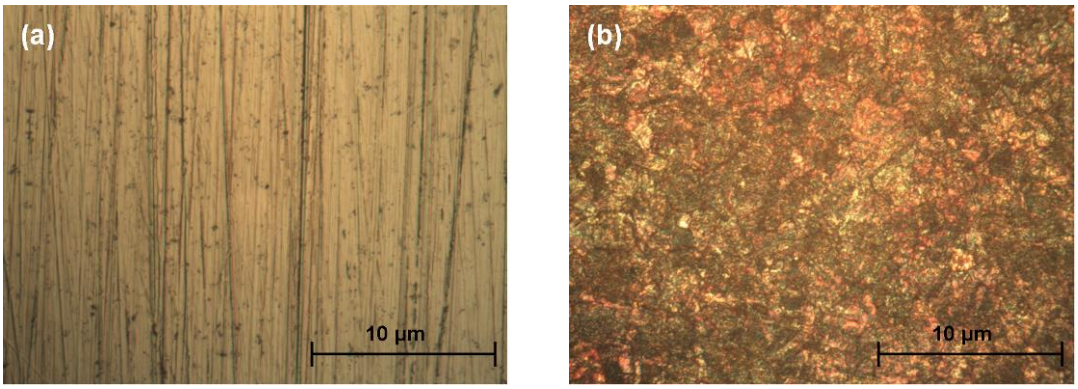

Fig. 6. *Optical microscopy images of pure copper (a) before and (b) after corrosion experiments*

In Fig 6 (a) it is shown copper surface before corrosion with some polished tracks. After corrosion, the surface of copper is uniformly covered with a thin layer of copper corrosion products (oxides with different colors.

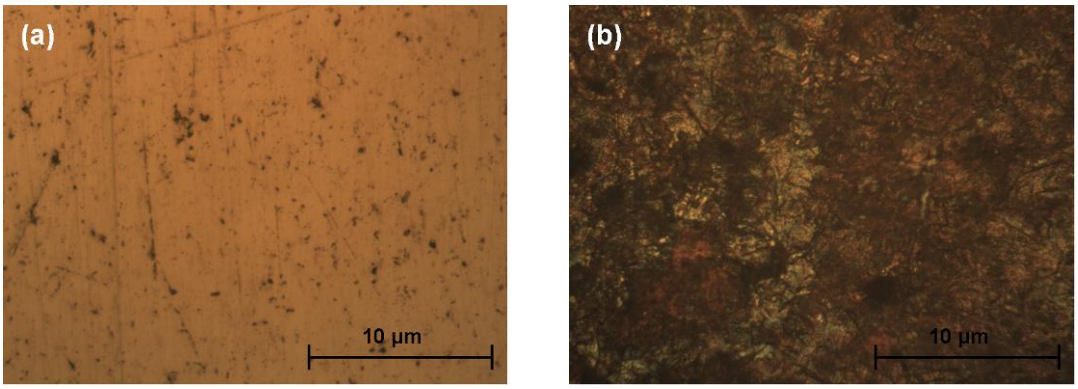

Fig. 7. *Optical microscopy images of brass (a) before and (b) after corrosion experiments*

The surface of brass from Fig 7 (a) before corrosion tests presents some polishing tracks but also some inclusions. After corrosion tests, Fig. 7(b) the surface of brass shows mainly a corrosion film product very similar to copper. The corrosion products of zinc are easily soluble, and being white, it is difficult to distinguish from other colored oxides of copper.

4. Conclusions

Corrosion of materials is a very important issue to consider when choosing a material that must operate in a specific environment.

After evaluating the results of laboratory research work on the two types of materials, the following have been drawn.

The free potentials values of pure copper are nobler than that for their alloy with zinc (brass), according to evolution of potential at immersion in 3.5% NaCl solution.

By assessing polarization resistance through 30 linear polarization measurements and dimensional mass loss (mm / year) it was observed the same trend of best corrosion resistance of copper compared with brass.

From cyclic voltammograms and specific corrosion reactions identified at specific potentials, it

was shown that even on brass surface the corrosion process is dominated by copper reactions.

The optical microscope micrographs before and after corrosion tests confirm the above-mentioned conclusions.

References

[1]. Davis J. R., *Corrosion: Understanding the basics*, ASM International, p. 1-17., 2000

[2]. Burstein G. T., Bia H., Kawaley G., *The Persistence of Inhibition of Copper Corrosion in Tap Water*, Electrochimica Acta, 191, p. 247-255, 2016.

[3]. Yohai L., Vázquez M., Valcarce M. B., *Brass corrosion in tap water distribution systems inhibited by phosphate ions*, Corrosion Science, 53, p. 1130-1136, 2011.

[4]. Santana Jiménez Y., Tejera Gil M., Torrado Guerra M., Baltes L. S., Mirza Rosca J. C., *Interpretation of open circuit potential of two titanium alloys for a long-time immersion in physiological fluid*, Bulletin of the Transilvania University of Brasov, vol. 2, (51), p. 197-204, 2009.

[5]. Choudhary S., Garg A., Mondal K., *Relation between open circuit potential and polarization resistance with rust and corrosion monitoring of mild steel*, Journal of Materials Engineering and Performance vol. 25(7), p. 2969-2976, 2016.

[6]. Blanco M., Barragan J. T. C., Barelli N., Noce R. D., Fugivara C. S., Fernández J., Benedetti A. V., *On the electrochemical behavior of Cu–16%Zn–6.5%Al alloy containing the β-phase (martensite) in borate buffer*, Electrochimica Acta, 107, p. 238-247, 2013.

[7]. Tadeja Kosec, Ingrid Milošev, Boris Pihlar, *Benzotriazole as an inhibitor of brass corrosion in chloride solution*, Applied Surface Science, 253, p. 8863-8873, 2007.

[8]. Valcarce M. B., de Sánchez S. R., Vázquez M., *Localized attack of copper and brass in tap water: the effect of Pseudomonas*, Corrosion Science, 47, p. 795-809, 2005.

THE ANNALS OF "DUNAREA DE JOS" UNIVERSITY OF GALATI
FASCICLE IX. METALLURGY AND MATERIALS SCIENCE
Nº. 2 - 2016, ISSN 1453 – 083X

ELECTROCHEMICAL CORROSION OF STAINLESS STEELS IN COMMERCIALLY AVAILABLE SOFT DRINKS

Laurențiu MARDARE, Lidia BENEA*
Competences Center: Interfaces-Tribocorrosion-Electrochemical Systems, Faculty of Engineering, "Dunarea de Jos" University of Galati, Domnească Street, 47, RO-800008, Galați Romania
*e-mail: Lidia.Benea@ugal.ro

ABSTRACT

In recent years, there has been a developing trend towards the use of advanced materials in the dental replacement industry. Corrosion mechanisms of 316L Stainless Steel in electrolyte containing common household soft drinks have been studied through investigating the corrosion performance by using electrochemical methods to measure the in-situ corrosion current during the immersion in four commercially available soft drinks. The objective of this research work was to evaluate the effect of electrochemical behavior on the corrosion performance of the material. 316L Stainless Steel was selected because it is commonly used as a dental replacement material. This is an important area of work as the use of steel retainers as well as other stainless steel dental replacements are still widespread and the effectiveness of these devices will be determined by their corrosion resistance performances.

KEYWORDS: stainless steel, soft drinks, electrochemical corrosion

1. Introduction

One of the goals of the implantology research is to design devices that induce controlled, guided, and rapid integration into surrounding tissues. Austenitic stainless steels as 316 L are the materials chosen for many load bearing surgical implants because they combine mechanical strength, excellent corrosion resistance and good biocompatibility [1]. AISI 316 L stainless steel has been successfully applied in medicine due to its biocompatibility and relatively low cost [2, 4]. Different surface engineering techniques can be performed to increase the corrosion resistance of the base metal, in particular when exposed to electrolytes simulating a body and oral fluid, which leads to diverse applications as biomaterial [1]. There is always concern about the corrosion resistance of the 316 L stainless steel in physiological fluids. For this reason, the development of the biomedical implants requires the improvement of their corrosion resistance [3].

There are different procedures established for the surface treatment of biomaterials, some of which depend on the particular application, like orthopedic surgery. The biofunctional behavior of these implant materials are generally governed by volume properties but the interaction with the biologic medium is determined by the characteristics of the surface films [4]. 316L Stainless steel has been employed to fabricate joint screws, prostheses, brackets for a long time due to its excellent mechanical and biomedical properties. However, it has some bioactivity and biocompatibility issues [5]. The corrosion resistance and mechanical properties of stainless steels make them a suitable material for use in medical applications, including dental purposes and orthopedic treatments. The main quality of stainless steel is its resistance to corrosion, which can vary depending on the grade of stainless steel used, where the formation of a passive chromium oxide film (passivation) can protect the material [6].

Most orthodontic appliances are made of a stainless-steel alloy, containing approximately 6% to 12% nickel and 15% to 22% chromium, and, because they are continuously exposed to saliva, the metals must exhibit corrosion resistance. All metals and alloys are subject to corrosion. The alloy ability to be biocompatible appears to be related to its pattern and mode of corrosion [7].

Increased consumption of soft drinks in the population led to the emergence of a new enemy for metallic materials used in orthodontic implants. The fluoride present in commercially available soft drinks

is a factor that leads to corrosion of biomedical materials used in dentistry [8].

Fluoride ion concentrations present in soft drinks range from 0.02 to 2.80 parts per million, in part because of variations in fluoride concentrations of water used in production [9].

In dentistry, orthodontics is the branch in which the problem of biocompatibility is most felt, since patients are young and, therefore, more susceptible to develop inflammatory reactions; also, alloys might have toxic effects. It is important to evaluate the biocompatibility and the corrosion resistance of materials used in orthodontic mini-implants and temporary anchorage devices, because their materials are directly inserted to the periodontal tissues and alveolar bones. Metallic ions released from orthodontic mini-implants and temporary anchorage devices might cause a reaction (inflammation or necrosis) in adjacent tissues, such as the oral mucosa and gingival, or alveolar bone [10].

A reason to conduct research in biomedical steel corrosion is given by the fact that some metallic biomaterials such as nitinol alloy releases toxic ions during corrosion causing allergic reactions, local anaphylaxis, and inflammation [11].

For the purpose of hygienic health of the oral cavity, especially for the prevention of tooth decay, fluorides are widely introduced into the oral environment by means of toothpastes, mouth rinses, orthodontic gels and other therapeutic dental products. Additionally, systemic fluorides may be ingested orally through tea, soft drinks, and fluoridated bottled water. Therefore, orthodontic wires, mini implants, and anchorage device, are readily exposed to fluoride medium. [12], an environment that favors the appearance of degradation processes, in particular corrosion of biomedical material. Numerous aggressive anions have been reported for various alloys. Out of these aggressive anions, halides are the most important group which provoke localized corrosion for a lot of metals and alloys such as stainless steel [13].

The principal aim of this research work attempts to evaluate the behaviour and effect of corrosion resistance properties of stainless steel SS 316 L in some commercially available soft drinks solutions and to make a comparison between the specific corrosive characteristics. In this experimental research work it is investigated comparatively the corrosion resistance of 316L stainless steel. All samples have been subjected to corrosion in commercially available soft drinks. The corrosion properties were studied using electrochemical methods such as: open circuit potential (OCP), polarization resistance (Rp) and potentiodynamic polarization (PD).

2. Experimental set-up

The corrosion experiments were performed on stainless steel 316 L. For corrosion measurements, all the samples were cut to the dimensions of 25 x 25 x 2 mm.

Samples used in the experimental protocol have been bonded with copper wire and insulated with epoxy resin to obtain a well determined active measurable surface area. The stainless steel (SS) 316 L samples were degreased with alcohol and acetone.

The chemical composition of SS 316 L can be found in the Table 1.

Table 1. *Chemical composition of 316 L stainless steel, in %*

Grade		C	Mn	Si	P	S	Cr	Mo	Ni	N
SS316L	Min	-	-	-	-	-	16.0	2.00	10.0	-
	Max	0.03	2.0	0.75	0.045	0.03	18.0	3.00	14.0	0.10

In order to perform the corrosion experiments it was used a standard three-electrode cell consisting of the tested samples as working electrode, a Pt-Rh grid used as auxiliary electrode and saturated calomel electrode (SCE) (saturated KCl solution, E = -244 mV vs. normal hydrogen electrode (NHE)) as reference electrode.

Table 2. *Characteristic of soft drinks*

Type of soft drink	pH	Conductivity [mS]	Salinity [ppt]	TDS [mg/L]	E [mV]
Energizing soft drink	3.63	1.82	0.9	0.11	89
Orange Juice	2.87	0.84	0.4	446	110
Cola Soft drink	2.85	1.16	0.6	0.61	108
Orange soda	2.87	0.738	0.4	394	109

As the electrolytes were used four commercially available soft drinks. In Table 2 are shown the characteristics of soft drinks.

The experiments were done using a Potentiostat / Galvanostat PGZ 100 and the data were recorded with VoltaMaster 4 software and edited with graphical software.

3. Results and discussion

3.1. Open circuit potential (OCP)

The potential-time measurements of the stainless steel 316 L surface studied in four different commercially available soft drinks are shown in Fig. 1. The evolution of OCP was monitored for 1 hour of immersion for each sample.

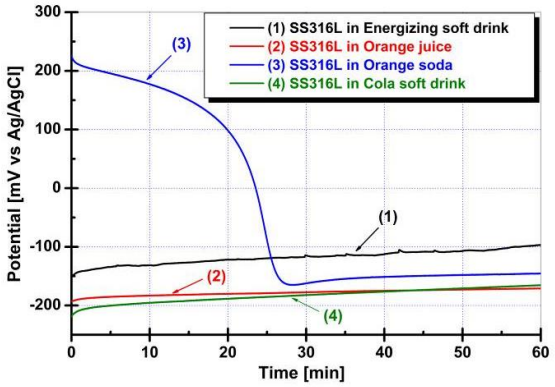

Fig. 1. *Variation of open circuit potential with time: (1) SS 316L immersed in energizing soft drink solution, (2) SS 316L immersed in orange juice solution, (3) SS 316L immersed in orange soda solution and (4) SS 316L immersed in cola soft drink solution*

For the samples immersed in energizing soft drink solution, the OCP increases slightly and reaches a steady-state around -115 mV vs. Ag/AgCl. The increasing trend of potential reveals the increase of protective layer and improvement of corrosion resistance. The same growth trend can be seen in the case of SS 316 L immersed in orange juice and cola soft drink. The potential of SS 316 immersed in orange juice is stabilized at a value around -197 mV vs. Ag/AgCl, and in the case of SS 316 L immersed in cola soft drink the potential value is stabilized around -175 mV vs. Ag/AgCl. This is associated with an improved behavior of corrosion resistance.

The OCP of SS 316 L immersed in orange soda decreases gradually from the noble value of +226 mV vs. Ag/AgCl to a more active value of -145 mV vs. Ag/AgCl during about 30 minutes of the immersion time. After 30 minutes the free potential value is stabilized in this solution at a mean value of -145 mV vs. Ag/AgCl.

3.2. Evolution of polarization resistance during immersion time

Linear polarization resistance (R_p) is the only corrosion monitoring method that allows corrosion rates to be measured directly, in real time.

The evolution of polarization resistance was performed by linear polarization method around free potential value with a very small overvoltage value of (± 40 mV) in order to keep the steady state of the surface.

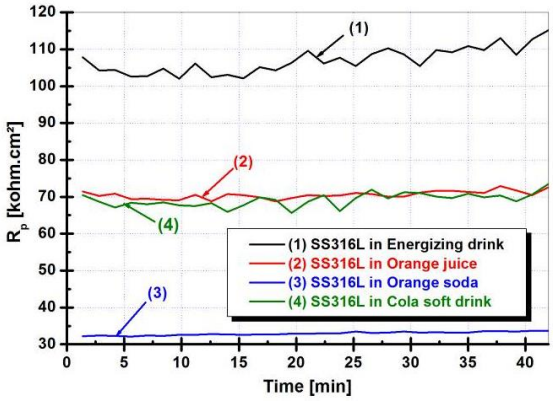

Fig. 2. *The evolution of R_p values during immersion time of: (1) SS 316L immersed in energizing soft drink solution, (2) SS 316L immersed in orange juice solution, (3) SS 316L immersed in orange soda solution and (4) SS 316L immersed in cola soft drink solution*

The polarization resistance values of the 316L stainless steel surfaces studied in four different commercially soft drinks are presented in Fig. 2. In Fig. 2 it can be seen that the higher polarization resistance value is attained by the SS 316 L immersed in energizing soft drink solution, being equal to 115 kohm·cm^2, this value increasing slowly during the immersion time.

In Fig. 2. it can be seen that the lowest polarization resistance (R_p) value is attained by the SS 316 L immersed in orange soda being equal to 33 kohm·cm^2. In the case of stainless steel SS 316 L immersed in orange juice, R_p reaches a mean value of 72 kohm·cm^2 and for stainless steel 316 L immersed in cola soft drink the free potential mean value is similar to 72 kohm·cm^2.

According to the data presented in Fig. 3 it can be seen that the higher corrosion rate corresponds to SS 316 L immersed in orange soda. From the

corrosion rate evolution shown in Fig. 3 it can be also seen a good stability of SS 316L immersed in energizing soft drink having a very low value of corrosion rate.

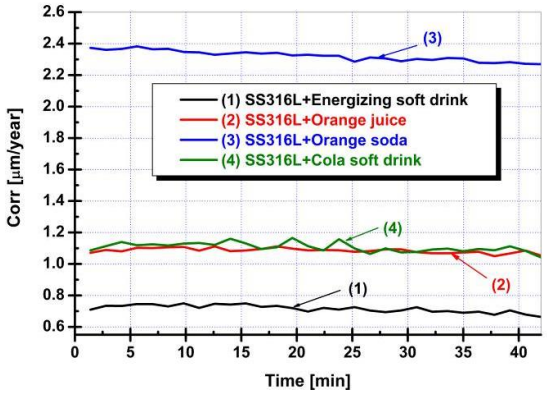

Fig. 3. *Evolution of corrosion rate during immersion period for: (1) SS 316L immersed in energizing soft drink solution, (2) SS 316L immersed in orange juice solution, (3) SS 316L immersed in orange soda solution and (4) SS 316L immersed in cola soft drink solution*

An increased value of polarization resistance means a lower corrosion current density and therefore a lower corrosion rate, as it can be seen in Figs. 2 and 3.

In the case of SS 316 L immersed in orange juice and cola soft drink solutions the corrosion rate values obtained are almost equal for both drinks.

3.3. Potentiodynamic polarization

The diagrams I = f(E) (current density-potential curves) were recorded in a range of potentials starting from -1500 mV vs. Ag/AgCl to +1500 mV vs. Ag/AgCl at a scan rate of 5 mV/s. Potentiodynamic polarization diagrams were performed to assess the polarization domains of stainless steel 316 L, immersed in four commercially soft drinks. The passive state is usually studied with respect to corrosion protection. If the passive state covers a higher potential domain and the passivation current value is smaller, then the metal or alloy shows a high corrosion resistance in this environment.

In Fig. 4 are presented the potentiodynamic polarization diagrams of these four surfaces which were studied in four commercially available soft drinks. It can be observed a higher current density values for 316 L Stainless Steel in cathodic domains for all solutions and a large passive domain only for three solutions. The higher current in the anodic domain for 316 SS immersed in orange soda suggests a general dissolution with a high corrosion rate. The passive current densities of SS 316 L immersed in energizing soft drinks, orange juice and cola are very low, being close to zero, revealing a better corrosion resistance compared with SS 316 L immersed in orange soda. In the zoom of Fig. 4, which is presented in Fig. 5, it can easily be observed the differences revealed for SS 316 L immersed in the four commercially available soft drinks. Practically, the stainless steel immersed in orange soda drink solution did not present a passive domain, having a continuous dissolution behaving as if the passive film was dissolved by this solution.

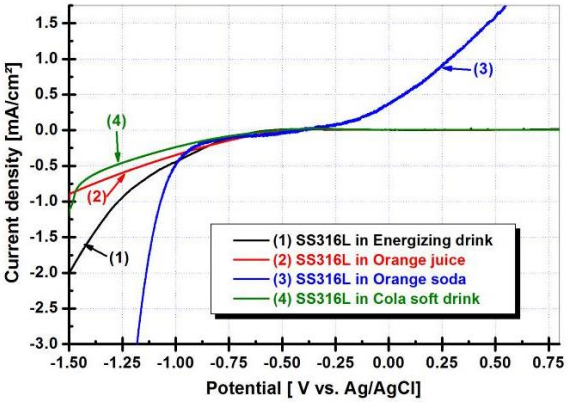

Fig. 4*. Potentiodynamic polarization curves of: (1) SS 316L immersed in energizing soft drink solution, (2) SS 316L immersed in orange juice solution, (3) SS 316L immersed in orange soda solution and (4) SS 316L immersed in cola soft drink solution*

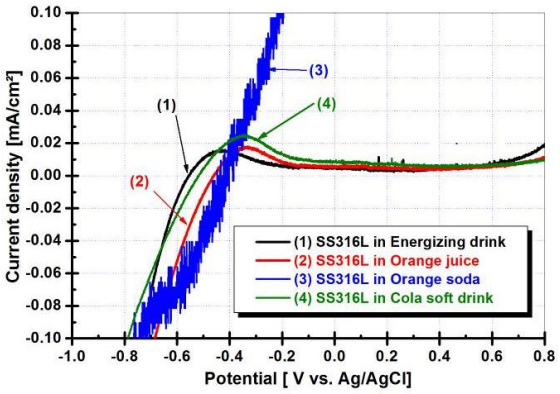

Fig. 5. *Zoom at lower passivation current density of potentiodynamic polarization curves of: (1) SS 316L immersed in energizing soft drink solution, (2) SS 316L immersed in orange juice solution, (3) SS 316L immersed in orange soda solution and (4) SS 316L immersed in cola soft drink solution*

In Fig. 4 in the monitored potential interval, there were identified three different potential domains for SS 316 L immersed in orange soda drink solution: cathodic domain, passive domain and transpassive domain. In the cathodic domain, the passive film is destroyed by the hydrogen reduction reaction, while in passive domain the passive film is formed by the oxidation process. In transpassive domain the passive film is damaged and the dissolution occurs through passive film.

For the stainless steel immersed in orange juice, energizing, and cola drinks solutions, in the monitored potential interval it can be identified only a cathodic and the passive domain which is comprised in very large potential range. Also, these three types of solution show very low passive current densities values compared with SS 316 L immersed in orange soda drink, fact which reveals a good corrosion performances SS 316 L immersed in energizing soft drinks, orange juice and cola, as it is shown in Fig. 5. The lowest passive current density values are almost equal for stainless steel immersed in the three commercially available solutions of orange juice, cola and energizing drink.

4. Conclusions

The corrosion behavior of SS 316 L immersed in four commercially available soft drinks solutions - energizing soft drink, orange juice, orange soda and cola soft drink - was investigated in this work. The following conclusions can be drawn.

- The evolution of open circuit potentials during immersion time in the four commercially available drink solutions show the nobler value for stainless steel immersed in energizing drink. The orange soda affects the surface of stainless steel by dissolving the natural oxide passive film and making the free potential to shift down to more active values. The other two drinks like orange juice and cola have about the same corrosive effect on 316 stainless steel, which shows about the same free potential values at immersion in these solutions.

- The SS 316 L immersed in energizing soft drink solution presents the highest polarization resistance in comparison with other solutions, suggesting an increased corrosion resistance.

- The higher corrosion rate corresponds to SS 316 L stainless steel immersed in orange soda juice compared with other three types of soft drinks solution.

- The passive states cover a higher potential domain and the passivation current values are smaller for 316 L stainless steel immersed in energizing soft drink, orange juice and cola soft drink than those values of SS 316 L immersed in orange soda drink, proving once again a high corrosion resistance, and good behavior of SS 316 L immersed only in three drinks.

- By using stainless steel 316 L in dental implantology as it is recommended by its good behavior in corrosion environments of soft drinks, much attention must be paid to consuming orange soda.

- The long lifetime of the stainless steels in dental replacements have to be under recommendations concerning some forbidden commercially available drinks.

Acknowledgements

UEFISCDI - Ministry of Education and Research is acknowledged for the financial support to Competences Centre Interfaces - Tribocorrosion and Electrochemical Systems (CC-ITES) - Dunarea de Jos University of Galati - Research Project: *HyBioElect*, contract 10 /30-08-2013 (2013 - 2016) in the frame of National Research Programme Romania - PN II PCE.

References

[1]. Barriuso S., Chao J., Jimenez J. A., Garcıa S., Gonzalez-Carrasco J. L., *Fatigue behavior of Ti6Al4V and 316 LVM blasted with ceramic particles of interest for medical devices*, Journal of the mechanical behavior of biomedical materials, 30, p. 30-40, 2014.

[2]. Mejía-Caballero I., Palomar-Pardavé M., Martínez Trinidad J., Romero-Romo M., Pérez Pasten-Borja R., Lartundo-Rojas L., López-García C., Campos-Silva I., *Corrosion behavior of AISI 316 L borided and non-borided steels immersed in a simulated body fluid solution*, Surface & Coatings Technology, 280, p. 384-395, 2015.

[3]. Djahida Sidane, Didier Chicot, Sabeha Yala, Salima Ziani, Hafit Khireddine, Alain Iost, Xavier Decoopman, *Study of the mechanical behavior and corrosion resistance of hydroxyapatite sol–gel thin coatings on 316 L stainless steel pre-coated with titania film*, Thin Solid Films, 593, p. 71-80, 2015.

[4]. Peredaa M. D., Kanga K. W., Bonettoc R., Llorente C., Bilmes P., Gervasi C., *Impact of surface treatment on the corrosion resistance of ASTM F138-F139 stainless steel for biomedical applications*, Procedia Materials Science, 1, p. 446-453, 2012.

[5]. Muhammad Akmal, Muhammad Asif Hussain, Haris Ikram, Tahir Sattar, Sarah Jameel, Ju Young Kim, Fazal Ahmad Khalid, Jung Won Kim, *In-vitro electrochemical and bioactivity evaluation of SS316L reinforced hydroxyapatite functionally graded materials fabricated for biomedical implants*, Ceramics International, 42, p. 3855-3863, 2016.

[6]. Holmes D., Sharifi S., Stack M. M., *Tribo-corrosion of steel in artificial saliva*, Tribology International, 75, p. 80-86, 2014.

[7]. Luciane Macedo de Menezes and Cátia Cardoso Abdo Quintão, *The Release of Ions from Metallic Orthodontic Appliances*, Seminars in Orthodontics, vol. 16, no. 4, p. 282-292, 2010.

[8]. Carolina Simonetti Lodi, Irene Ramires, Juliano Pelim Pessan, Lucimara Teixeira das Neves, Marília Afonso Rabelo Buzalaf, *Fluoride concentrations in industrialized beverages consumed by children in the city of Bauru, Brazil*, J Appl Oral Sci., 15, (3), p. 209-212, 2007.

[9]. Mary C. Kiritsy, Steven M. Levy, John J. Warren, Nupur Guha-Chowdhury, Judy R. Heilman, Teresa Marshall,

Assessing fluoride concentrations of juices and juice-flavored drinks, J Am Dent Assoc, 127, p. 895-902, 1996.

[10]. Siddik Malkoc¸ Firat Ozturk, Bayram Corekci¸ Buket S. Bozkurt, and Sema S. Hakki, *Real-time cell analysis of the cytotoxicity of orthodontic mini-implants on human gingival fibroblasts and mouse osteoblasts*, American Journal of Orthodontics and Dentofacial Orthopedics, vol. 141, issue 4, p. 419-426, 2012.

[11]. Xia Li, Xiangmei Liu, Shuilin Wu, Yeung K. W. K., Yufeng Zheng, Paul K. Chu, *Design of magnesium alloys with controllable degradation for biomedical implants: From bulk to surface*, Acta Biomaterialia, vol. 45, p. 2-30, 2016.

[12]. Xiaoji Li, Jianqiu Wang, En-hou Han, Wei Ke, *Influence of fluoride and chloride on corrosion behavior of NiTi orthodontic wires*, Acta Biomaterialia, 3, p. 807-815, 2007.

[13]. Pahlavan S., Moazen S., Taji I., Saffar K., Hamrah M., Moayed M. H., Mollazadeh Beidokhti S., *Pitting corrosion of martensitic stainless steel in halide bearing solutions*, Corrosion Science, 112, p. 233-240, 2016.

THE ANNALS OF "DUNAREA DE JOS" UNIVERSITY OF GALATI
FASCICLE IX. METALLURGY AND MATERIALS SCIENCE
Nº. 2 - 2016, ISSN 1453 – 083X

INFLUENCE OF THE UNCONVENTIONAL TREATMENT APPLIED TO A STEEL ON THE CORROSION EVOLUTION

Carmen-Penelopi PAPADATU
Faculty of Engineering, "Dunarea de Jos" University of Galati, 47 Domneasca street, 800008, Galati, Romania
e-mail: papadatu.carmen@yahoo.com

ABSTRACT

The study of an alloyed steel with Cr Mo with an important content of aluminum (0.9…1.2%), unconventionally treated in magnetic field, is attractive because of the durability which increases along with the improvement of the corrosion resistance. Through the thermo-magnetic treatments applied before thermo-chemical treatment, the mechanical properties of this material have been improved. The hardness of the superficial layers has been increased after thermo-magnetic and thermo-chemical treatment because of the superficial layers' characteristics obtained after the unconventional treatment. The behavior of steel in corrosion tests was used as criterion.

This paper is a review of personal research and presents the changes of corrosion resistance, using non-conventional treatments and corrosion tests for a Cr Mo alloyed steel, after thermo-magnetic treatment, respectively thermo-chemical treatment. The evolution of the superficial layer for non-conventionally treated steel during the corrosion tests was studied.

KEYWORDS: steel, superficial layer depth, unconventional treatment, corrosion

1. Introduction

The magnetic field can modify the residual stresses which were obtained by hardening/tempering treatment and the resistance of the corrosion process in marine medium or in fog. The resistance of corrosion depends on the treatments and the content of the carbon from the structure of the steel. The cooling within the magnetic field during the thermo-magnetic treatment regimes modifies the characteristics of steel, compared with the classic treatment results. During the improvement treatment of steel through thermo-magnetic treatment, the residual stresses realized by hardening decreases, the residual austenite quantity decreases too and the magnetic field has a positive effect on the mechanical and corrosion properties because the hardness of the steel and the corrosion resistance increase [1, 2].

If Aluminum and Chromium contents increase in the structure of steel, the residual austenite quantity decreases more rapidly. The martensitic quantity and the hardness of steels increase significantly, more than in the case of the steels with approx. the same content of Carbon but with a lower quantity of aluminum. As a consequence, the magnetic field intensity, the content of the Carbon and the content of the aluminum from steel have an important influence. Because of these aspects, the tendency of breaking decreases and the probability of the fragile breakage no longer exists.

An important quantity of aluminums in the structure of steel increases the thermo-magnetic treatment power and the results are the best. At the same time, the existence of aluminum content in the structure of steel causes some hardening problems which are countered by the Chromium existence [3].

2. Materials and experiment

The materials used for this study was a steel grade for the construction of machine parts which have the following principal components: 0.38 % C, 1.18 % Al, 1.38 % Cr, 0.17 % Mo, 0.5 % Mn, 0.058 % Cu, 0.25 % Si, 0.26 % Ni, 0.026 % P, 0.026 % S.

For the experimental program, samples (rollers) from steel were considered. The outer diameter of the rollers is of 40 mm and the inner diameter of the rollers is of 16 mm.

The first stage from the complex program of treatments consists in thermo-magnetic treatment.

The treatment t1 represents a Martensitic hardening process at 920 °C and high tempering at 620 °C, a classic treatment of improvement (Magnetic field intensity doesn't exist). The other treatment, t3, represents a hardening process (just cooling in water in strong alternative current (A.C.) of magnetic field and a high tempering process (just the cooling in water in strong A.C. magnetic field). The treatment t4 represents a hardening process with cooling in water, in direct current (D.C.) of magnetic field and high tempering process (just cooling in water, in D.C. magnetic field).

The second stage from the complex program of the treatments consists in applying the thermo-chemical treatment: a plasma (ion) nitriding at 530 °C, after thermo-magnetic treatment. The treatments were noted such as: Tca' = T3 = t3 + plasma nitriding; Tcc' = T4 = t4 + plasma nitriding, T1'= Tclassic, applied to the different samples from the same steel grade considered.

The corrosion tests were done to detect the evolution of the superficial layer using a fog chamber, testing time [1]. Experimental tests were done in a fog chamber using the following components: 27 g/L NaCl, 6 g/L $MgCl_2$, 1 g/L $CaCl_2$, 1 g/L KCl.

It was established the influence of the corrosion conditions on the superficial layers, determining the mass loss (Δm_1) after 100 hours, the mass loss (Δm_2) after 200 hours and (Δm_3) after 300 hours of corrosion process, for each treatment regime.

3. Results and discussion

In Figure 1 was presented the evolution of the micro-hardness values in the ion nitrided layer versus the treatments; the micro-hardness values were measured at 0.02 mm distance from the surface of the samples [1].

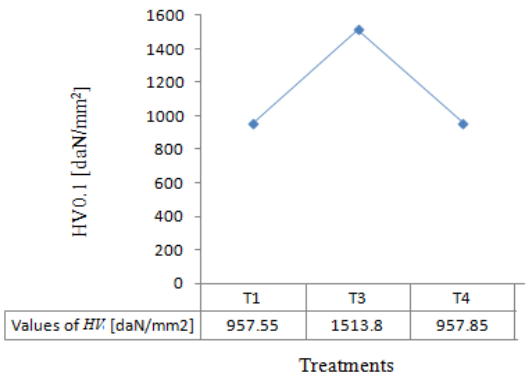

Fig. 1. *Micro-hardness values at 0.02 mm distance from the surface of the ion nitrided layer versus the treatments*

In Figure 2 were presented the depths of the superficial layers evolution versus the treatment applied to steel with 1.18% Al.

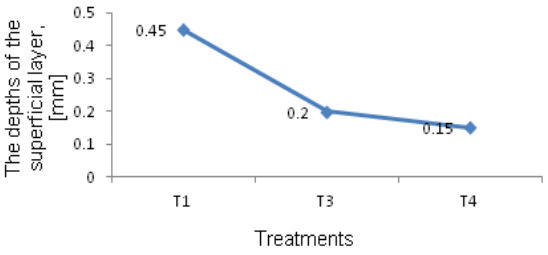

Fig. 2. *The depth of the superficial nitrided layer versus the treatment*

The results of the corrosion process were presented in Figures 3, 4 and 5 [1].

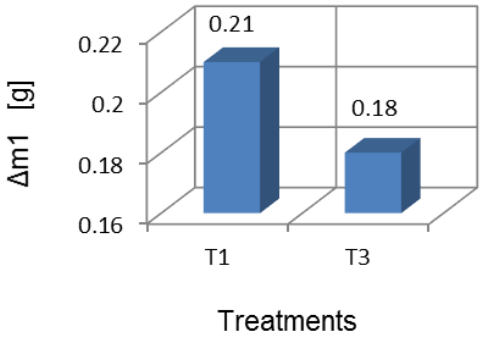

Fig. 3. *The evolution of the Mass loss (Δm_1) after 100 hours of corrosion process vs. treatments*

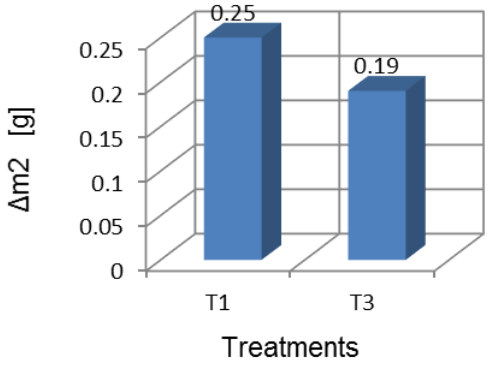

Fig. 4. *The evolution of the Mass loss (Δm_2) after 200 hours of corrosion process vs. treatments*

In Figure 6 was presented the evolution of the Mass loss value in the case of T1 treatment applied to steel versus duration of the corrosion process.

In Figure 7 was presented the evolution of the Mass loss value in the case of T3 unconventional

treatment applied to steel versus duration of the corrosion process.

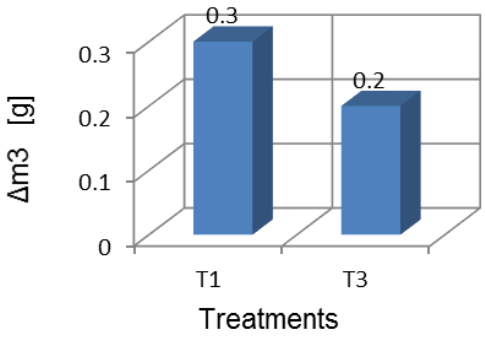

Fig. 5. *The evolution of the Mass loss (Δm_3) after 300 hours of corrosion process vs. treatments*

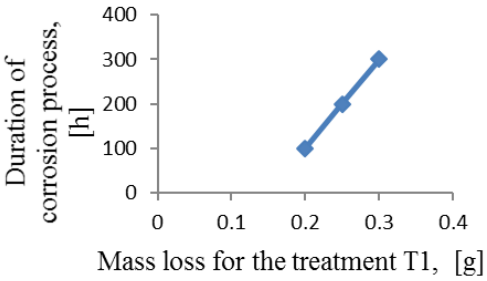

Fig. 6. *Mass loss evolution for T1, after each hour of corrosion process*

Considering Figures 6 and 7, the mass loss had higher values in the case of classic treatment (T1) than in the case of the unconventional treatment (T3). For this reason, the unconventional treatment improved the resistance of the corrosion for the steel with 1.18% Al.

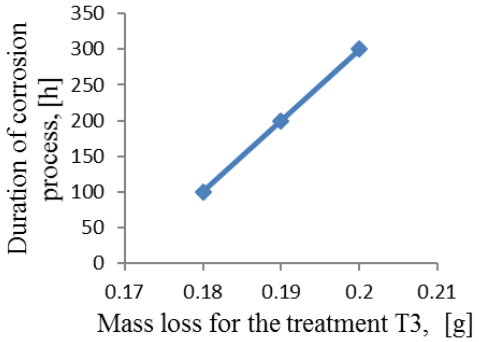

Fig. 7. *Mass loss evolution for T3, after each hour of corrosion process*

Considering Figures 6 and 7, the mass loss had higher values in the case of the classic treatment (T1) than in the case of the unconventional treatment (T3). For this reason, the unconventional treatment improved the resistance of the corrosion for the steel with 1.18% Al.

The properties of the nitrided superficial layer depend on the nature of nitrides phases. With the increasing of the temperature of the nitriding, the nitriding duration is reduced, but decreases the hardness of the superficial layer because of the coalescence of the nitrides of alloying elements.

Inside, in the superficial layer thermo-chemically treated with plasma nitriding, there are the following important phases: $Fe_{\alpha}(M)$, Fe_3N and Fe_4N. The phase Fe_2N (ξ)- has a rhombic structure (the deformed structure of the phase ε) and small values of the hardness. This phase did not appear in the structure of the steel considered.

The explanation is that phase Fe_2N (ξ) is stabile in equilibrium with ammonia until to maximum 450 ˚C [2-4]. The nitriding treatments have been carried out at 530 ˚C, a temperature higher than 450 ˚C. This phase was decomposed and disappeared from the superficial layer. The micro-hardness and the wear resistance of the steel increase because of this situation.

The distributions of the phases in the depth of the nitrided superficial layers is uneven. That is why the nitriding process is not uniform [1-3, 5]. The quantity of the $Fe_{\alpha}(M)$ phase (martensite phase) and nitrides of chromium increase in the T3 treatment case. As a consequence of this phenomenon, both the wear resistance and the corrosion resistance increase.

4. Conclusions

The evolution of the superficial layer for the unconventionally treated steel during the corrosion tests was studied. If applied to a magnetic field (an unconventional treatment), the micro-hardness of the superficial layer for the material with higher contents of aluminum and chromium has higher values.

Aluminum and chromium contents influence the characteristics of the superficial layers. The nitrides of these elements concentrate in the form of small particles at the grain size limits (boundary) of residual austenite and prevents their growth during heating at heat treatment. The corrosion resistance increases in the cases of the thermo-magnetic treatments applied.

References

[1]. Papadatu C. P., *Researches on improving the properties and reliability of some steel grades used for manufacturing metallurgical equipment*, PhD. Thesis, "Dunarea de Jos" University of Galati, 2006.
[2]. Sun Z. H. I., Guo M., *et al.*, *Strong magnetic field processing of metallic materials: A review*, Current Opinion in Solid State and Materials Science 16, p. 254-267, 2012.
[3]. Umoren S. A., Ly Y., Wang F. H., *Influence of aluminium microstructure on corrosion and Corrosion inhibitor performance*

in acidic medium, Journal of Materials and Environmental Science, vol. 1, no. 3, 2010.
[4]. Stefanescu I., *Contribuţii la studiul influenţei tratamentelor termomagnetice asupra unor caracteristici mecanice ale oţelurilor de rulmenţi RUL1*, Suceava, 1981.
[5]. Papadatu C. P., *Posibilități de îmbunătățire a calității unor oțeluri utilizate în industria metalurgiă*, Editura Fundației Universitare "Dunărea de Jos", Galați, 2007.

THE ANNALS OF "DUNAREA DE JOS" UNIVERSITY OF GALATI
FASCICLE IX. METALLURGY AND MATERIALS SCIENCE
Nº. 2 - 2016, ISSN 1453 – 083X

INDUSTRIAL RESEARCH IN THICKER HEAVY PLATES (70-80 MM) HSLA STEEL MICRO-ALLOYED WITH Mo-Nb-Ti THERMO-MECHANICAL CONTROL PROCESS IN ARCELORMITTAL GALATI

Costel DURDUC, Liviu GURAU, Elena DRUGESCU, Viorica MUSAT
"Dunarea de Jos" University of Galati, 47 Domneasca Street, RO-800008, Galati, Romania
e-mail: costel.durducroibu@arcelormittal.com, liviu.gurau@arcelormittal.com, elena.drugescu@ugal.ro, viorica.musat@ugal.ro

ABSTRACT

Thermomechanical rolling (TMR or TMCP) is a special rolling process resulting in an extremely high-strength, fine-grained substructure which simultaneously offers very good toughness and cold formability. TM products have much lower carbon content and consequently are much less susceptible to cold cracks during welding. In ArcelorMittal Galati the challenge was to increase for structural steel the feasibility from 50 up to 80 mm and targeted plate thickness without ACC mode. Slabs thickness produced in AMG with maximum 250 mm thickness corresponding to almost the maximum ratio of 3:1 between slabs and targeted plate thickness according to the EN 10025/4/2004. TM rolled steels performed in industrial trial presented in this paper were performed in Heavy Plate Mill no 2 in ArcelorMittal Galați using computer process SIROLL assisted by AGC system. The main goal of this experimental rolling is to provide a concise and complete overview of the rolling process with higher amount of deformation below T_{nr} (non-recrystallisation temperature) and close to A_{r3} in austenite region, and to address the potential to optimize it.

KEYWORDS: thermomechanical steel, thicker heavy plates, 70 mm, 80 mm, T_{nr}

Nomenclature:

B: flat background
c: sound velocity
α: scattering angle
T: fitting parameter for a constant radial temperature gradient

1. Introduction

In a world in continuous competition it is a challenge to perform higher strength steel like HSLA [1, 9, 10] (higher strength low alloyed). Usual thicker heavy plates over 30 mm thickness are produced by the most important players on the market steel in TMR [2] mode (thermo-mechanical control process) followed by ACC mode (accelerated control cooling). In ArcelorMittal Galati we managed to produce thicker plates up to 50 mm without ACC [3] mode for structural steel. Now, the challenge was to increase the feasibility up to 80 mm corresponding to almost the maximum ratio 3:1 between slab produced in AMG and end targeted plate thickness, from 250 to 80 mm. The trials were performed in ArcelorMittal Galati in industrial conditions - Heavy Plate Mill [4] (equipped with two quarto reversing mills stand). Rolling simulation with new chemical compositions based on low alloying on Mo [5], Nb [6], Ti [7] and rolling schedule was done using SIROLL Level 2 Automation system. We checked if the process parameters targeted, namely TBT (transfer bar thickness), SRT (start rolling temperature) and FRT (final rolling temperature) below the non-recrystallization temperature T_{nr} close to critical point A_{r3} can be reached without the overall stand technical limit: force, torque, speed. The value of T_{nr} and A_{r3} is raised by the addition of micro-alloying elements: Nb and Ti. For these trials were used two slabs with 250 thicknesses and two plates were rolled, with 70 and 80 mm targeted thickness in TMR mode. The parameters monitored, that is TBT, SRT, FRT, pre-calculated in simulation, were reached in industrial rolling conditions with a delta admitted for each parameter: TBT = ± 3 mm; SRT and FRT = ± 10 °C. Total amount of deformation ≈ 58% below T_{nr} was

distributed in 6 rolling passes. The speed of WR (work rolls) was constant at 2 m/s, leading to uniformity of grain size in rolling direction, despite the high targeted thickness. Plates were cooled in pile for dehydrogenation purpose. All the tests were performed in the authorized lab of AMG in order to characterize the mechanical properties [5] of material:

- Spectral analysis: to compare heat analysis on ladle with end product;
- Mechanical tests:
  - Tensile test: UTS [MPa]; Ys [MPa]; Elongation E [%];
  - Charpy-V notch test – toughness – KV values [J];
- Metallographic analysis, SEM and Optical: microstructure, substructure, segregations and inclusions.

2. Experimental setup

SIROLL rolling simulation was done and screenshot of HMI was captured in Figure 1.

SIROLL software – level 2 automation of rolling process in current use has a simulation module. the process parameters were checked: force, torque and speed supposed to be in stand limits. The metallurgical parameters checked were: SRT_Q1; TBT; SRT_Q2; FRT_Q2 supposed to be in the established theoretical domain with max ± 5% of deviation. A screenshot image with rolling simulations for a plate targeted with 55 mm in TMR is shown in Fig. 1:

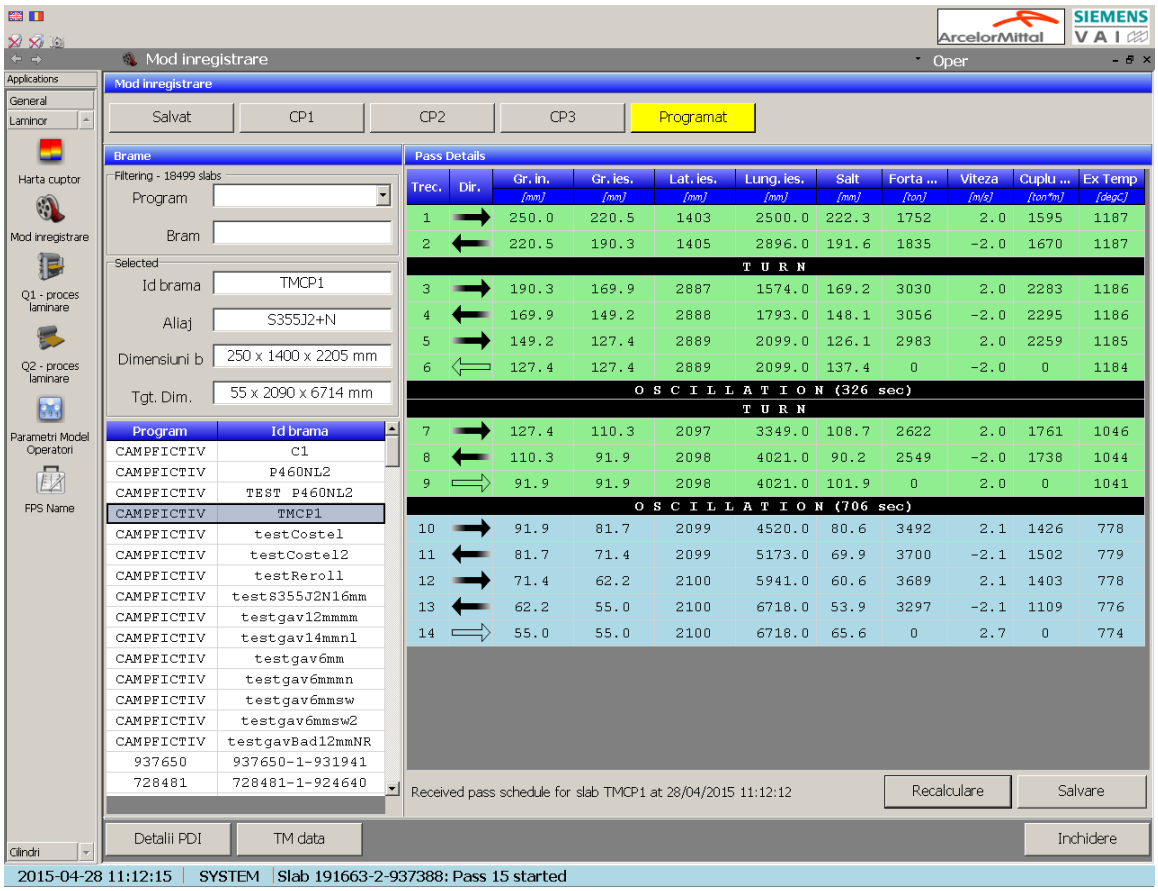

Fig. 1. *Rolling simulation on 55 mm plate targeted - SIROLL*

2.1. Matrix chemical composition

2 slabs with M1 - chemical composition in target and realized elements (Table 1) were allocated to this industrial trial.

The improved property combination of strength and toughness was made possible by maximizing grain refinement thus substituting for the strengthening effect of carbon. In addition, modern steel making processes allow the mass production of low sulfur steels [8]. Figure 1 indicates, which improvements in ductility are achieved, especially in transverse and through thickness direction (5), by lowering the sulfur content.

Table 1. *Chemical composition in mass percentage %*

M1									
C min	C max	Mn min	Mn max	Si min	Si max	Si target	S realized	P min	P realized
0.085	0.100	1.250	1.400	0.250	0.400	0.330	0.004	0.000	0.012
N max	N target	∑ **(Ni+Cu+Cr)**	Mo min	Mo max	∑ **min (Nb+Ti+V)**	∑ **max (Nb+Ti+V)**	Ca min	Ca max	H2 realized
0.007	0.006	0.50	0.055	0.065	0.050	0.078	0.0005	0.0015	0.00026

Table 2. *Data identifications for slabs used in trial*

Traceability				**Slab dimensions [mm]**			**Mother plate target [mm]**			
Program	**Daughter slab**	**Heat no.**	**Bauman class**	**Length**	**Width**	**Thickness**	**Length**	**Width**	**Thickness**	**Qty.**
171121	1	935090	1	2620	1500	250	6000	2000	70	7.70
171122	1	935090	1	2995	1500	250	6000	2000	80	8.80

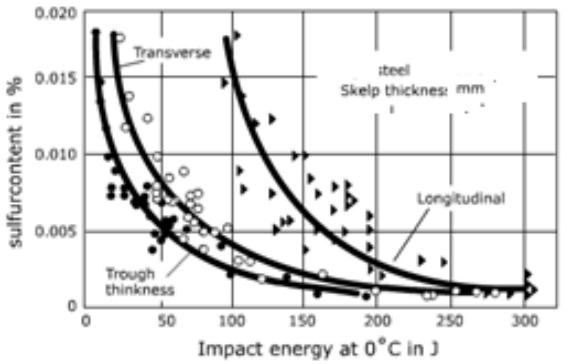

Fig. 2. *Sulphur content*

In order to obtain the required properties in thermomechanical rolling of heavy plate, a high deformation in the temperature range of non-recrystallization of austenite is to be introduced. The finish rolling temperature reaches in the metastable austenite the critical point A_{r3}.

The mechanical properties required are presented in Tables 3-5 according to the European standard for structural steel with delivery conditions in thermo-mechanical rolling state EN 10025/4 of 2009.

Afterwards, rolling process sampling was taken in order to check mechanical characteristics.

Table 3.

EN10025/4 requirements: Yield strength; Tensile strength, Elongation and carbon equivalent						
Thickness	**Steel grade**	**YS min [MPa]**	**TS min [MPA]**	**TS max [MPa]**	**E %**	**CEV [%]**
<40 mm <=63 mm	S355M	335	450	610	22	0.40
	S355ML	335	450	610	22	0.40
<63 mm <=80 mm	S355M	325	450	610	22	0.45
	S355ML	325	450	610	22	0.45

Table 4.

Minimum values of impact energy for impact tests on longitudinal V-notch tests pieces for thermomechanical rolled steel in Joules [J] at test temperature in Celsius degrees [°C]								
Thickness	Steel grade	+20	0	-10	-20	-30	-40	-50
60-80mm	S355M	55	47	43	40	-	-	-
	S355ML	63	55	51	47	40	31	27

Table 5.

Z Test units for flat products - extract from EN10164-2004				
Quality class	Test units for S>0.005%		Test units for S<=0.005% Cast *d*	*d* Products with the same heat treatment. *e* Unless otherwise agreed at the time of the order.
	Parent plate		max 40 t	
Z15	if agreed	xe	x	
Z25	x	-	xe	
Z35	x	-	xe	

3. Thermomechanical rolling process

Our purpose is to avoid the accelerate cooling, that means the rolling schedule will target the frt close to Ar_3. Rolling process will be divided in two phases. One phase will be in roughing area with equalizing and broadsiding sequence up to transfer bar thickness between two stands – roughing mill and finishing mill. After oscillation time to achieve SRT in finishing mill, finishing sequence will be rolled. FRT will reach the limit of Ar_3 in austenitic zone.

Trial summary:

4 slabs used; Total qty = 37 t; Thickness targeted: 60; 70 and 80 mm.

Results:

70 mm - 1 slab - 1 pass in full auto mode;

80 mm - 1 slab - 1 pass in full auto mode;

TMR = Thermomechanical rolling process;

TBT = transfer bar thickness;

SRT = start rolling temperature;

FRT = final rolling temperature.

For both plates rolled with thickness 70 and 80 mm tension tests were performed in transverse direction

Table 6. *Process parameters data*

Rolling process parameters								
Type of Rolling process	**Preset L2 AGC [°C]**	**SRT Q1 [°C]**	**Preset L2 AGC TBT [mm]**	**TBT exit thick [mm]**	**SRT preset L2 AGC [°C]**	**SRT Q2 [°C]**	**FRT preset L2 Q2 [°C]**	**FRT Q2**
Auto	1148	1147	133	130	856	853	783	778
Auto	1153	1150	133	131.2	853	839	781	776

4. Trial lab results

For toughness properties Charpy V-notch test was performed. Tests were performed at top and bottom of surface plate, the toughness guarantee being at -20ºC. For S355ML with toughness guarantee at -40ºC, the minimum limit is 325 MPa and it was accomplished.

Z trough-thickness coefficient is very good for such thicker plate of 7-80 mm, with an average value higher than Z35 condition at 38% (see Fig. 4).

Very good values for TS in middle of the targeted range, and for YS it is in sustainable average with 40 MPa, higher than the required minimum limit of 335 MPa for S355M - meaning toughness guarantee at -20 ºC. For S355ML with toughness guarantee at -40 ºC the minimum limit is 325 MPa and this was accomplished.

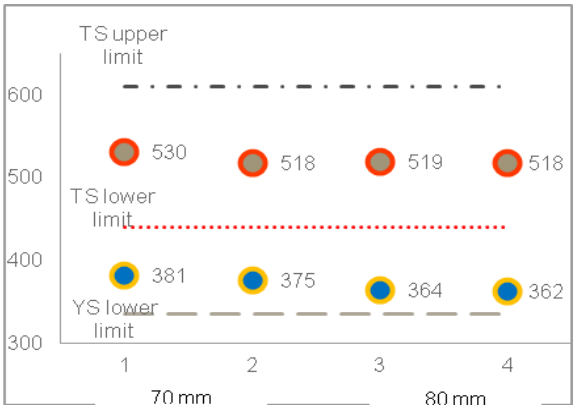

Fig. 3. *Mechanical properties TS and YS*

Z trough-thickness coefficient is very good for such thicker plate of 7-80 mm with an average value higher than Z35 condition at 38% (see Fig. 4).

Table 7. *Mechanical properties: TS and YS in [MPa] and elongation in percentage %*

Lab sample no.	Program	mother plate	heat no.	Thickness [mm]	Steel grade fit	Steel grade fit	Standard fit	TS min S355 M	TS min S355 ML	TS lab	TS max S355 M	TS max S355 ML	YS min S355 M	YS min S355 ML	YS lab MPa	E %
3317 top	171121	1	935090	70	S355M	S355ML	EN10025/4	450	440	530	610	600	335	325	381	34
3317 bottom	171121	1	935090	70	S355M	S355ML	EN10025/4	450	440	518	610	600	335	325	375	35
3316 top	171122	1	935090	80	S355M	S355ML	EN10025/4	450	440	519	610	600	335	325	364	32
3316 bottom	171122	1	935090	80	S355M	S355ML	EN10025/4	450	440	518	610	600	335	325	362	32

Table 8. *Trough-thickness Z coefficient*

Lab sample no.	Thickness [mm]	Z min [%]	Z [%]
3317	70	35	39.3
		35	38.2
		35	39.1
3316	80	35	36.9
		35	38.2
		35	38.3

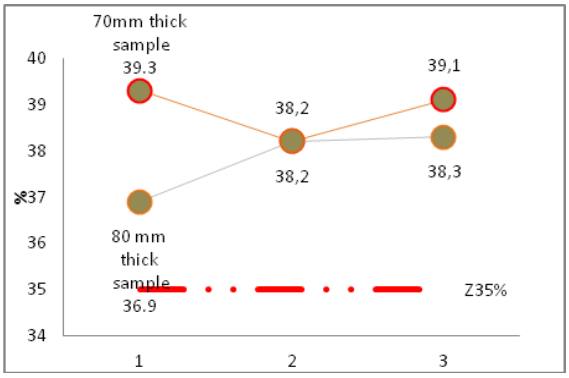

Fig. 4. *Z coefficient*

Table 9. *Charpy V-notch test at -20 ºC in longitudinal direction*

Lab sample no.	Thickness [mm]	V-notch test directions	Test Temperature [°C]	KV1	KV2	KV3	KV average	KV min S355M	KV min S355ML
3317/F1 1/4	**70**	longitudinal	-20	238	240	229	235.7	40	47
3317/F1 1/2 middle	**70**	longitudinal	-20	110	98	107	105.0	40	47
3317/F2 2 mm at bottom	**70**	longitudinal	-20	192	202	184	192.7	40	47
3316/F1 1/4	80	longitudinal	-20	210	224	218	217.3	40	47
3316/F2 1/2 middle	80	longitudinal	-20	58	59	42	53.0	40	47
3316/F2 2 mm at bottom	80	longitudinal	-20	220	219	208	215.7	40	47

Charpy V-notch tests were performed at two temperatures in order to check both steel grade S355M and S355ML do to the fact that the differences are given by the test temperatures: -20 ºC, and -40 ºC. *(see Table 9 and 10)*.

Figure 5 shows very good value for toughness also in middle thickness, in average higher than 100 J.

In Figure 6 we can observe good toughness values for 80 mm thickness on surface, meeting the standard requirement - in the middle of lower limit.

Very good toughness values [Joules] can be noticed in Fig. 7 on surface as standard requirements demand, but lower than minimum limit in average 20 Joules at -40 ºC test temperature.

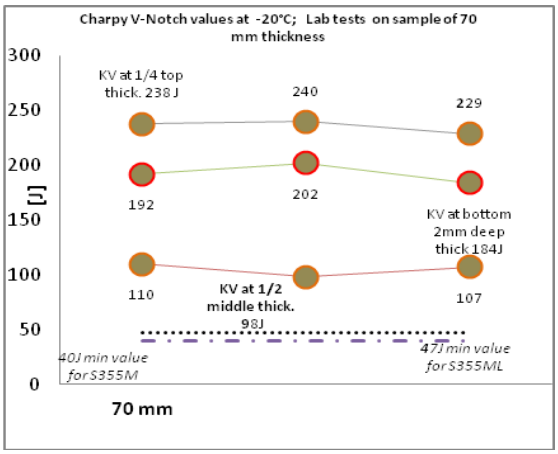

Fig. 5.

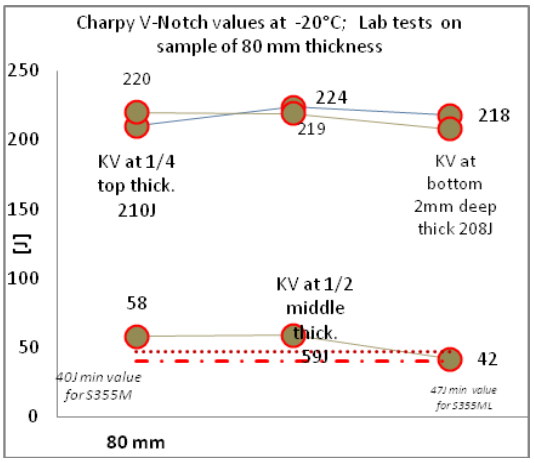

Fig. 6.

Table 10.

Lab sample no.	Thickness [mm]	V-notch test directions	Test Temperature [°C]	KV1	KV2	KV3	KV average	KV min S355ML
3317/F1 1/4	**70**	longitudinal	-40	120	116	101	112.3	31
3317/F1 1/2 middle	**70**	longitudinal	-40	68	19	20	35.7	31
3317/F2 2mm at bottom	**70**	longitudinal	-40	162	184	168	171.3	31
3316/F1 1/4	80	longitudinal	-40	170	168	28	122.0	31
3316/F2 1/2 middle	80	longitudinal	-40	8	9	8	8.3	31
3316/F2 2mm at bottom	80	longitudinal	-40	162	158	30	116.7	31

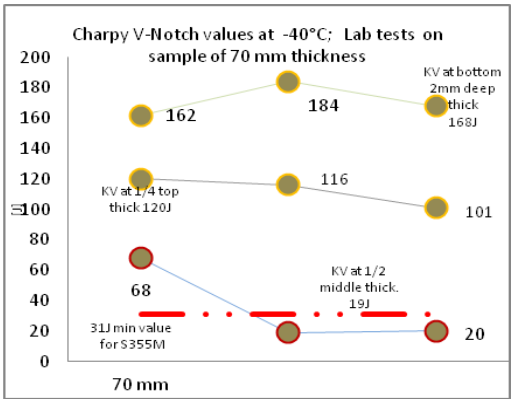

Fig. 7.

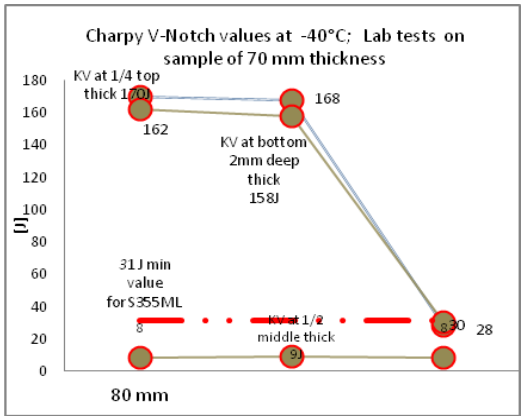

Fig. 8.

Variations on toughness values [Joules] in Fig. 8 on surface according to standard requirements, lower than the minimum limit, also in average 8 Joules at -40 ºC test temperature for 80 mm thickness.

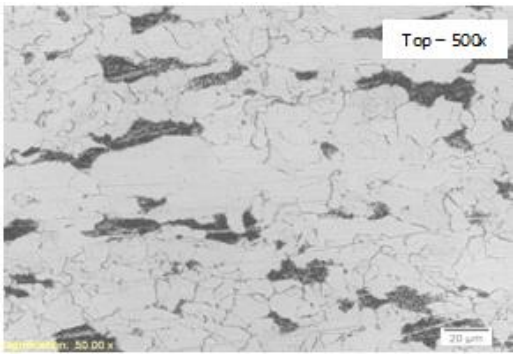

Fig. 9. *Metallographic analysis - sample no. 3317 - thick. 70 mm at surface - 2 mm deep in thickness*

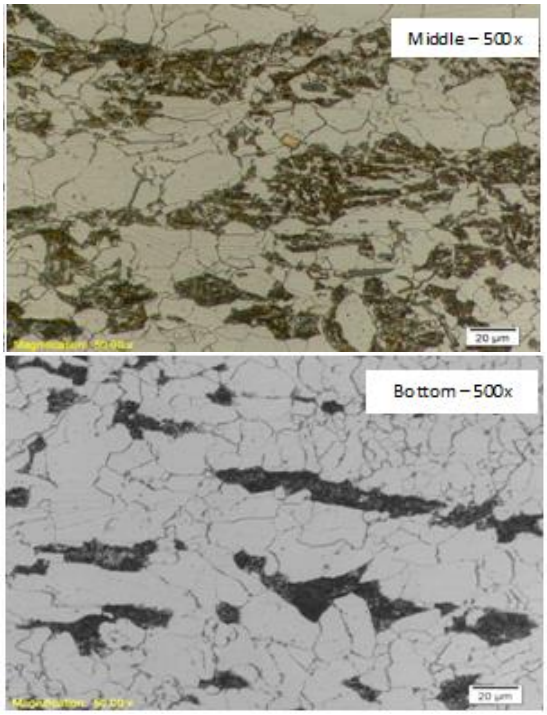

Fig. 10. *Metallographic analysis - sample no. 3317 - thick. 70 mm and SEM in middle and bottom*

Discussion on metallographies 70 mm thickness:

- Lamellar type of ferritic-pearlitic structure, partial decarburization 115 µm on the edge, accicular aspect;
- Cementite presence at the grain boundaries;
- Pearlitic structure has a different grade of dispersion;
- Lamellar type of coarse sorbite-pearlitic disbanded structure;
- Small segregations; 1. nitrides presence - orange in middle.

Grain size:

1. top - 7÷9.5 points;
2. middle - 6÷9 points;
3. bottom - 7÷9.5 points.

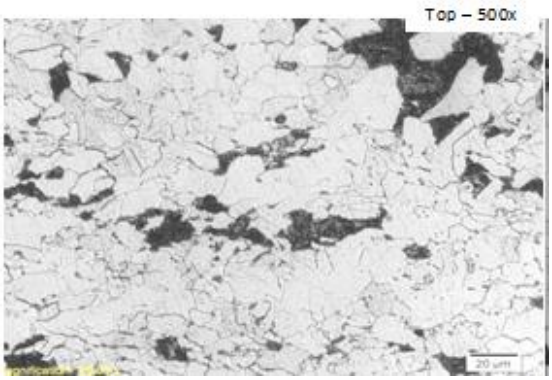

Fig. 11. *Metallographic analysis - sample no. 3316 - thick. 80 mm at surface - 2 mm deep in thickness*

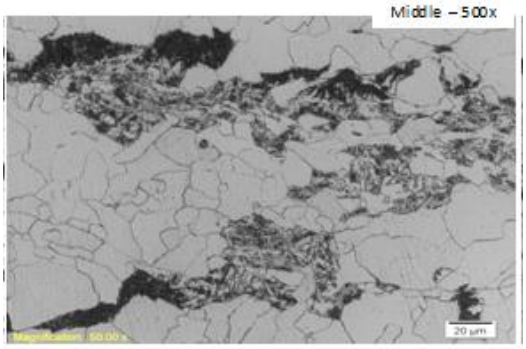

Fig. 12. *Metallographic analysis - sample no. 3316 thick. 80 mm in middle thickness*

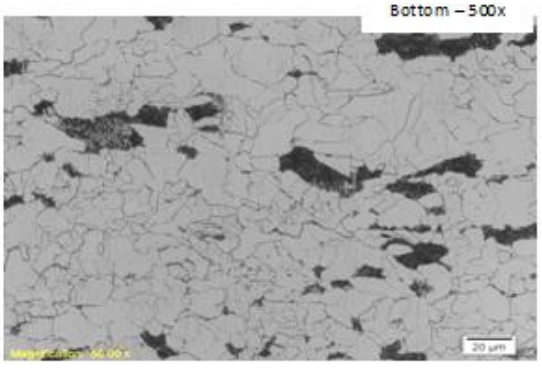

Fig. 13. *Metallographic analysis - sample no. 3316 thick. 80 mm at 2 mm deep thickness from bottom surface*

Discussion on metallographies 80 mm thickness:

- Lamellar type of ferritic-pearlitic structure, partial decarburization 270 µm on the edge, accicular aspect.
- Pearlitic structure has a different grade of dispersion.
- Lamellar type of coarse sorbite-pearlitic disbanded structure.

Grain size:

1. top - 7÷9.5 points;
2. middle - 6÷9 points;
3. bottom - 7÷9.5 points.

SWOT analysis:

Strength:

- S355M steel grade will cover the thickness range from 50.01 ÷ 80 mm.
- Thermo-mechanical rolling process – full auto mode.

Weakness:

- Time of production around 18 minute/mother plate.

Opportunities:

- Increased thickness range up to 84 mm.
- Preservation of the same chemistry.
- Added value.
- Fine tuning of rolling process.

Threats:

Occurrence of segregations in the middle of the higher thickness.

5. Conclusions

With the actual chemical compositions used in this experimental rolling we are confident about the feasibility for steel grade S355M to cover the thickness range from 50.01 up to 80 mm.

In order for the steel grade S355ML to start to increase the thickness range, in the first step the slab dimensions should be changed or different type of rolling should be used do to the lowest toughness achieved in the middle thickness.

References

[1]. *,** *ASM Handbook*, vol. 1, Properties and Selection: Irons, Steels, and High Performance Alloys, Section: Carbon and Low-Alloy Steels, HSLA Steels. 01 Sep 2005.

[2]. Prabal Gumar Ray, Ratan Indu Gangulay, Ashok Kumar Panda, *Determination of Recrystallization stop temperature (TR) of an HSLA steel*, Journal of Steel and related Materials - published in 2004.

[3]. Jian Fang, *Experimental study on the relationship between impact fracture properties and titanium addition for HSLA steels*, Technical Center, Baoshan Iron and Steel Co., Ltd., Shanghai 201900, China.

[4]. ***, http://galati.arcelormittal.com/about-s/arcelormittal-profile.

[5]. Hashimoto Shunichi, *et al*., *Effects of Nb and Mo addition to 0.2% C-1.5% Si-1.5% Mn steel on mechanical properties of hot rolled TRIP-aided steel sheets*, ISIJ, p. 1590-1598, 2004.

[6]. Craven A. J., He K., Garvie L. A., Baker T. N., *Complex heterogeneous precipitation in titanium-niobium microalloyed Al-killed HSLA steels-I. (Ti, Nb) (C, N) particles*. Acta Materialia, 48 (15), p. 3857-68, 25.09.2000.

[7]. Kunishige K., Nagao N., *Strengthening and toughening of hot-direct-rolled steels by addition of a small amount of titanium*, ISIJ International, 29 (11), p. 940-946, 1989.

[8]. Costel Durduc-Roibu, Elena Drugescu, *Effect of intercritical hot rolling deformation on steel grade for welded pipes with lean chemistry*, The annals of "Dunarea de Jos" University of Galati, Fascicle IX, Metallurgy and Materials Science, p. 171-178, 2012.

THE ANNALS OF "DUNAREA DE JOS" UNIVERSITY OF GALATI
FASCICLE IX. METALLURGY AND MATERIALS SCIENCE
Nº. 2 - 2016, ISSN 1453 – 083X

RESEARCH IN INDUSTRIAL TRIALS TO IMPROVE THROUGH-THICKNESS Z35 PROPERTIES OF HOT ROLLED HEAVY PLATES UP TO 60 MM THICKNESS FOR STRUCTURAL STEELS

Costel DURDUC, Liviu GURĂU, Elena DRUGESCU, Viorica MUȘAT
"Dunarea de Jos" University of Galati, 47 Domneasca Street, RO-800008, Galati, Romania
e-mail: costel.durducroibu@outlook.com

ABSTRACT

The main purpose of this industrial experimental rolling, done in ArcelorMittal Galati in the Heavy Plate Mill is to check the correlation between mechanical properties and the microstructure of chemical compositions used in trial in order to reach through-thickness Z properties. First chemical composition is C_Mn steel with mechanical properties designed to reach at least 275 MPa on yield strength. The other chemical composition is based on Nb and Ti alloying elements with mechanical properties designed to be equal or higher than 360 MPa. In total, four slabs with 250 mm thickness were rolled. Two slabs with targeted plates thickness of 22.5 mm and 60 mm were used in trial per each chemical composition in order to check the thickness feasibility of targeted through-thickness Z properties.

KEYWORDS: trough-thickness, Z25, Z35, structural steels, ship structures, offshore structures, beams in bridge constructions

1. Introduction

Z35 through-thickness mechanical properties is a specially processed steel grade, which takes into consideration the requirements of heavy steel construction. The possibility of lamellar tearing occurring in stiff welded joints has been prevented by improving the perpendicular properties of steel.

Definition of Z plates, quality classification and dimension range: the properties of the Z plates perpendicular to the plate surface are better than those properties of the corresponding grade of general structural steel. The letter Z refers particularly to the thickness in xyz-coordinates of the plate width x length x thickness. The through-thickness deformation properties are determined with the tensile test using test pieces that are machined in through-thickness direction of the plate. The result is the perpendicular reduction of area at fracture, that is, the so-called Z value. The Figure indicates the reduction of the cross-sectional area of the tensile test piece during the tensile test, i.e. perpendicular reduction of area in percentage. This calculated Z value sets a basis for the quality classification of Z plates, as shown in Table 1.

Table 1. *Z quality classes and the corresponding reduction of area values for Z plates according to EN 10164*

Z quality class	**Requirements for reduction of area value (Z values)**	
Quality class designation	**Minimum average value, requirement for three tests %**	**Minimum individual value requirement %**
Z15	15	10
Z25	25	15
Z35	35	25

For plates of thickness less than 15 mm the standard EN 10164 does not require through-thickness tensile tests and these tests are not carried out. However, the same manufacturing process is used for all the Z plates regardless of the thickness

For Z plates the standard ASTMA 770 also deals with the steel plates having improved through-thickness properties. In this standard, Z plates are defined as plates that have reduction of area value Z ≥ 20%. Z plates with improved through-thickness properties can be delivered within the thickness range of ≥ 25 mm. Z guarantees for thinner plates according to separate agreement. For other dimensions the corresponding dimension range of heavy plates is effective.

For steel grades, product shapes and properties Z plates can be ordered in any of the steel grades included in the heavy plate production programmed. Z plates are used in all parts of the world as structural steels, pressure equipment steels, ship construction steels and offshore steels. In addition to heavy plates, shop-primed plates and a wide selection of prefabricated plate products are also available. Prefabricated products that are ready for installation can be tailor-made, cut, bent and/or beveled in accordance with the customer's requirements. The chemical composition, mechanical properties as well as usability in the engineering shop are determined by the steel grade.

Z plates are manufactured and tested primarily according to the requirements set in the relevant steel standard or in the Rules of the classification society in question. During the manufacture of the steel, special additional treatment is used to improve the through-thickness properties of the finished plates. If the material standard does not specify requirements for Z plates and the purchaser does not indicate any specific requirements, the standard EN 10164 will be applied.

Regarding the occurrence of lamellar tearing in steel structures, the lamellar tearing as a failure type of steel structures is extremely uncommon and when it occurs, it usually takes the form of cracking parallel to the surface of the plate and in association with a welded joint. The cracks are on different planes and are connected to one another in a step-like form. Most sensitive to this are stiff, fillet and butt welded L and T joints, where large through-thickness stresses may occur. When assessing the possibility of occurrence of lamellar tearing, the empirical values for through-thickness reduction of area presented in Table 2 can be used. The industrial trials were done in ArcelorMittal Galati.

Table 2. *Values for reduction of area in the through-thickness direction*

Reduction of area in the through-thickness direction %	Probability of occurrence of lamellar tearing
Z ≥ 35	Extremely unlikely.
20 ≤ Z < 35	Extremely rare.
15 ≤ Z < 20	Possible in welded joints highly loaded in the through-thickness direction of the plate.
10 ≤ Z < 15	Possible in welded joints moderately loaded in the through-thickness direction of the plate.
Z < 10	Possible in welded joints only lightly loaded in the through-thickness direction of the plate.

2. Tracking and traceability of products followed in Z35 industrial trials

For the trial designation on drawing the heavy plates according with DNV rules of the steel grade A to EH36 with Z quality class reaching Z35 according to EN 10164 were designated with the following example: DNV rules + EN 10164-Z35.

Flow production process starts from SMS (SMS = steel melting shop) and CC (Continuous casting); HPM (heavy plate mill) hot rolling and normalizing and further heat treatment with laboratory tests for 4 plates with two thickness plates target, namely 22.5 mm and 60 mm, taken from 4 different heats scheduled, elaborated and casted, were rolled and normalized. In Table 3 are shown dimensional slabs used in trial.

The first analysis concerned the macrostructure of slabs used in trial.

In Table 4 we have the Bauman prints for each slab. We can observe small center lines in the middle of the thickness.

Table 3. *Dimensions of slabs used in Z35 trial*

Trial no	Slab thickness	Slab width	Slab length	Plate thickness	Slab width	Slab length
1	250	1500	1999	22.5	3120	11000
2	250	1500	2035	22.5	3120	11000
3	250	1500	4040	60	3100	10000
4	250	1500	3570	60	3100	9000

Table 4. *Macrostructure analysis – Bauman print - central segregation and core defects – class 2*

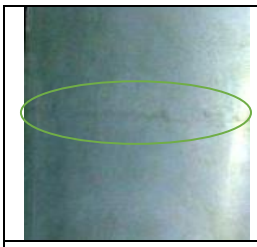			
Trial no. 1	Trial no. 2	Trial no. 3	Trial no. 4

3. Hot rolling

3.1. Processing conditions for trials

The delivery conditions of Z plates are defined in standards with N – normalizing heat treatment in furnace. Our purpose is to have the final rolling temperature in austenitic area above Ar_3, which means the rolling schedule will be in two phases. One phase will be in roughing area were the transfer bar thickness between two stands will increase s – roughing mill and finishing mill. In finishing mill, the transfer bar will be rolled in one phase with one cooling point. The cooling point will be 60 °C above Ar_3 in austenitic zone. We prepared 4 chemical compositions of steel grade equivalent with NVE and NVE36 according with DNV rules. Preliminary laboratory tests showed that the combination of austenitic rolling followed by normalizing heat treatment can increase the Z35 trough-thickness properties. The lab trials were focused on Z25 through-thickness properties of thick plates with a similar chemical composition used in the described trial as it can be seen in Table 5. Now the objective is to determine up to which degree of thickness such a lean chemistry composition could be used to reach Z35 properties. Purposed chemistry and the traceability of trial are described in Table 5.

Table 5. *The chemical composition used in trial*

No.	C	Mn	Si	P	S	Al	Ni	Cu	Cr	Ti	Mo	Nb	V	N
1	0.170	1.09	0.21	0.011	0.003	0.038	0.016	0.016	0.027	0.002	0.003	0.002	0.002	0.0051
2	0.172	1.45	0.22	0.012	0.005	0.034	0.014	0.019	0.025	0.009	0.003	0.036	0.028	0.0057
3	0.157	1.34	0.27	0.013	0.003	0.042	0.239	0.014	0.024	0.018	0.002	0.018	0.025	0.0054
4	0.180	1.31	0.27	0.010	0.004	0.038	0.240	0.017	0.022	0.019	0.003	0.037	0.055	0.0055

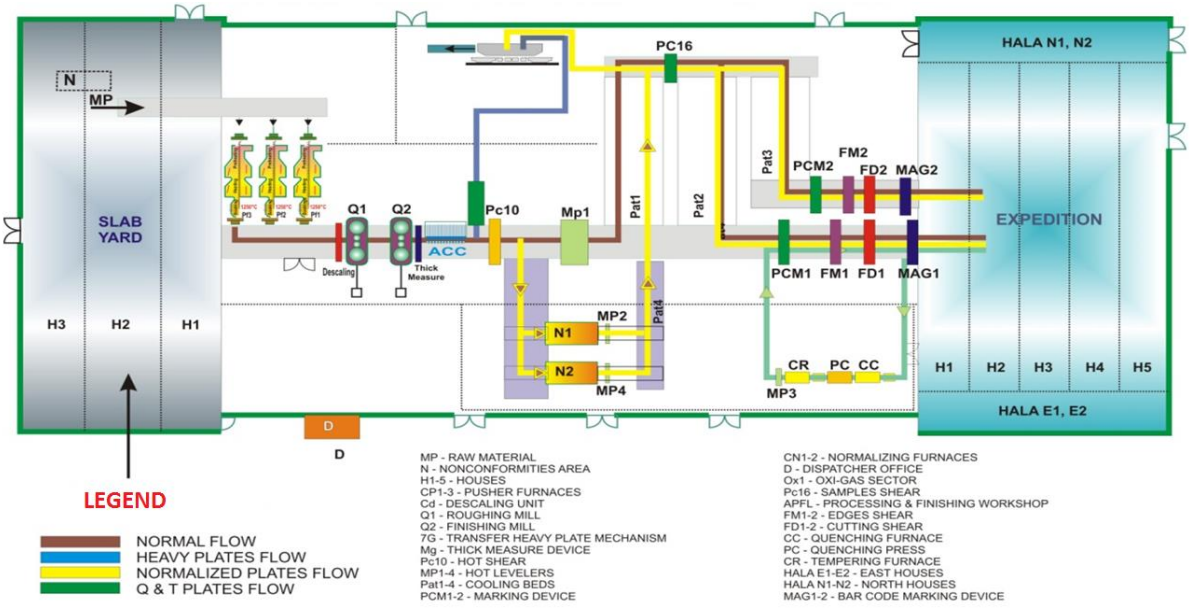

Fig. 1. *Heavy Plate Mill flow production process*

Table 6. *Pushing furnace data (reheating data)*

Trial no.	CP Line	Preheating time [hours]	Heating time [hours]	Soaking time [hours]	Average temperatures preheating zone [°C]	Average temperatures heating zone [°C]	Average temperatures soaking zone degrees [°C]	Discharging temperature [°C]
1	2	1:18	2:10	1:37	1065 / 1001	1269 / 1278	1259 / 1259	1187
2	1	1:17	2:00	1:36	1061 / 1060	1270 / 1281	1259 / 1259	1165
3	2	1:20	2:10	1:37	1061 / 1060	1269 / 1278	1252 / 1252	1160
4	1	1:22	2:00	1:31	1061 / 1060	1270 / 1281	1259 / 1259	1173

Specific time to reheating slabs of the steel grades equal to 1.5÷2 min/mm

Rolling data:

- Q1 roughing mill stand; reversible quarto mill stands; locked frame: Maximum dimensions on plates: thickness > 14 mm / width: 1500-4600 mm / maximum length: 16500 mm. Transfer bar thickness for Q2 = 30-120 mm.

- Q2 finishing mill stand; reversible quatro mill stands; open frame: Maximum dimensions on plates: thickness: 6 ÷ 150 mm / width: 1500÷4200 mm / maximum length: 50000 mm.

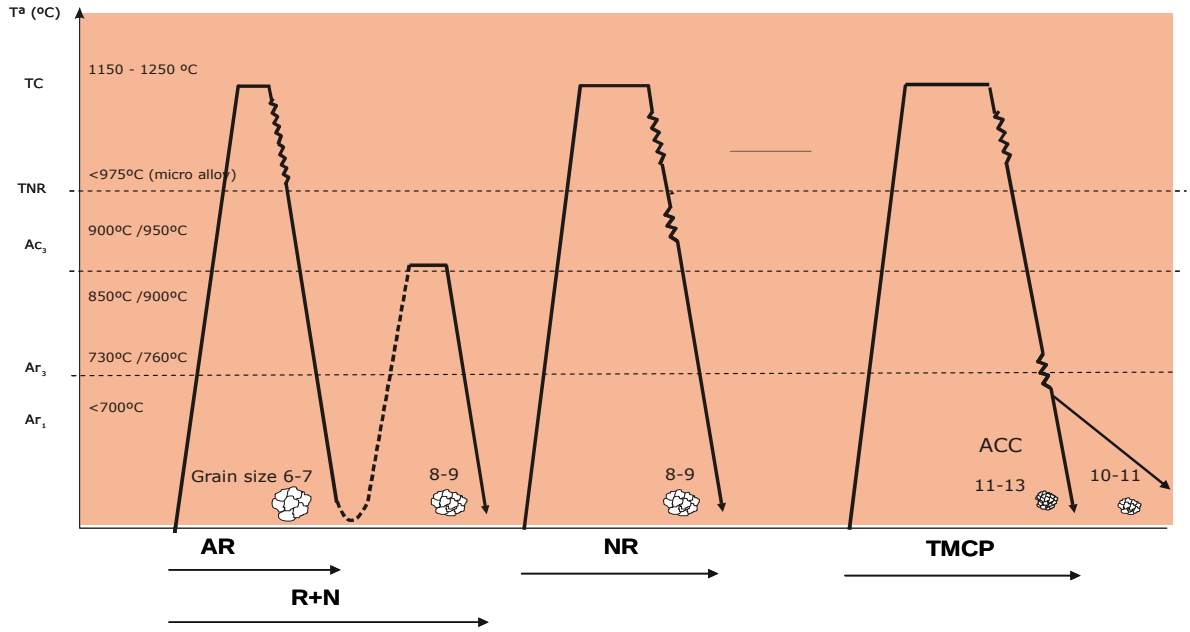

Fig. 2. *Type of rolling = R + N control rolling followed by normalizing heat treatment*

Table 7. *Rolling process data*

No.	Slab thick [mm]	Slab width [mm]	Slab length [mm]	Plate thick [mm]	Plate width [mm]	Plate length [mm]	Descaling pressure [bar]	Start rolling temperature in Q1 [°C]	Transfer bar thick. [mm]	Start rolling temperature in Q2 [°C]	End rolling temperature in Q2 [°C]	Total percentage reduction in Q2 [%]
1	250	1500	1999	22.5	3120	11000	170	1170	67	870	814	33.58
2	250	1500	2035	22.5	3120	11000	170	1150	67	870	815	33.58
3	250	1500	4040	60	3100	10000	170	1150	110	840	812	54.54
4	250	1500	3570	60	3100	9000	170	1170	110	840	816	54.54

About the control rolling process the discharging from the pushing furnace, followed by descaling at 170 bar pressure will be Q1 the entry temperature around 1150 ºC and the rolling strategy = pre-sizing sequence and the broad-sizing sequence from 2 turns; followed by realizing the transfer bar

thickness; cooling time in oscillation are to achieve Q2 start temperature, rolling passes to achieve final thickness at the temperature aimed. The total percentage reduction in Q2 is equal or higher than 55%. Next step is normalizing heat treatment. All data are in the next table and the next figures will show rolling temperatures function of thickness, and exit thickness function of rolling passes.

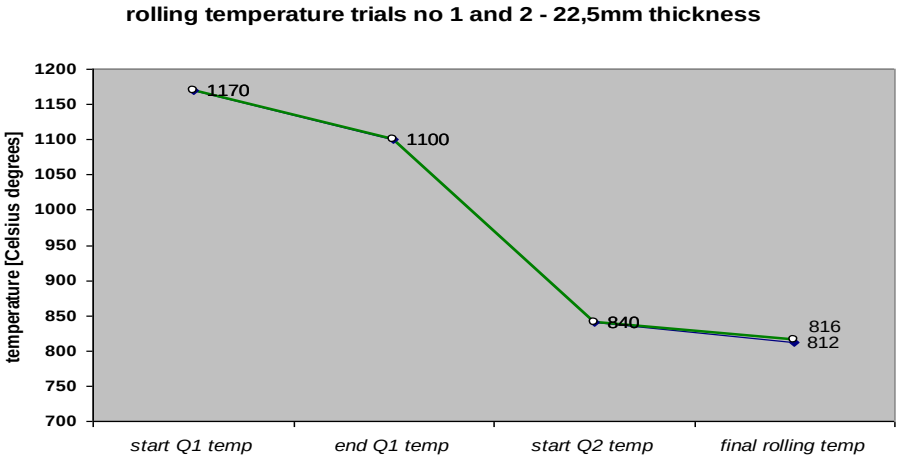

Fig. 3. *Rolling temperature for plates with 22.5 mm final thickness*

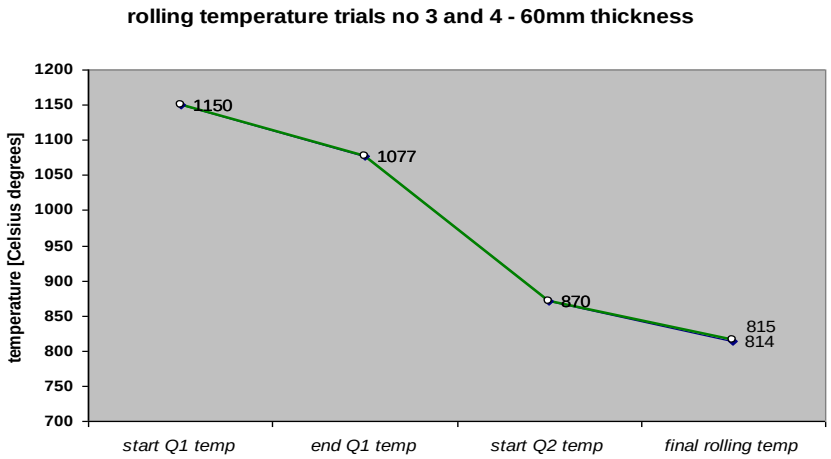

Fig. 4. *Rolling temperature for plates with 60 mm final thickness*

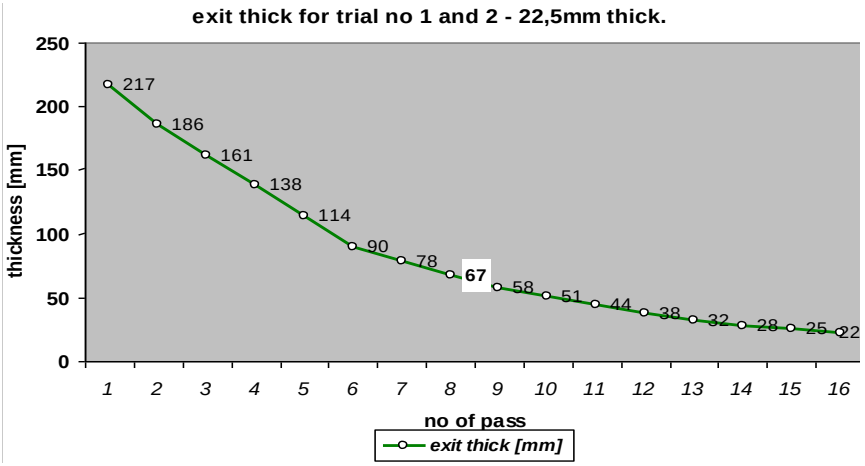

Fig. 5. *Exit thickness at rolling pass for plates with 22.5 mm thickness*

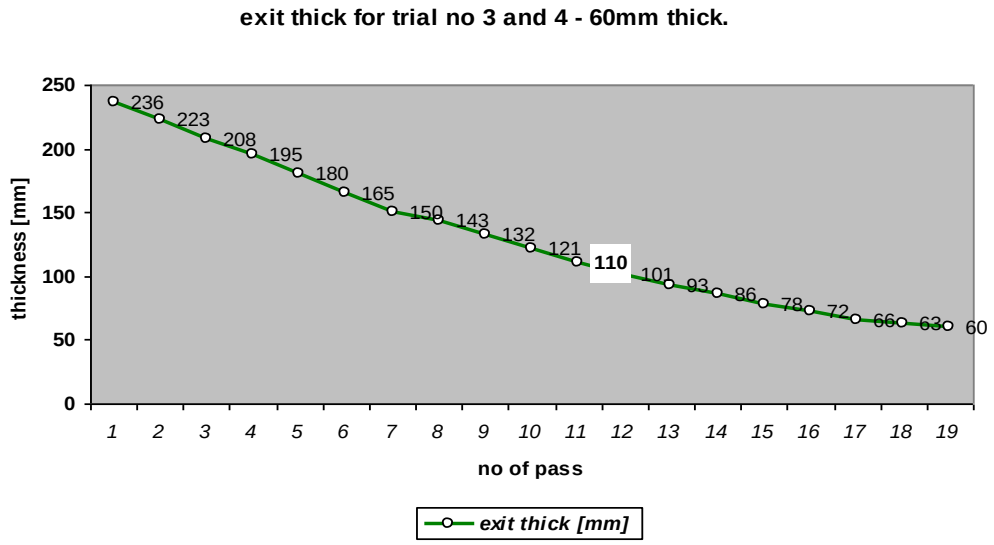

Fig. 6. *Exit thickness at rolling pass for plates with 60 mm thickness*

3.2. Normalizing data

Normalizing N metallurgical route is a separate heat treatment after rolling involving austenitising (above the transformation range Ac_3). Normalizing relieves the internal stresses caused by previous working, and while it produces sufficient softness and ductility for many purposes, it leaves the steel harder and with a higher tensile strength.

Table 8. *Normalizing furnace data*

No.	Slab thick. [mm]	Slab width [mm]	Slab length [mm]	Plate thick. [mm]	Slab width [mm]	Slab length [mm]	Temperature set on burners zone 1-12 [°C]	Total time spent in furnace [minutes]
1	250	1500	1999	**22.5**	3120	11000	**880**	**49**
2	250	1500	2035	**22.5**	3120	11000	**880**	**50**
3	250	1500	4040	**60**	3100	10000	**880**	**101**
4	250	1500	3570	**60**	3100	9000	**880**	**120**

Specific time to normalize plates depends of the thickness range and steel grades between 1.6÷2.2 min/mm

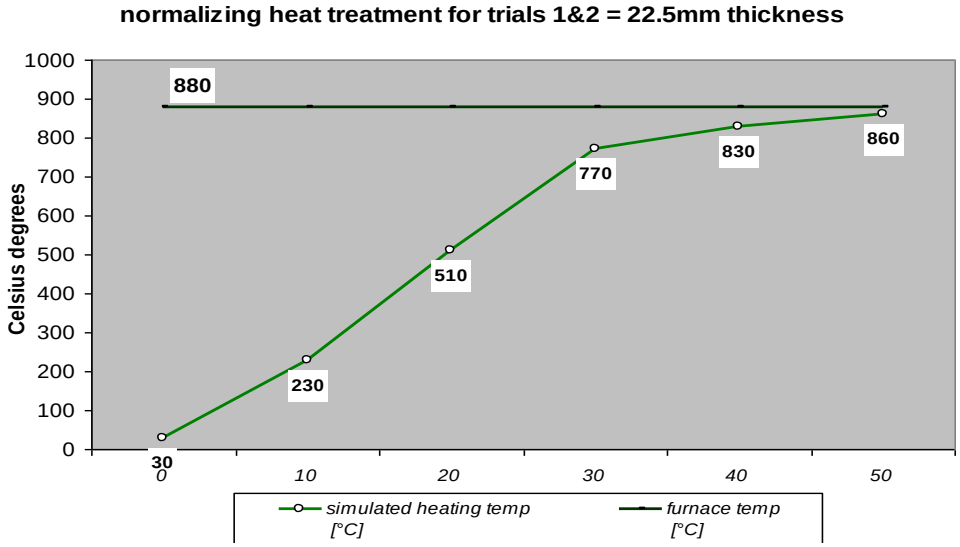

Fig. 7. *Normalizing plate temperature plate with 22.5 mm thickness*

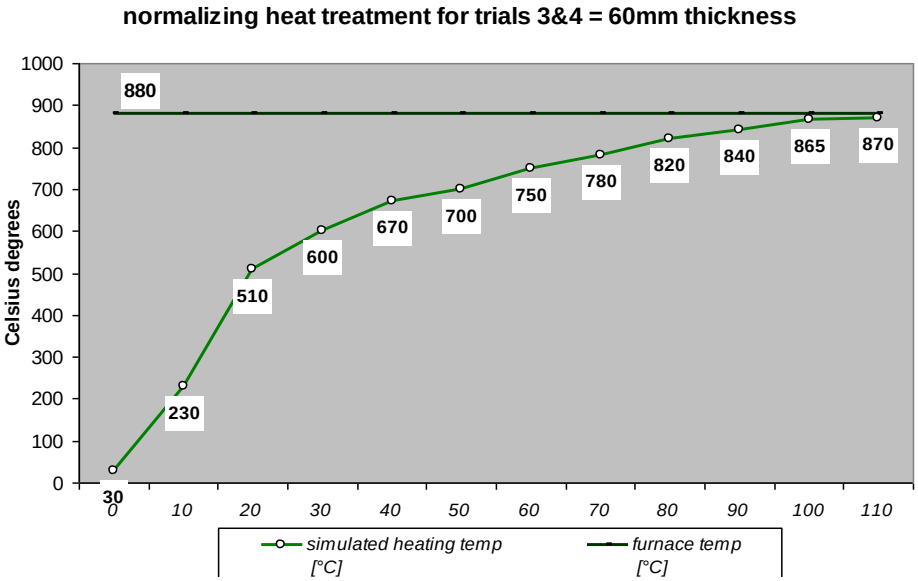

Fig. 8. *normalizing plate temperature - plates with 60 mm thickness*

3.3. Material testing and sampling

Z plates are manufactured and tested primarily according to the requirements set in the relevant material standard or in the rules of Classification Society in question. If the standard does not specify requirements for Z plates and the purchaser does not indicate any specific requirements, standard EN 10164 will be applied. A test unit and the sampling are defined in EN 10164. The through-thickness tensile test and the calculation of the through-thickness reduction of area are defined in the standard EN 10002-1. The test result assessment is based on the sequential method defined in the standard EN 10021.

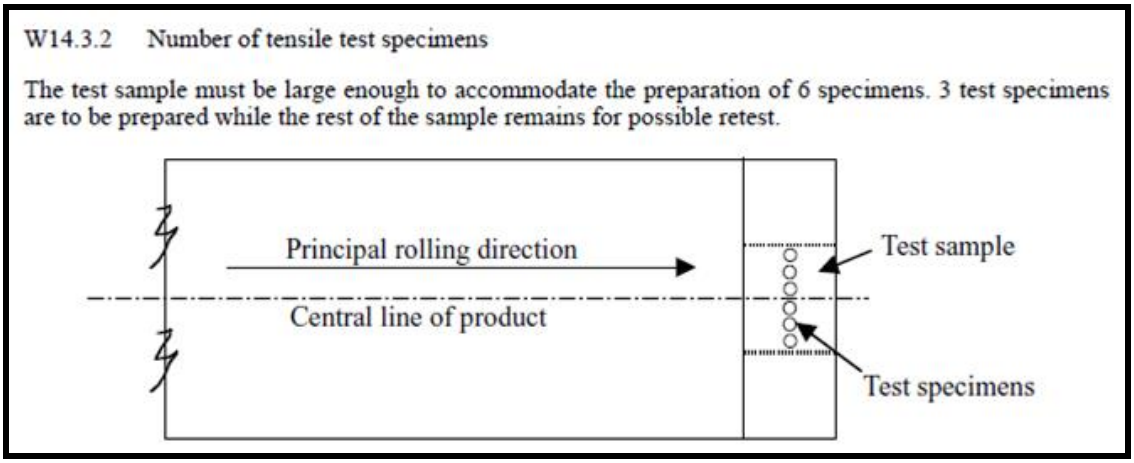

Fig. 9. *Test sample according to EN 10002-1*

Ultrasonic test performed S1E1 conf. EN10160:2009: the testing of Z plates always includes ultrasonic testing which is carried out according to the requirements of EN 10160 class S1. It must be noted that the normal ultrasonic technique cannot be used for determining resistance to lamellar tearing. UT test was performed with Olympus Flaw detector, model EPOCH600: probe diameter φ = 21 mm, test frequency = 4 MHz, scanning area between 100-200mm. The results are shown below.

Mechanical tests performed on INSTRON testing machine are listed below.

- One tensile test for each sample in transverse direction according to DNV Rules for classification of Ships / High Speed, Light Craft and Naval Surface Craft, Section 1, chapters B and C / 2011;

- One Charpy test notch in transverse direction KV at -40 °C (negative Celsius degrees) for each sample transverse test according to DNV rules / 2011;
- Z35: 2 tests with 3 samples according with EN 10164/2004;
- Table 10 presents data of INSTRON testing machine presets for tensile test;
- Table 11 presents results of the mechanical properties of plates rolled.

In Figure 10 we can observe very good toughness properties with an average of 100 Joules for 22.5 mm thickness and around 80 Joules for 60 mm thickness in comparison with the minimum value requirement of 27 J.

In Figure 11 we can observe very good elongation properties in comparison with minimum value requirement of 21%.

Table 9. *UT results*

Trial no. 1	Dimensions T x Wx L [mm]	Specification for examination	Specification for acceptance
1	22.5 x 3000 x 9000	EN10160/1999 – S1E1	EN10160/1999 – **S2E2**
2	22.5 x 3000 x 9000	EN10160/1999 – S1E1	EN10160/1999 – **S2E2**
3	60 x 3000 x 9000	EN10160/1999 – S1E1	EN10160/1999 – **S1E1**
4	60 x 3000 x 8000	EN10160/1999 – S1E1	EN10160/1999 – **S1E1**

Table 10. *Summary of sample data and presets of INSTRON testing machine*

Trial no.	1	2	3	4
Plate thickness [mm]	22.5	22.5	60	60
Section	23.7 mm x 25.1 mm	23.2 mm x 25 mm	Φ 14 mm	Φ 14.1 mm
Original Gauge Length Lo [mm]	140	135	70	70
Final Gauge Length Lu [mm]	180	181	91	95
Maximum Force Fm [N]	320	275	84	80
Flow Force F [N]	235	190	57.5	65
Z Section [mm]	Φ6	Φ6	Φ10	Φ10

Table 11. *Mechanical properties result after tensile test*

Trial no.	1	2	3	4
Tensile Strength [MPa]	538	474	546	513
Yield Stress [MPa]	395	328	374	416
Elongation E [%]	29	34	30	36
KV, transverse at -40 ˚C	171; 186; 191	98;115; 106	98; 92; 80	89; 102; 74
Z test 1 [%]	46; 44; 46;	65; 62; 56;	56; 51; 54;	70; 71; 71;
Z test 2 [%]	46; 41; 49	56; 60; 60	55; 59; 59	71; 71; 73

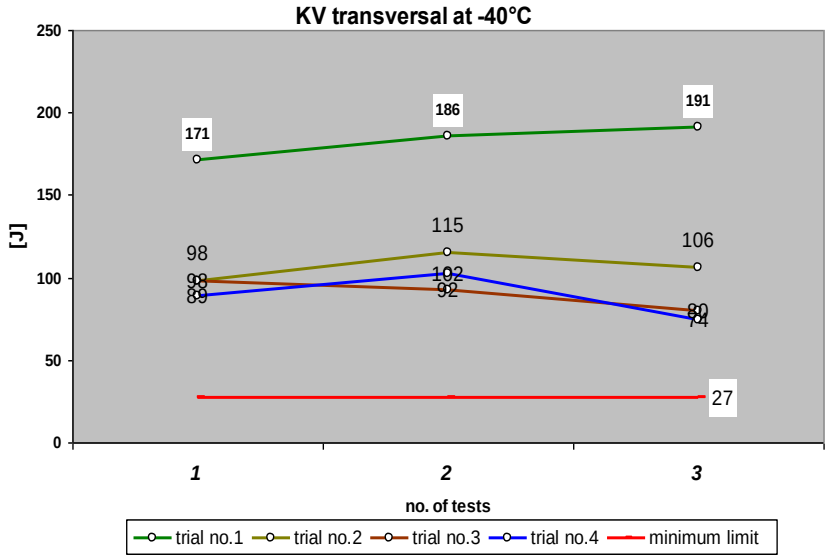

Fig. 10. *Toughness results*

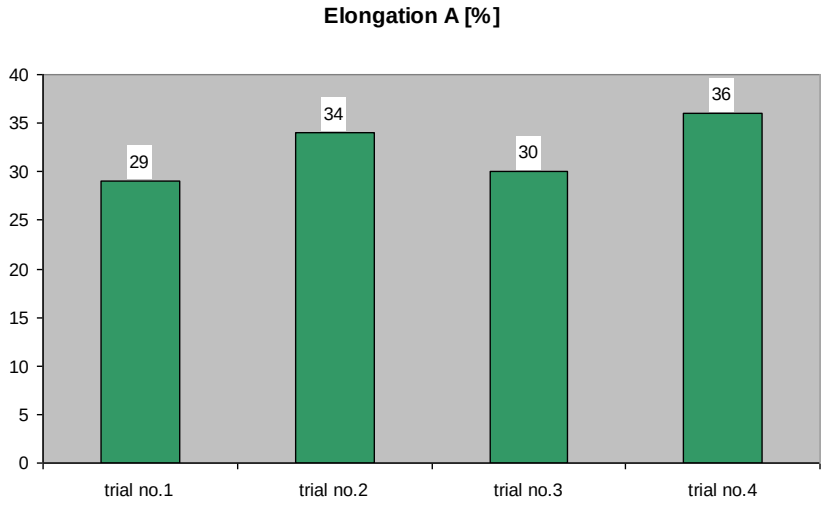

Fig. 11. *Elongation result*

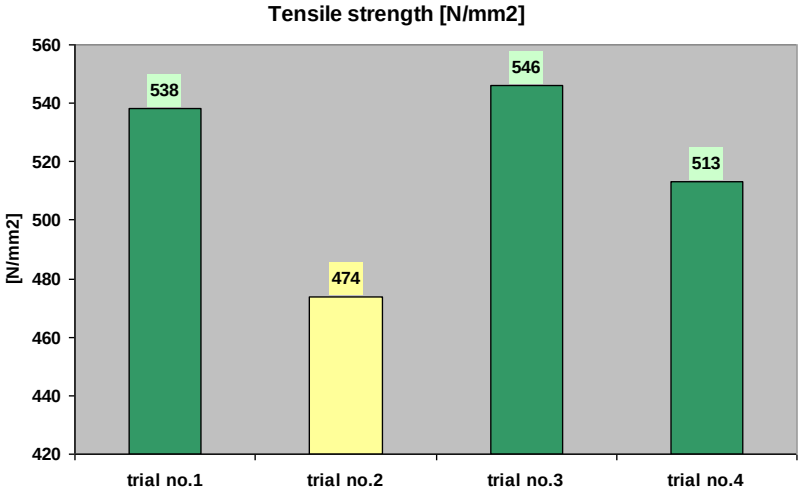

Fig. 12. *Lab results of TS*

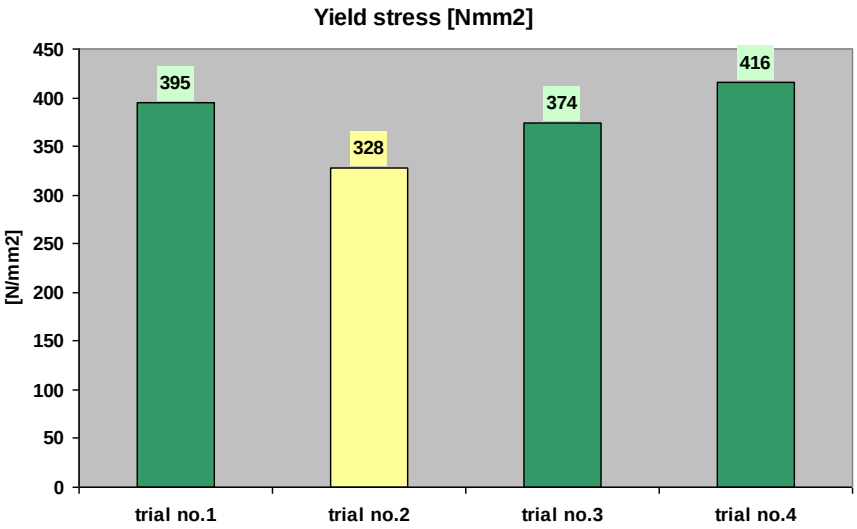

Fig. 13. *Lab results of YS*

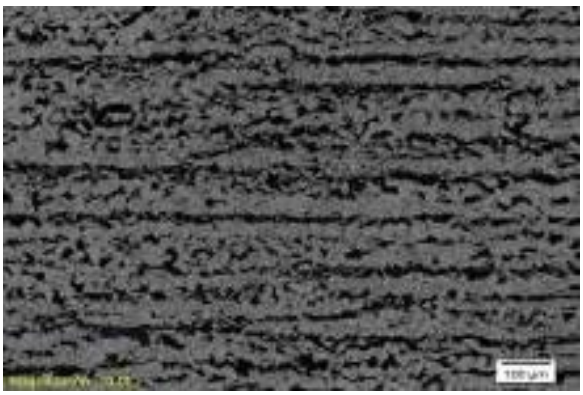

Fig. 14. *Rolling sample top surface at 100 x magnifications Ferrite-perlite relative uniform structure, grain size 8.5 - 10; KV (-40 °C) = 46 / 40 / 48 J*

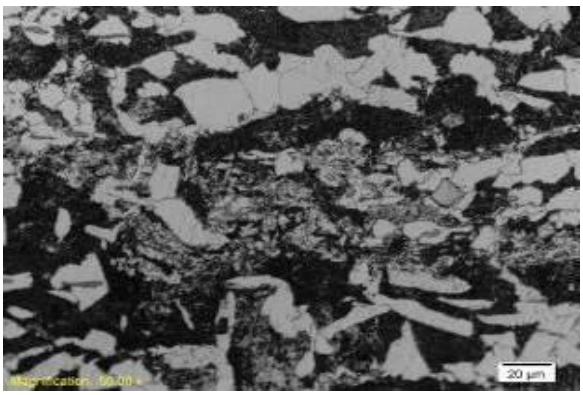

Fig. 15. *Rolling sample in middle at 500x magnifications Perlite conglomerations in large area grain size 7.5 - 9: KV (-40 °C) = 18 / 18 / 24 J*

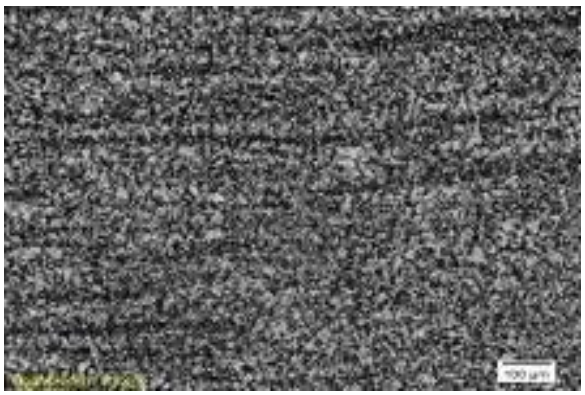

Fig. 16. *Normalized sample at 100x magnification - Ferrite-perlite uniform structure, grain size 10; KV (-40 °C) = 89 / 102 / 74 J*

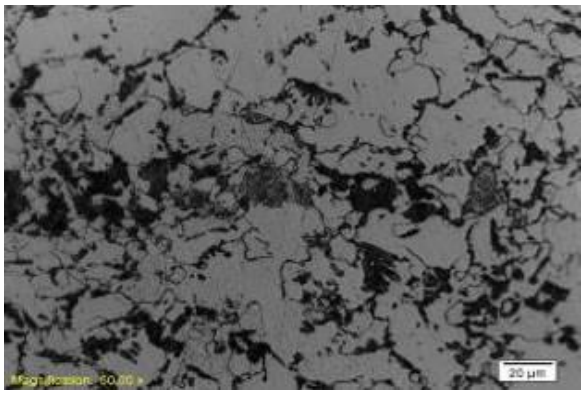

Fig. 17. *Normalized sample in middle at 500x magnification; Ferrite-perlite uniform structure, grain size 9.5; KV (-40 °C) = 52 / 48 / 58 J*

Good results on TS properties higher than 470 MPa were obtained. Except for trial no. 2, the rest of

the results are very good, the TS properties on higher steel grade having limits between 485-630 MPa.

Good results on YS properties higher than 320 MPa were obtained. Except for no. 2, the rest are very good, the YS properties on higher steel grade with minimum limit being 355 MPa.

The metallography of trial no. 4 - 60 mm thickness is presented in Figures 14-19.

Fig. 18. *Rolling sample bottom surface at 100x magnification Non-uniform ferrite-perlite structure; grain size 8-9.5; KV (-40 °C) = 59 / 62 / 60 J*

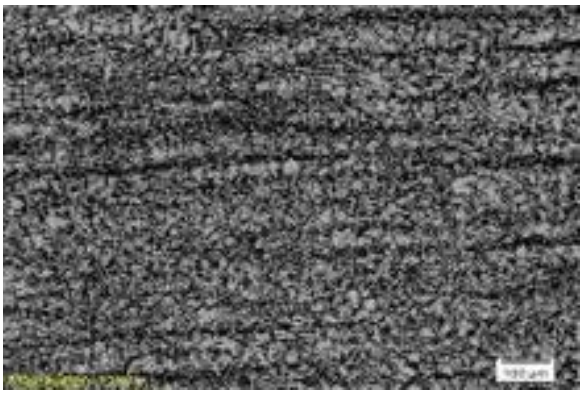

Fig. 19. *Normalized sample bottom surface at 100x magnification; Ferrite-perlite uniform structure oriented in rolling direction, grain size 10; KV (-40 °C) = 92 / 100 / 84 J*

4. Conclusions

The use of this material known as 'Z' quality steel is recommended when plate material, intended for welded construction, is subject to significant strain in a direction perpendicular to the rolled surfaces. These strains are usually associated with thermal contraction and restraint during welding, particularly for full penetration of "T"- butt welds, but may also be associated with loads applied in service or during construction. Where these strains are of sufficient magnitude, lamellar tearing may occur. Two 'Z' quality steels are specified: Z25 for normal ship applications and 'Z35' for more severe applications. As possible applications, we ca mention the frame structures, in which the plates are heavily loaded in the through-thickness direction, Beams in bridge construction, overhead bridge crane structures, ship structures, machine beds, heavily loaded structures such as crushers, propeller blade structures, oil rig cross frames, other offshore structures.

The chemical composition used in trial can be used in accordance with the followed standards ASTMA 131/2001; BV 2011; GL 2009; NKK 2008; ASME SA 612; ABS 2012; RINA 2008; LR 2013; DNV 2013; EN 10028-3-2003; EN 10025-2-2004.

Carbon equivalent was calculated according to IIW formula

$$C_{eq} = C + \frac{Mn}{6} + \frac{Cr+Mo+V}{5} + \frac{Ni+Cu}{15},$$

and the following results were obtained

trial no. 1; Ceq = 0.36
trial no. 2; Ceq = 0.43
trial no. 3; Ceq = 0.41
trial no. 4; Ceq = 0.43,

offering possibilities to produce, in industrial conditions, plates with Ceq max 0.43% for both chemical compositions used in trial.

The sum of micro-alloying elements from chemical composition $\sum(Nb+V+Ti) \leq 0.12$ are in accordance with DNV rules described in the Standard for certification no. 2.9 / Approval Programme No. 301B, / Rolled ferritic steel plates, sections and bars section 4.3 and with EN 10025-3-2004 and with EN 10028/3-2009:

trial no. 1 = 0.0053
trial no. 2 = 0.0740
trial no. 3 = 0.0615
trial no. 4 = 0.1110

Nb and Ti alloying elements influence microstructure, provide fine grains in rolled state and in normalized state.

Normalizing heat treatment has higher influence in the Z trough-thickness coefficient, achieving almost double value than the minimum requirement of the highest quality Z3.5.

This trial can cover plates from structures, ships to pressure and steel grades vessels.

Trials 1 and 3 can be covered in naval section from NVE36, AH36, LRE36 below until reaching A grade. For a structure it can be achieved the S355

grade and for pressure vessels it can be achieved until P355.

Trial 2 and 4 can cover the A naval grade until A32, structural grade until S275 and pressure vessels until P275. With the combination of control rolling plus the normalizing heat treatment in the furnace, the Z35 through-thickness properties can be reached for thicknesses up to 60 mm, with the chemical composition as indicated in Table 5.

Even the matrix chemistry is only CMn without micro alloying (see trial no 1), with a good combination between control rolling and heat treatment in furnace, the Z35 properties can be achieved for thickness up to 40 mm AH32 (S275; P275).

For future research, a thickness higher than 60 mm (up to 100 mm) can be approached following the minimum micro alloyed chemistry presented in this research combined with a very good control rolling parameters and a specific normalizing heat treatment with very well defined values of time and temperatures.

References

[1]. Joseph R. Davis, *Alloying: understanding the basics - high-strength low-alloy steels*, ASM International, Chapter 38, 2001.
[2]. Florentina Potecaşu, Octavian Potecaşu, Elena Drugescu, Petrică Alexandru, *The influence of cold rolling on the microstructure for drawing steels*, The Annals of "Dunarea de Jos" University of Galati, Fascicle IX Metallurgy and Material Science, no. 2, p. 40-46, 2007.
[3]. Zhang L., Kannengiesser T., *Austenite grain growth and microstructure control in simulated heat affected zones of micro-alloyed HSLA steel*, Materials Science and Engineering, A, 2014.
[4]. Potecaşu F., *Metalurgie fizică*, vol. 1, Editura FRM-ISBN-978-973-8151-48, 2007.
[5]. George E. Totten, *Heat treatment handbook steel heat treatment - metallurgy and technology*, Second edition, Taylor & Francis Group, p. 134, 159, 162, 2006.
[6]. Ginzburg, Vladimir B., Ballas Robert, *Fundamentals of flat rolling manufacturing engineering and materials processing publisher: CRC Press*, Chapter 12.3 - Continuous-Type Slab Reheating Furnaces, 2000.
[7]. ***, *HSLA Steels 2015, Microalloying 2015 and Offshore Engineering Steels 2015*, The Chinese Society for Metals.
[8]. Kunishige K., Nagao N., *Strengthening and toughening of hot-direct-rolled steels by addition of a small amount of titanium*, ISIJ International, 29 (11), p. 940-946, 1989.
[9]. ***, ASTMA A 131/A 131M - 2001 - Standard Specification for Structural Steel for Ships, p. 3-7.
[10]. ***, *Rules on materials and welding for the classification of marine units German's Lloyd 2009, Section 1 - Principles covering the manufacture and testing of materials*, Bureau Veritas, p. 3-7, 2011.
[11]. Hashimoto Shunichi, *et al.*, *Effects of Nb and Mo addition to 0.2% C-1.5% Si-1.5% Mn steel on mechanical properties of hot rolled TRIP-aided steel sheets*, ISIJ international 44.9, p. 1590-1598, 2004.
[12]. Nippon Kaiji Kyokay, *Guidance for the survey and construction for the ship steel contents*, p. 2-5, 2008.
[13]. ***, *Section 1 rolled steel plates, sections and bars*, RINA 2008, p. 3-10.
[14]. ***, *Rules for the manufacture, testing and certification of materials*, Lloyd's Register, p. 3-7, 2013.
[15]. ***, *Rules for classification of ships / high speed, light craft and naval surface craft new buildings; Materials and welding*, Det Norske Veritas, p. 3-7, 2013.
[16]. ***, *Flat products of steel for pressure purpose – Part 3 – Wieldable fine grain steels, normalized*, European Norm 10028-3-2003, p. 2-12, 2003.
[17]. ***, *Hot rolled products of structural steels - Part 3: Technical delivery conditions for normalized/normalized rolled and wieldable fine grain structural steels*, European Norm 10025-2-2004, p. 2-12, 2004.
[18]. ***, *Steel products with improved deformation properties perpendicular to the surface of the product. Technical delivery conditions - Through-thickness properties*, European Norm 10164, p. 2-15.

THE ANNALS OF "DUNAREA DE JOS" UNIVERSITY OF GALATI
FASCICLE IX. METALLURGY AND MATERIALS SCIENCE
Nº. 2 - 2016, ISSN 1453 – 083X

STATISTICAL CORRELATIONS BETWEEN CHEMICAL COMPOSITION AND MECHANICAL PROPERTIES OF A516 GRADE 65 STEEL

Anișoara CIOCAN, Beatrice TUDOR
"Dunarea de Jos" University of Galati, 111 Domnească Street, 800201, Galaţi, Romania
e-mail: aciocan@ugal.ro

ABSTRACT

In order to respond to required demands associated to certain operation conditions, the steels used in petroleum, petrochemical and chemical processing industries must have significant improved mechanical properties. These can be obtained by constant monitoring and controlling of parameters of steelmaking process. The determining factors responsible for improving the mechanical properties of steel are chemical composition, purity and the technological parameters. The injection of an inert gas or by vacuum exposure is effective in reducing non-metallic inclusions and for chemical composition control. These treatments are comprised in the secondary metallurgy and require special installations. It is cheaper to create a modeling tool that can be used for the prediction of mechanical properties, directly in the steel production process by variating its chemical composition. In this paper, by using the linear regression technique, the relationships between certain mechanical properties and the chemical composition of steel A516 Grade 65 have been determined.

KEYWORDS: steel, mechanical characteristics, chemical composition, statistical correlation

1. Introduction

In standard specification, A516 steel, with grades 55, 60, 65, and 70, refers to a range of steels used to produce pressure vessels [1-4]. These steels are mainly used to manufacture pressure vessels and boilers for the petrochemical industry that work at moderate and lower temperature. The steels have good weldability and excellent notch toughness. A516 Grade 65 has greater specified tensile and also higher yield strength. The chemical composition of steel plates may vary for different products thicknesses so as to meet particular mechanical properties requirements. These ask for high levels of purity and the precise control of chemical composition. The mechanical properties are in direct relation with parameters of steel produced in traditional furnace. Also, special processing of steel bath, like the vacuum degassing for control of inclusions and chemical composition, is a solution to obtain improved mechanical properties [5-7]. Today, there are many techniques available in the steelmaking industry for correction and control of the characteristics of non-metallic inclusions. The secondary treatment of melted steel is carried out in special metallurgical installations with supplementary costs [8]. It is cheaper to create a modeling tool able to predict the mechanical properties of steels directly, during the steel making process by varying their chemical composition [9-11]. In this paper the linear regression technique was used to determine relationships between certain mechanical properties and the chemical composition of steel A516 Grade 65.

2. Method and materials

Sample size of industrial heats of A516 Grade 65 steel were made using the traditional method in an electric arc furnace. All steels were poured into ingots and then were rolled into slabs than finally as plates. The material properties were improved by normalization treatment, applied in accordance with the specifications required for this steel. The data regarding the mechanical properties and chemical composition of steel from the monitored heats were obtained from the laboratory of a steel integrated plant.

3. Experimental data and discussion

The data set comprising measurements of the parameters for 93 sample from 31 industrial heats of A516 Grade 65 steel were statistically processed. The variables taken into consideration concerned the element content: carbon, manganese, phosphorus, sulfur, silicon and nickel. Figure 1 below shows statistical distributions of data regarding chemical composition of steel obtained in electric arc furnace.

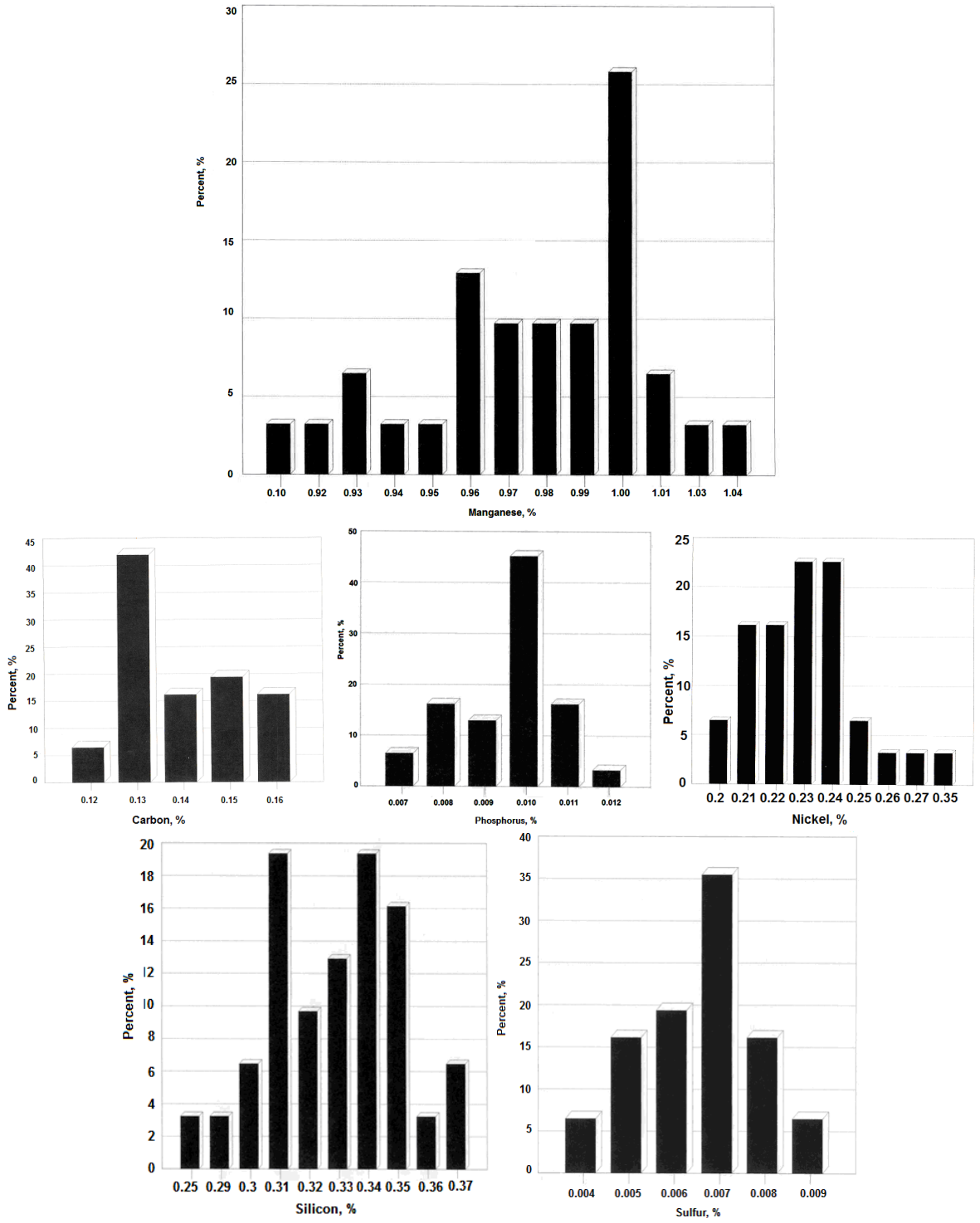

Fig. 1. *Distribution of elements content in the steel*

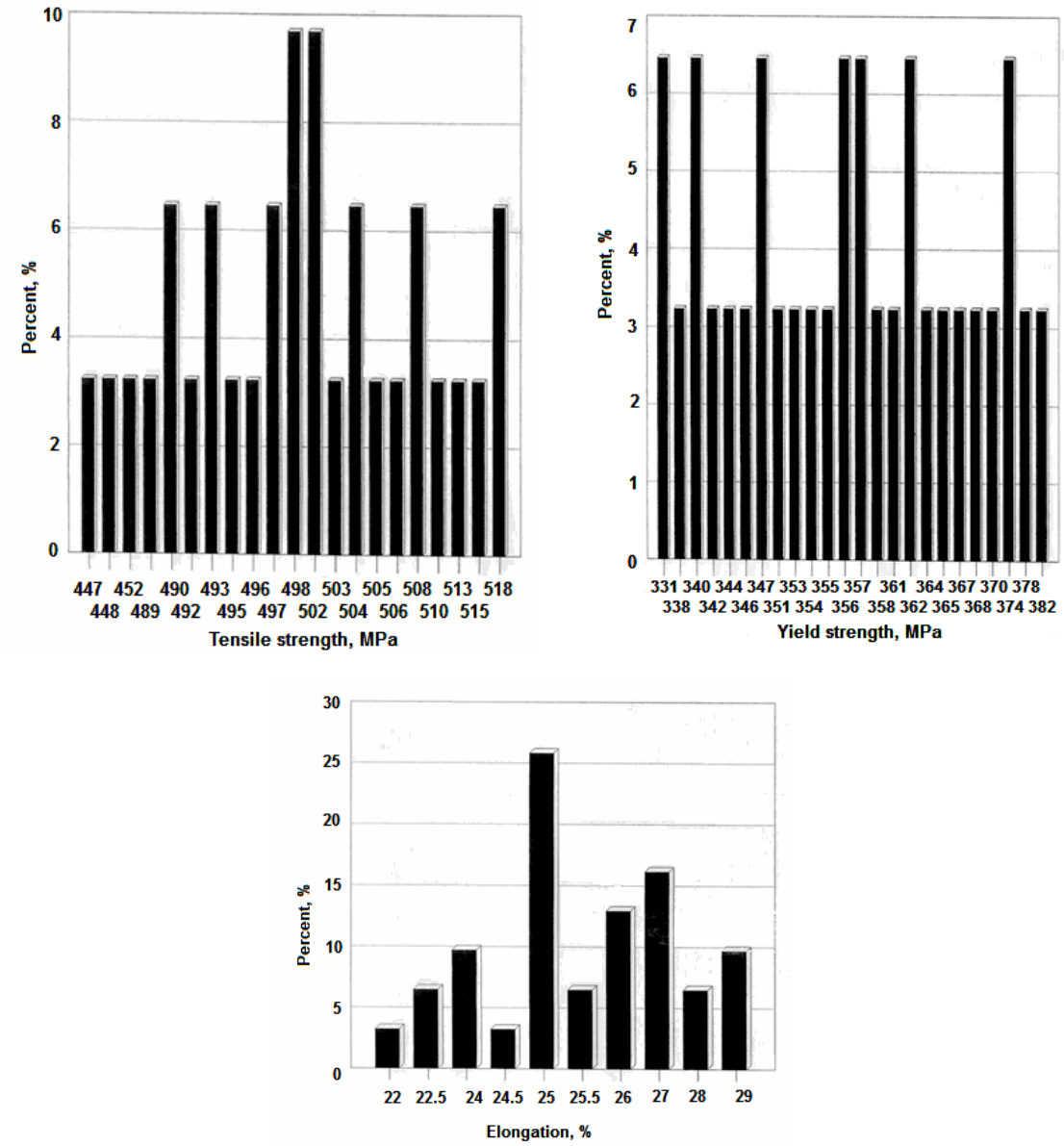

Fig. 2. *Distribution of mechanical properties of monitored steel (measured data)*

The distribution of the data used for the mechanical properties of steel from the monitored heats are shown in Figure 2.

The data calculated for correlation and regression analysis are listed in Table 1. There, ″Mean″ is the arithmetic mean of distribution and ″Standard_dev″ is the standard deviation of distribution.

Regarding the range (minimum, maximum or the smallest and largest content of element), carbon varied from 0.12% to 0.16%, manganese from 0.92% to 1.04% (with the exception of a single value, namely 0.1%, which in fact also explains the greater standard deviation of 0.025 from Table 1), phosphorus from 0.007% to 0.012%, sulfur from 0.004% to 0.009%, silicon from 0.25% to 0.37% and nickel from 0.2% to 0.35%. Equally, the tensile strength varied from 447 MPa to 518 MPa, yield strength from 331 MPa to 382 MPa and elongation from 22% to 29%.

In order to determine the correlation between the final elements content of the steel analyzed and their mechanical properties we determined the individual correlation coefficient between the parameters analyzed. The sign (+) or (-) in front of the coefficient indicates direct or inverse relationship between parameters.

Table 1. *Statistical data for correlation and regression analysis*

Parameter	Mean	Dispersal	Standard_dev
Carbon, %	0.140	0.012	0.000
Manganese, %	0.952	0.158	0.025
Phosphorus, %	0.010	0.001	0.000
Sulfur, %	0.007	0.001	0.000
Silicon, %	0.328	0.025	0.001
Nickel, %	0.233	0.027	0.001
Tensile Strength, MPa	496.484	17.387	302.314
Yield Strength, MPa	355.806	13.005	169.124
Elongation, %	25.694	1.799	3.237

The equation is a function of the range of the chemical composition considered

$$Y = f(x_1, x_2, \ldots x_n)$$

were x_1, x_2, ... x_n are input random variables.

The linear relation between chemical composition of steel and each mechanical property of A516 Grade 65 steel are described as the equation

$$Y_{1...3} = f(c_0+c_1 x_1+c_2x_2+c_3x_3+c_4x_4+c_5x_5+c_6x_6)$$

where Y_1 is tensile strength (MPa), Y_2 yield strength (MPa) and Y_3 elongation (%), while $c_0...c_6$ are regression coefficients corresponding to the chemical element from steel, and $x_1...x_6$ are, respectively, the content of C, Mn, P, S, Si and Ni.

Finally, we obtained the following results for steel A516 Grade 65:

$Y_1 = f(x_1, x_2, x_3, x_4, x_5, x_6) = 553.937 - 71.658 * (\%C) + 1.423 * (\%Mn) - 1553.289 * (\%P) + 49.549 * (\%S) - 87.86 * (\%Si) - 23.277 * (\%Ni)$; $c_0 = 553.937$, $c_1 = -71.658$, $c_2 = +1.423$, $c_3 = -1553.289$, $c_4 = +49.549$, $c_5 = -87.86$, $c_6 = -23.277$ and $R^2 = 0.3015$

$Y_2 = 371.686 - 66.142 * (\%C) + 4.486 * (\%Mn) - 1859.868 * (\%P) + 1453.264 * (\%S) - 23.565 * (\%Si) + 21.777 * (\%Ni)$; $c_0 = 371.686$, $c_1 = -66.142$, $c_2 = +4.486$, $c_3 = -1859.868$, $c_4 = +1453.264$, $c_5 = -23.565$, $c_6 = +21.777$ and $R^2 = 0.4853$

$Y_3 = 28.219 - 7.694 * (\%C) - 4.458 * (\%Mn) + 560.673 * (\%P) + 13.628 * (\%S) + 5.886 * (\%Si) - 19.75 * (\%Ni)$; $c_0 = 28.219$, $c_1 = -7.694$, $c_2 = -4.458$, $c_3 = +560.673$, $c_4 = +13.628$, $c_5 = 5.886$, $c_6 = -19.75$ and $R^2 = 0.36678$.

The coefficient of R^2 determination (square multiple correlation coefficient) which has values within the range [0,1] was calculated. The values of R^2 can be interpreted as meaning that about 30%, 48.5% and respectively 367% of the variation of Y (tensile strength, yield strength or elongation) can be determined by the independent variables x (content of C, Mn, P, S, Si and Ni).

The ductility, as well as weldability properties of the steel decrease if the amount of carbon increases. Manganese has effects similar to those of carbon and also it is necessary in hot rolled steels for its role to form combinations with oxygen and sulfur. Phosphorus is generally regarded as an undesirable impurity because of its embrittling effect. Also, sulfur is normally regarded as an impurity and has an adverse effect on impact properties when steel is high in Sulphur and low in manganese. Elements such as silicon and nickel were also found to be beneficial to the strength properties. Silicon increases strength and hardness but to a lesser extent than manganese. The decrease of ductility could induce cracking problems. Ni is added to steels to increase hardenability. Nickel enhances the low temperature behavior of the material by improving the fracture toughness. The weldability of the steel is not decreased by the presence of this element. The nickel drastically increases the notch toughness of the steel [12].

From the regression analysis, carbon was found to reduce ductility (the elongation at fracture is a measure of ductility of the steel), which is probably related to the pearlite content and the strain hardening rate. Analyses of equations show that manganese improves the tensile strength and yield strength, but have an adverse effect on ductility. This influence is caused by grain refinement and by hardening of solid solution. Also, this effect can be put in relation with the role of manganese as deoxidiser in the steel bath. However, it adversely affects elongation. Silicon has negative effect on steel strength but not on elongation. The alloying of steel with nickel was beneficial to yield strengthening and harmful for tensile strength and elongation.

The effects of the monitored elements can be explained by the following considerations. The regression equations have derived from the available data and so, they have statistical significance only for the samples that were utilized. The equations are functions of the range of chemical composition considered. These linear equations enable the predictions of mechanical properties for steel A516 Grade 65 at the production of plates with variations in their chemical composition.

The accuracy of the regression analysis could be affected by the low number of data processed. Consequently, the regression analysis carried out based on available data is of lower significance level and can be misleading. They must be substantially improved by increasing the number of data and by using a relatively largest range of values for parameters.

4. Conclusions

Mechanical properties of steel plates are determined firstly by the chemical composition of steel. To obtain steels of adequate strength levels, the elements content can be constantly monitored and controlled. By means of regression analysis were obtained simple linear equations used to obtain some mechanical properties of steels by variation in chemical composition (C, Mn, Si, S, P, Ni). The relationships between mechanical properties and chemical composition of A516 Grade 65 Steel assist the specialists' control process to choose the optimum conditions during steel production. The statistically significant correlation between the analyzed parameters and the good correspondence with practical knowledge concerning how parameters affect behaviour of steel in service condition, create the suggestion concerning the practical applicability of the developed statistical models.

References

[1]. ***, *Standard specification for pressure vessel plates, carbon steel, for moderate and lower-temperature service*, ASTM A516 / A516M – 10, 2015.

[2]. ***, *Plate A516 and A387 Pressure Vessel Steels: A Technical Overview*, ArcelorMittal USA.

[3]. Kenneth E. Orie, Fred B. Fletcher, *Performance characteristics of special clean pressure vessel steel subjected to SSC and HIC testing*, paper no. 632, Corrosion 99, April 1999.

[4]. Ken Orie, Charles R. Roper, *The effect of PWHT on normalized base - metal properties of ASTM A516 steel*, Welding Research Council Bulletin, 481, 2003.

[5]. Turkdogan E. T., *Fundamentals of steelmaking*, Institute of Materials (ed.), Cambridge University Press, London, UK, 1996.

[6]. Krawczyk J., Pawłowski B., *Influence of non-metallic inclusions on the strength properties of screws made of 35B2+Cr steel after softening*, J. Achiev. Mat. and Manuf. Eng., 55, p. 721-726, 2012.

[7]. Anisoara Ciocan, Beatrice Tudor, *Effect of secondary vacuum treatment on performance characteristics of A516 grade 65 carbon steel*, Ugalmat 2016, The 7th Conference on material science and engineering, 19-21, Galati, Romania, May 2016.

[8]. Harada A., Miyano G., Maruoka N., Shibata H., Kitamura S., *Composition change of inclusions during ladle treatment by reaction with slag and refractory*, 8th International Conference on Clean Steel, Budapest, Hungary, 2012.

[9]. Lorentz Jäntschi, *Prezentarea şi procesarea datelor experimentale*, Cluj-Napoca, UTPress, 2013.

[10]. Sorana Bolboacă, *Corelaţia şi regresia liniară*, 2012.

[11]. Vlada M., *Calcule statistice si modele de aproximare*, Universitatea din Bucureşti, 2012.

[12]. Vacu S., *Elaborarea oţelurilor aliate*, vol. I and II, Editura tehnică, Bucureşti, 1980 and 1983.

THE ANNALS OF "DUNAREA DE JOS" UNIVERSITY OF GALATI
FASCICLE IX. METALLURGY AND MATERIALS SCIENCE
Nº. 2 - 2016, ISSN 1453 – 083X

THE DYNAMIC SIMULATION FOR A COLD ROLLING MILL MACHINE

Ștefan DRAGOMIR
"Dunarea de Jos" University of Galati, 111 Domnească Street, 800201, Galaţi, Romania
e-mail: stefan.dragomir@yahoo.com

ABSTRACT

For a cold rolling mill machine that represents a mechanical system, the dynamics problems may be solved by using the differential equations of their movement. We must consider all the connections and couplings for the mill machine that have too elastic elements like: springs, shafts and axes deformed through torsion, spring bars, work rolls and back-up rolls.

The vibrations of the mechanical system must be monitored in order to identify those components which cause problems when the damage of the mill occurs during the operation.

In these mechanical systems, mobile rigid permanent couplings are used - which transmit shocks and vibrations - or stretch couplings - which, due to the elastic element, dampen shock and vibration.

Vibrations can appear, too, because of rolling strip that can have undulations.

KEYWORDS: dynamic simulation, mechanical systems, elastic deformations

1. Introduction

This work focuses on aspects of mechanical torque and the aspects resulting from dings (impulsive movements) of a linear character and the vibrations that are produced during the milling impact. The values of the moments of mechanical inertia from electric motor rotors, the couplings, the brake drums and other components can be found in catalogs or can be determined.

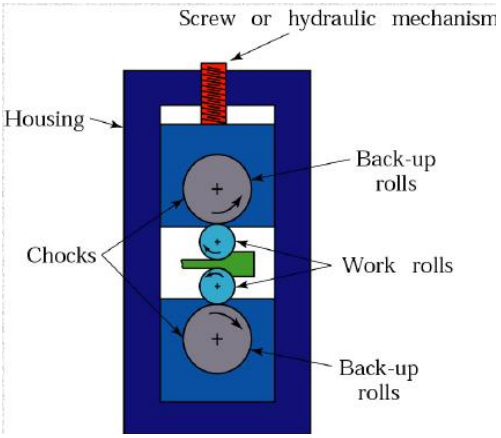

Fig. 1. *Schedule of a quarto rolling mill machine*

The drive system for a modern drive rolling mill machine has greatest accuracy if the rolls speed and strip tension in correlation with torque, laminated force and rotation angle are taken into account.

The monitoring system incorporates the gap control existing in the rolling mill machine (Fig. 1).

The simulation of the dynamic behavior of some components or parts of rolling mill has contributed to decreasing the hardness of this movement parts, a new and functional design, the decrease of energetical consumption.

Initially, the model accepted for a simulation is composed of resorts which substitute the actual masses in work. The hardware and the software for the function control in work are connected to the simulated model. The model must be simulated in real time function work.

The advantage of this system simulation is that both the hardware and software may be tested, regulated and optimized without any risk in comparison to the the existent system.

To investigate the behavior of rolling mills we must study first of all, the behavior of chosen model. The dynamic simulations show the influence of diverse cause on the stand of rolling mill, during work like: high-frequency torsion vibration in the drive system; eccentricity and state surface of work roll shape; mill speed; reduction; strip tension; roll

lubrication. The stands models satisfy the most stringent requirements on control dynamics and shock capacity and are largely free of maintenance. The equipment used has the following advantage: no limit in the drive rating; better control performance; the rotor of the engine (machine) has lower moments of inertia; less spare parts; greater flexibility of parts; simple start-up procedure; high reliability and availability; output frequencies from 0 to 600Hz; frequency control; highly accurate speed and torque control; positioning controls; parameter indicator, text display, graphic display.

Now, the modern tandem rolling mills have hydraulic gap controls on all stands. The control loops take into account the position control and work rolls tilt control. The roll forces are measured either indirectly, by pressure transducers attached to the hydraulic cylinders or directly by roll force transducers located in force line of the hydraulic cylinders.

2. Dynamic model of rolling mill machine

Dynamic loads are produced in cold rolling mill machine for strip when change technology parameter, stiffness and forces are periodical. The mathematical models for a mill dynamic model takes into consideration the equation of differential movement during the period of acceleration. For the kinematic schedule of drive mechanism, rigidities shall be regarded as usual at the electric motor shaft or at the input shaft of the work machine mechanism.

These loads appear on systems with variable stiffnesses, in different directions (transmissions) U-Joints, the coupling bars a.s.

Figure 2 shows a schedule of quarto rolling mill. By replacing a real system with an equivalent one, in energetic terms, an accuracy in determining its parameters which greatly affect the accuracy of the dynamic calculation must be kept.

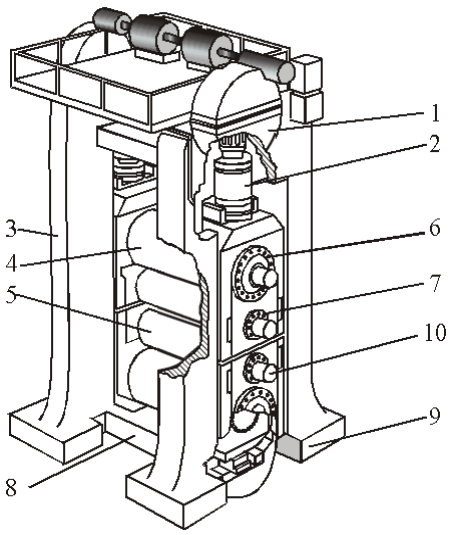

Fig. 2. *Quarto rolling mill machine* [2]*: 1-mechanism of positioning system; 2-positioning system; 3-mill frame; 4-back-up roll; 5-work roll; 6-back-up roll bearing; 7-work roll bearing; 8-lower traverse of rolling mill frame; 9-the sole of rolling mill frame; 10-work roll shaft*

The signals from the position transducers on each side of the stand are subtracted to produce the value for the roll tilt controller, which alters the tilt of centerline stand.

For the calculation of the dynamic rolling stands we can imagine a system with springs and masses in rotation as shown in Figure 3. The considered oscillating system is formed from a straight shaft (negligible mass) and the elastic constant of the torsion represents C = K. There can be treated oscillating systems with rotating masse from 2, 3 to n.

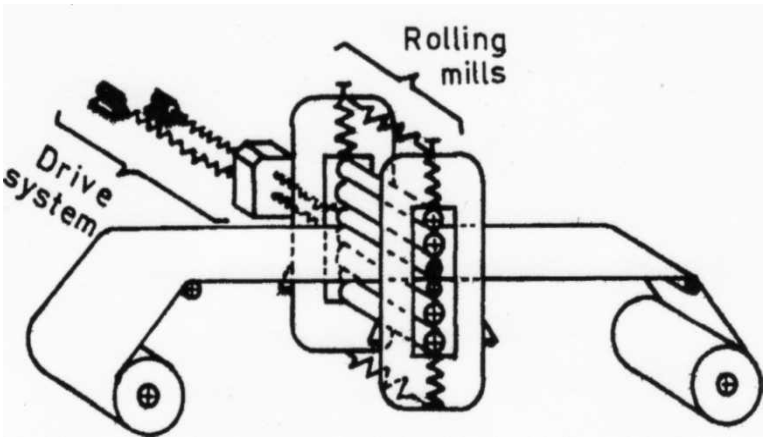

Fig. 3. *Stand for dynamical simulation* [3]

The roll force control is measured for each roll work. The total tension reference value is calculated in the control system in accordance with the rolling program and the strip dimensions and is sent to the tension controller.

The laminated torque can be estimated by [3]:

$$T = 0.5 * F * L \quad (1)$$

where T is torque (Nm); F-roll force (N); L-contact length (m).

The Power required by the rolling mill electrical engine is calculated as follows

$$P = 2\pi*N*F*L \quad (2)$$

where P is Power (in J/s =Watt or in-lb/min); N- rolls rotational speed (RPM); F- roll force (N).

The tension is measured by tension-meters mounted under the bearing blocks of the deflector rolls. The control system depends on the speed with respect to the gain and time response. The gain of the tension controller is matched out adaptively to the properties of the controlled system.

The equipment used has the following advantages [4]:

- total digital DC speed control in production line, closed loop control of tension and automatic control of speed;
- hydraulic automatic gauge control of five stands including pre-control AGC, monitoring AGC and mass flow AGC;
- positive/negative bending roll of working rolls, positive bending rolling of intermediate rolls;
- equipping with the collection system, display, storage and data output, including fault diagnosis and alarm system;
- five stands with the function of automatically decreasing speed and tension during passing welding seam;
- quick roll change;
- oil-air lubrication for all rolls;
- ferromagnetic filter and plate filter for rolls cooling system.

3. Schedule of reductions for cold rolling strip

Reduction schedule for obtaining cold rolled strip steel with dimensions of 0.3 × 1490 mm, the mill consists of five stands arranged in tandem.

For low carbon steel with percentage and reduced thickness ε_{tot} = 86%.is adopted

So, it will be used as a rough hot rolled strip and pickled (dimension 2 × 1490 mm) form of roller weighing 30 t.

3.1. Determining maximum reductions - admissible

By friction grease provided by technology, the friction coefficient varies from the first to the last pass on the rolling speed (v = 2.5 ...30 m / s) between f = 0.08 ...0.043 (anointing with oil). Based on these values, it results:

$$\Delta h_{max} = D\left(1-\frac{1}{\sqrt{1+f^2}}\right) = 585\left(1-\frac{1}{\sqrt{1+(0{,}08...0{,}043)^2}}\right) \quad (3)$$

$$\Delta h_{max} = 1.87...0.54 \text{ mm}$$

Depending on the driving engine power reduction is [4]

$$\Delta h_{max} = (32...33{,}8)\frac{K \cdot N_{nom}}{\psi \cdot p_m \cdot b \cdot v} \quad (4)$$

where k - is a driving motor overload factor, ranging from 1.5 ... 2 (K = 1.75 was adopted); Ψ = coefficient of rolling force positioning on arc length of contact. For cylinders with the leaf surface "mirror" Ψ = 0.48, p_m represents mean pressure lamination, which is approximatively as follows:

$$p_m = 1.15 \cdot \sigma_c \quad (5)$$

Knowing that the initial state annealed, strip has a flow limit equal to σ_0 = 22 daN / mm^2, there follows:

- for the first pass (admitting ε_1 reduction = 27%):

$$\sigma_{c1} = \sigma_0 + 17\,{}_1^{0.6} = 22 + 1.7 \cdot 27^{0.6} = 34.3 \text{ daN/mm}^2 \quad (6)$$

$$p_{m1} = 1.15 \cdot 34.3 = 39.4 \text{ daN / mm}^2$$

- for the final pass (in which ε_{tot} = 85%):

$$\sigma_{c5} = \sigma_{c0} + 3.4 \cdot \varepsilon_{tot}^{0.6} = 22 + 3.4 \cdot 85^{0.6} = 70.9 \text{ daN/mm}^2 \quad (7)$$

$$p_{m5} = 1.15 \cdot 70.9 = 81.5 \text{ daN / mm}^2$$

The amount of reduction to the first passage was adopted according to the final thickness. Depending on the deflection of the work rolls in the last pass,

$$\Delta h_{max} = (F_{max} / p_m.b)^2 \cdot 1/R \quad (8)$$

where F_{max} is the rolling force, which can ensure an arrow (bending) for rolling cylinders with Δd_{max}, respectively strip thickness tolerance that is:

$$\Delta d_{max} = \pm\ 0.05 \text{ mm} \quad (9)$$

$$F_{max} = \frac{37.6 \cdot \Delta d_{max} \cdot E \cdot D_s^4}{L^2\left(10 \cdot L \cdot +24 \cdot l \frac{15D_s^2}{L}\right)} \quad (10)$$

E = modulus of elasticity of the back-up rolls. E = $2.2 \cdot 10^4$ daN/mm^2; D_s = diameter of back-up rolls D_s = 1525 mm; L = roll length; l = spindles roll length; L = 1700 mm; l = 1000 mm.

Depending on the adopted values, we obtain

$$F_{max} = 12.6 \cdot 10^5 \text{ daN} \quad (11)$$

and it results

$$\Delta h_{max} = 0.14 \text{ mm} \quad (12)$$

Given the maximum value reductions - allowable, calculated according to three limiting criteria it results that, regarding the reduction scheme to be fixed, higher reductions than 1.87 mm at first pass and 0.14 mm at the last pass will not be allowed.

Considering the maximum reduction values - allowable calculated according to three limiting criteria, results that the established reductions scheme, will not allow larger reductions of 1.87 mm at first pass to 0.14 mm at the last pass.

3.2. Establishing the crossing reductions

For the first pass, we adopted, depending on the final strip thickness (h_5 = 0.3 mm), a ε_1 equal reduction = 27%. For other passages, the following factors shall be taken to reduce the degree of amplification from a switch to another: C = 1.555; C' = 0.90.

Depending on the values of these degrees of reduction per pass, the absolute reduction in thickness of the strip passes will be:

$$\Delta h_2 = \varepsilon_2 \cdot h_1 = 0.46 \text{ m}; \ h_2 = h_1 - \Delta h_2 = 1.00 \text{ mm} \quad (14)$$
$$\Delta h_3 = \varepsilon_3 \cdot h_2 = 0.36 \text{ mm}; \ h_3 = h_2 - \Delta h_3 = 0.64 \text{ mm} \quad (15)$$
$$\Delta h_4 = \varepsilon_4 \cdot h_3 = 0.21 \text{ mm}; \ h_4 = h_3 - \Delta h_4 = 0.43 \text{ mm} \quad (16)$$
$$\Delta h_5 = \varepsilon_5 \cdot h_4 = 0.13 \text{ mm}; \ h_5 = h_4 - \Delta h_5 = 0.30 \text{ mm} \quad (17)$$

Setting the stress values of each pass band will be according to: $\sigma_n = (0.2...0.5)\sigma_{c.med}$.

Calculation of average yield strength of the material after each pass is:

$$\sigma_{cn} = \sigma_{c0} + a \cdot \varepsilon_{tot_n}^{0.6} = 22 + 3.4 \cdot \varepsilon_{tot_n}^{0.6} \quad (18)$$

Calculation of tensile forces inside of strip is done by the next equation:

$$T_i = \sigma_i \cdot S_i = \sigma_i \cdot h_i \cdot b_i \quad (19)$$

3.3. Establishing the minimum speed rolling

Speed of the last mill stand is adopted with a value v_5 = 30m / s.

Minimum speed to other stands will be: v1 = 6.16 m / s, v2 = 9.0 m / s; v3 = 14.06 m / s; v4 = 20.93 m / s.

3.4. Calculation of the rolling forces

For the case of cold rolling it is recommended rolling force calculation using the Stone formula [5]:

$$F = p_m \cdot B \cdot l_c = (K_0 - \sigma_m).(e^m - 1)\ B.l_c / m \quad (20)$$

where: $K_0 = 1.15 \cdot \sigma_{c.med}$

The calculation of rolling force is performed in two stages: determining a first approximation rolling force without taking into account the elastic deformation of the cylinder. In this case:

$$I_c = \sqrt{R \cdot \Delta h} \quad (21)$$

The value obtained for the rolling force is calculated by the arc length of contact, taking into account the elastic deformation of rolls.

For rolling of carbon steel, the coefficient of friction when using emulsions of mineral oils is f_0 = 0.06 ...0.11.

It was found that the elastic deformation of the rolling mill work rolls, in contact with the arc length

of the first passage increases by about 9.5%, which entails an increase in the rolling force by about 13.0%. Also, as the material of the strip is hardening, the relative increase in length of the contact arc is the greatest.

For other passages similarly resulting calculation were obtained, and the results were summarized in Table 1.

Table 1. *Schedule of reduced for rolling a strip of 0.3 × 1500 mm carbon steel as a continuous train of five rolling stands*

Number of passes	h mm	Δh, mm	Reduction on passing ε, %	total reduction ε_{tot}, %	σ_c daN/mm^2	σ_0 daN/mm^2	v m/s
0	2.0	-	-	-	22	6	-
1	1.46	0.54	27	27	46.56	10	6.16
2	1.00	0.46	21.2	50	57.55	21	9.0
3	0.64	0.36	36.0	68	64.75	30	14.06
4	0.43	0.21	32.4	78,5	68.60	33	20.93
5	0.30	0.13	29.1	85	70.88	17	30.0

f	I_c^*, mm	I_c^{**}, Mm	P_m^*, daN/mm^2	P_m^{**}, daN/mm^2	Mill force*, tf	Mill force**, tf	Tensile strength tf
-	-	-	-	-	-	-	15
0,061	12.57	13.76	40.16	41.08	757	848	21.9
0,057	11.60	13.28	58.74	61.30	1022	1221	31.5
0,051	10,26	12,04	62,72	66,70	965	1205	28,8
0.047	7.84	9.68	66.77	73.15	785	1062	21.3
0.043	6.17	8.30	81.15	93.65	751	1166	7.65

* -- for undeformed rolls
** -- for deformed rolls

A lot of tracking tests on the work and backup rolls were contours of the roughing mill and have been finished. Generally, work roll wear contours are wearing and the partial peak exists while the backup roll wear is generally non-uniform along the entire length of the roll.

4. Vibration analysis

The dynamic behavior of rolling mill is related to the vibrations that occur during operation. These vibrations can occur because of wear in bearings and spacing due to component wear rolling mill, cylinder roughness or even destruction of the strip surface which is laminated. The vibrations in the rolling tandem occur when acceleration or deceleration different underlain by different reasons.

This analysis shows that the alternating shear stress of a certain depth from the roll surface caused by roll contact pressure is very important.

The type of conventional wear of rolls makes contact stress between the edge of backup and work rolls increase significantly, contact stress between rolls in the middle of the roll had little change in the edge of the roll occurs sometimes [5].

The ideal solution is to obtain a uniform distribution of the pressure by improving the surfaces and the contour of the backup rolls and of the work rolls (Cao, J. G. 1999).

This wear is in correlation with the amplitude of the vibration measured in the stand 3, 4 and 5 of rolling mill machine.

The axial distribution of contact stress between the work roll and the backup roll could be influenced by the strip width and wear in different service period. It could be known by comparative analysis: the peak of the contact stress between rolls gradually increases with the increase of the strip width.

When the strip width increases, the peak of contact stress between rolls is increased with 106.3%. The rolling force per strip width is increased from 16 kN/mm to 27 kN/mm.

The distribution trends of contact stress between rolls are the same for different width strips, and the non-uniformity coefficient of contact stress distribution between the rolls are 1.35, 1.39 and 1.43, respectively [5]. It could be seen by the analysis of contact pressure between rolls that the peak position of contact stress between rolls is essentially the same, which is about 205mm from the edge side of the backup roll barrel.

The position control is in action when the gap is open, during the beginning of the operation and a subsystem of the gauge control.

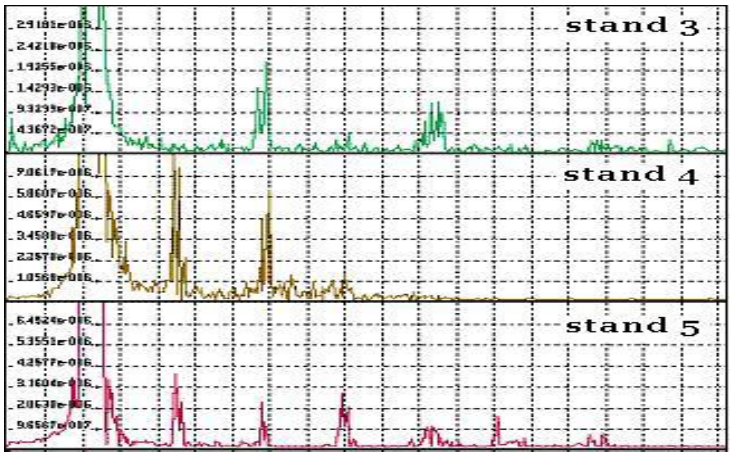

Fig. 3. *Vibrations spectrums in the stands no. 3, 4 and 5* [6]

For the rolls tilt control the signals from the position transducers on each side of the stand are subtracted to produce the actual value for the tilt controller, which alters the tilt about the centerline of the stand. Atypical response time is approx. 25 ms. The control loop is effective during rolling and is only switched during calibration after the calibration force has been reached. A typical response time is approx. 30 ms.

The gain of the tension controller is matched to the properties of the controlled system.

5. Conclusion

Nowadays, the modern rolling mills have hydraulic gap controls on all stand loops, positioning control, tilt control, speed, forces and tensions control. The roll forces are measured either indirectly by pressure transducers attached to the hydraulic cylinders or, directly by roll force transducers located in the line of force of the hydraulic cylinders. To predict the real roll force, it is necessary to introduce all variables into a corrective neural network. A corrective neural network can eliminate the errors in the roll force prediction.

This network can reduce the prediction errors at 21%. The additional variables, which are not introduced in the mathematical model, were necessary for the substitutive model only. The chemical composition of coil and temperature variable must be considered for the network.

The use of proposed system milling (stand) improves the accuracy of work parameters (in particular rolling force).

Some parameters not considered in the mathematical model can be easily introduced in a system neural network.

The system proposed can predict the work parameters and also correct wrong work milling as an option for the final adequate configuration (thickness and flatness and mechanical characteristic) for rolling sheet.

References

[1]. Goodwin G. C., Grebe S. F., Salgado M. E., *Control system design*, Prentice Hall, Inc., New Jersey, 2001.
[2]. Olaf Norman Iepsen, Gunter Kneppe-System, *Simulation and mill modelling ilustrated by the example of chattering tandem cold rolling mills*, MPT Internationa, p. 80-86, l6/1996.
[3]. Dragomir Stefan, Tudor Beatrice, *Cold rolling mill driving and dynamic behaviour for some important components*, Annals metallurgy and material sciences, UDJ, 1999.
[4]. Portmann N., *Application of neural network rolling mill automation*, Iron and Steel Eng., vol. 72, no. 2, p. 33-36, 1995.
[5]. Dobrucki W., Bar A., *Changes in roll-gap shape in the case of vibration in a four-high rolling mill stand*, Journal of Materials Processing Technology, vol. 61, p. 328-338, 1996.
[6]. Krot P. V., Pryhodko I. Y., Chernov P. P., *Regenerative chatter vibrations control in the tandem cold rolling mills JSC*, Novolipetsk Metallurgical Combine (NLMC), Lipetsk.

MANUSCRISELE, CĂRŢILE ŞI REVISTELE PENTRU SCHIMB, PRECUM ŞI ORICE CORESPONDENŢE SE VOR TRIMITE PE ADRESA:

MANUSCRIPTS, REVIEWS AND BOOKS FOR EXCHANGE COOPERATION, AS WELL AS ANY CORRESPONDANCE WILL BE MAILED TO:

LES MANUSCRITS, LES REVUES ET LES LIVRES POUR L'ÉCHANGE, TOUT AUSSI QUE LA CORRESPONDANCE SERONT ENVOYÉS À L'ADRESSE:

MANUSCKRIPTEN, ZIETSCHRITFTEN UND BUCHER FUR AUSTAUCH SOWIE DIE KORRESPONDENZ SID AN FOLGENDE ANSCHRIFT ZU SEDEN:

After the latest evaluation of the journals by the National Center for Science Policy and Scientometrics (**CENAPOSS**), in recognition of its quality and impact at national level, the journal will be included in the B^+ category, 215 code (http://cncsis.gov.ro/userfiles/file/CENAPOSS/Bplus_2011.pdf).

The journal is already indexed in:

EBSCO: http://www.ebscohost.com/titleLists/a9h-journals.pdf

Copernicus: http://journals.indexcopernicus.com/karta.php

The papers published in this journal can be viewed on the website: www.fascicula9.ugal.ro

Name and Address of Publisher:
Contact person: Elena MEREUȚĂ
Galati University Press - GUP
47 Domneasca St., 800008 - Galati, Romania
Phone: +40 336 130139, Fax: +40 236 461353
Email: gup@ugal.ro

Name and Address of Editor:
Prof. Dr. Eng. Marian BORDEI
Dunarea de Jos University of Galati, Faculty of Engineering
111 Domneasca St., 800201 - Galati, Romania
Phone: +40 336 130208
Phone/Fax: +40 336 130283
Email: mbordei@ugal.ro

AFFILIATED WITH:

- THE ROMANIAN SOCIETY FOR METALLURGY
- THE ROMANIAN SOCIETY FOR CHEMISTRY
- THE ROMANIAN SOCIETY FOR BIOMATERIALS
- THE ROMANIAN TECHNICAL FOUNDRY SOCIETY
- THE MATERIALS INFORMATION SOCIETY (ASM INTERNATIONAL)

Edited under the care of the FACULTY OF ENGINEERING

Annual subscription (4 issues per year)

Editing date: 15.06.2016
Number of issues: 200
Printed by Galati University Press (accredited by CNCSIS)
47 Domneasca Street, 800008, Galati, Romania